TUBULIN MODIFICATIONS IN HUMAN GAMETES:

From the oocyte spindle to the sperm flagellum

Characterization of tubulin post translational modifications in female meiosis and sperm pathologies

PARASKEVI KARAMTZIOTI

TESI DOCTORAL UPF / 2020

Thesis supervisor

Dra. RITA VASSENA, Clinica EUGIN

Thesis co-supervisor

Dra. ISABELLE VERNOS, CRG

THESIS DEPARTMENT
Department of Experimental and Health Sciences

Universitat Pompeu Fabra Barcelona

Στην αγαπημένη μου κυρία Φυλακτακίδου Κωνσταντίνα

To Prof. Fylaktakidou Konstantina

Acknowledgements

My utmost gratitude goes to my thesis director Dr. Rita Vassena, my thesis co-supervisor Dr. Isabelle Vernos and my laboratory supervisors Dr. Gustavo Tiscornia and Dr. Montse Barragán. Their scientific insight, research experience, professional attitude and unique character have crafted my identity as a scientist and researcher. Rita is the adamant and grounded captain that steers the ship to new horizons. Isabelle, a role model of graceful leadership and passion for new discoveries. Gustavo, discussions with you improved my scientific rationale, communicating clear ideas, and what I like to call "perform a paper x-ray". I will always remember your encouraging words for writing this thesis: "Go Nike about it", so "just do it"! Montse, thank you so much for all the troubleshooting and the constructive criticism that stimulated improvement.

Along with doing experiments in this lab, I will miss even more my colleagues. David, I have to admit, around you I felt more within my comfort zone so thanks for making my integration in the group easier and smoother. Paula, I appreciate you being the other "grandma" in the lab, and not making me feel too old for this! Without you agapi, I wouldn´t have survived the David-Marc combination. Which brings me to Marculito. Thanks for making my desk a mess with your coffee and all your artistic decorations in the lab. Sharing responsibilities, learning new techniques and in general "playing scientists" has been a pleasure next to you guys. Anna, you are my oocyte-confocal mentor and I can´t express how

lucky I felt to have your guidance and advice! Filippo, I enjoyed the data analysis discussions, your quick-thinking and input really boosted the lab´s dynamics. Finally, Alexandra´s and Raquel´s energy electrified the lab´s atmosphere, giving the spark that was needed in the absence of the "PMD" trio. Their eagerness to learn and enthusiastic personality was motivating in moments of hardship and disappointment. Speaking of which, no experimental or professional challenge compares to life´s punches in the face when it comes to health issues. Agus, I really missed you in the lab but seeing your fighting power, I have faith that things will turn out …supercalifragisticexpialidocious!

Ana, Alejandra, Christel, Ivan, Pragya, Ennio, Jiju, Manuel, Pablo and Robert have been like co-travellers either physically or mentally to this journey. I hope this network will give birth to new collaborations in the future.

Farners, Georgina, Alvaro, Aitor, Leo, Christian and Nuria thanks for welcoming and helping me in Isabelle's lab, it was lovely to have met you all, sharing science or even a few words.

My significant others… the incarnation of hope and love, you have literally brought and kept me to life. There is no thank you enough for that. Dad, mama and sis you have no clue about what I do but you've always supported me because it makes me happy (among some bursts of tears!). Mama, thank you for never ever giving up. Grandpa and grandma, the strongest couple I have known, you've given me and my sis love, attention and pure devotion, always

there, always present, always understanding. George, the years with you have been a journey with many ups and downs, and I wouldn't change a single moment. Eirini, Chara and Giota, thank you for every laugh and every tear we've shared together and looking forward to the many more to come. Eirini, your enthusiasm, your faith in me and your support in tough moments of the PhD were crucial for pushing through them and coming out stronger.

Finally there is this one person. My person. The paradox is that contrary to the meaning of its name, DivIDE, right before its end, led to our union and I am grateful for this. It is up to us now, my Pierre, to stick together for the years to come, contributing with new "deliverables"!...

Abstract

This thesis aimed to characterize the tubulin PTM profile of human oocytes and spermatozoa. Tubulin rich structures play critical roles in the cellular behavior of human gametes. Mutations in tubulin or related proteins can affect oocyte maturation and flagellum motility. We first focused on tubulin post-translational modifications (PTMs) in the oocyte spindle and sperm flagellum. We characterized the PTM spindle profile of MII oocytes cultured *in vitro* and matured *in vivo,* and compared PTM enzyme transcript levels with two additional groups: GV and failed to mature oocytes. Further determination of the transcripts' translational fate was performed using the cytoplasmic polyadenylation element code with verification experiments on Xenopus oocytes. Additionally, we sought to deteremine the pattern and levels of tubulin PTMs along the sperm tail and correlate these profiles with pathologies like asthenozoospermia and teratozoospermia.

Resumen

Esta tesis tuvo como objetivo caracterizar el perfil de PTM de los microtúbulos de ovocitos y espermatozoides humanos. Las estructuras ricas en tubulina juegan un papel fundamental en el comportamiento celular de los gametos humanos. Las mutaciones en la tubulina o proteínas relacionadas pueden afectar la maduración de los ovocitos y la motilidad del flagelo. En primer lugar, nos centramos en las modificaciones posteriores a la traducción (PTM) de la tubulina en el huso del ovocito y el flagelo del esperma.

Caracterizamos el perfil de PTM del huso en ovocitos de MII cultivados in vitro y madurados in vivo, y comparamos los niveles de transcripción de PTM enzimas con dos grupos adicionales: GV y ovocitos que no maduraron. Además se estudió la regulación de la transcripción de los RNA mensajeros por el código del elemento de poliadenilación citoplásmica con experimentos en oocitos de Xenopus. Además, investigamos el patrón y los niveles de PTM de tubulina a lo largo de la cola del esperma y su correlacioón potencial con patologías como la astenozoospermia y la teratozoospermia.

Preface

The work presented here was mainly conducted in the basic research laboratory of Clínica Eugin and partially in the Cell and Developmental Biology Program at the Center for Genomic Regulation (CRG). This work has been supervised by Dr. Rita Vassena (Clínica Eugin). The project was funded as part of the DiViDE consortium (project number 675737) focused on elucidating the mechanisms and principles of cell division and to reproduce them *in vitro* with synthetic approaches.

Our study aims to expand our knowledge in the field of human gamete biology focusing on tubulin post translational modifications (PTM). Basic research in reproduction has gained momentum as initial *in vitro* fertilization procedures by Robert Edwards were successful in 1978 and have since spawned a global industry based on assisted human reproduction techniques. A central and complex question in the field is the following: how can the oocyte and spermatozoon of the best quality be selected? What exactly do we mean by 'quality' and how do we measure it? The findings presented in this thesis explore previously unkown territory. We have characterized the spindle microtubule PTM profile of human oocytes cultured *in vitro* and matured *in vivo,* compared the levels of PTM enzymes of the previous groups with immature oocytes and oocytes that have failed to mature. Furthermore, we have optimized a protocol for determining and quantitatively comparing the PTM pattern along the human sperm flagellum.

Abbreviations List

ART	Assisted Reproduction Technologies
ATP	Adenosine Triphosphate
cAMP	Cyclic Adenosine Monophosphate
cDNA	Complementary DNA
CPE	Cytoplasmic Polyadenylation Element
DNA	Deoxyribonucleic Acid
ET	Embryo Transfer
FSH	Follicle Stimulating Hormone
FTM	Failed to Mature
GV	Germinal Vesicle
GDP	Guanosine Diphosphate
GIFT	Gamete Intra-fallopian Transfer
GnRH	Gonadotropin Releasing Hormone
GTP	Guanosine Triphosphate
hCG	Human Chorionic Gonadotropin
ICC	Immunocytochemistry
ICSI	Intracytoplasmic Sperm Injection
IF	Immunofluorescence
IVC	*In vitro* Cultured Oocytes
IVM	*In vitro* Maturation
IVO	*In vivo* Matured Oocytes
LH	Luteinizing Hormone
MI oocyte	Meiosis I Oocyte
MII oocyte	Meiosis II Oocyte
mRNA	messenger RNA

MTOCs	Microtubule Organizing Centers
NEBD	Nuclear Envelope Breakdown
ODC	Oocyte Developmental Capacity
PBS	Phosphate-Buffered Saline
PCR	Polymerase Chain Reaction
PFA	Paraformaldehyde
PGCs	Primordial Germ Cells
PGT	Pre-implantation Genetic Testing
PTMs	Post-translational Modifications
WHO	World Health Organization

Table of contents

List of Figures

List of Tables

INTRODUCTION

INTRODUCTION

1. Basic research in infertility: focus on the gametes

Infertility (or subfertility) is defined as involuntary childlessness after one year of regular unprotected intercourse (Zegers-Hochschild *et al.*, 2017). In western countries, one in six couples are affected (Farquhar *et al.*, 2019), resulting in significant psychological and financial burden for individuals, couples and society at large. Infertility can occur due to pathologies of the male and/or female reproductive system or idiopathic reasons (unexplained infertility). More than half of infertility cases are due to male factor (Inhorn and Patrizio, 2014).

Assisted reproduction technologies (ART) are defined as "all interventions that include *in vitro* handling of human gametes or embryos for the purpose of reproduction. This includes, but is not limited to, IVF and embryo transfer (ET), intracytoplasmic sperm injection (ICSI), embryo biopsy, preimplantation genetic testing (PGT), assisted hatching, gamete intrafallopian transfer (GIFT), zygote intrafallopian transfer, gamete and embryo cryopreservation, semen, oocyte and embryo donation, and gestational carrier cycles" (Zegers-Hochschild *et al.*, 2017). The field of ART started with the birth of Louise Brown, the first human to be born with the technique of *in vitro* fertilization developed by Robert Edwards in 1978. Since then, the field has thrived, with more than 5 million live births to date using IVF and ICSI (Chen and Heilbronn, 2017).

A major cause for infertility is gamete dysfunction. Research on cryopreservation, *in vitro* culture of follicles, *in vitro* oocyte maturation and "omics" studies have widened the range of medical approaches for assisted reproduction treatments.

1.1) Oocyte quality

Oocyte developmental capacity (ODC) is the ability of the oocyte to produce a healthy embryo capable of reaching the blastocyst stage after fertilization with non-compromised sperm and implantation into a healthy uterus (Kempisty *et al.*, 2015). ODC is determined by molecular and cellular aspects of the oocyte, such as structural and accessory proteins, signalling elements, antioxidant stores, the calcium response machinery, and the state of the MII spindle, chromosomes and organelles (mitochondria, cortical granules and the endoplasmic reticulum) (Coticchio *et al.*, 2013a). Less than 5% of the total number of oocytes collected for fertility treatment result to a live birth, failing at the stages of maturation, fertilization or embryonic divisions (Albertini, 2014). The low efficiency can be due to intrinsic compromised function, advanced maternal age, lifestyle factors and medical conditions (obesity, diabetes) as well as major ART interventions that can interfere with oocyte quality, such as ovarian hyperstimulation, cryopreservantion and *in vitro* maturation.

Folliculogenesis

Folliculogenesis is the process of antral follicle formation, the spherical cyst that encapsulates the maturing oocyte. Follicles in the ovary can be found in four different stages: primordial, primary,

secondary and antral. During the latter half of human fetal life, the first step of folliculogenesis occurs (Fig.1). Oocytes that survive the germ cell cluster apoptotic breakdown are encapsulated in a single-layer of squamous somatic pre-granulosa cells, forming the primordial follicles. Follicle rectruitment can occur as initial activation of primordial follicles throughout life until menopause and after puberty, as cyclic recruitment of a specific number of follicles from the growing cohort, out of which a portion is selected for dominance and ovulation (Baerwald *et al.*, 2012). The morphology of the somatic cells changes to cuboidal when the transition to primary oocytes occurs. The pool of existing primary oocytes are arrested in prophase I at the diplotene stage (also known as dictyotene) during which the synaptonemal complex disappears, the chiasmata are visible and RNA synthesis is maintained at basal levels (Lenormand *et al.*, 2016). The next stage of preantral follicle formation is marked by oocyte growth, granulosa cell proliferation and appearance of a second somatic cell layer, the theca cells. Upon formation of the antrum, the fluid-filled cavity granulosa cells form either the lining of the follicle (mural) or enclose the oocyte (cumulus). The meiotic arrest in antral follicles is achieved by high cAMP levels within the oocyte, which are maintained by cGMP-mediated PDE3A inhibition. cGMP is diffused in the oocyte through its gap junctions connecting it with the cumulus and mural granulosa cells (Edson *et al.*, 2009; Adhikari and Liu, 2014).

Oocyte maturation

Natural ovulation cycles are initiated once every month when the female enters into puberty. Upon the release of follicle-stimulating hormone (FSH) from the pituitary gland, the oocyte will enter a growth phase during which its volume increases, cellular components are accumulated (RNA, proteins, lipids and organelles) while structures like the zona pellucida and the cortical granules are formed. The luteinizing-hormone (LH) peak triggers ovulation of the mature oocyte that has undergone both nuclear and cytoplasmic modifications, organelle redistribution and cytoskeleton remodeling as well as establishment of polarity for the resumption of the asymmetric division until metaphase II (Verlhac and Terret, 2016). In particular, the signaling cascade affected by the LH receptor leads to decreased cGMP levels and thus increased phosphodiesterase activity which results to the drop of cAMP levels. Within the GV nucleus, the key event is the activation of cyclin B1-cyclin dependent kinase1 (CDK1) (Coticchio *et al.*, 2013a).

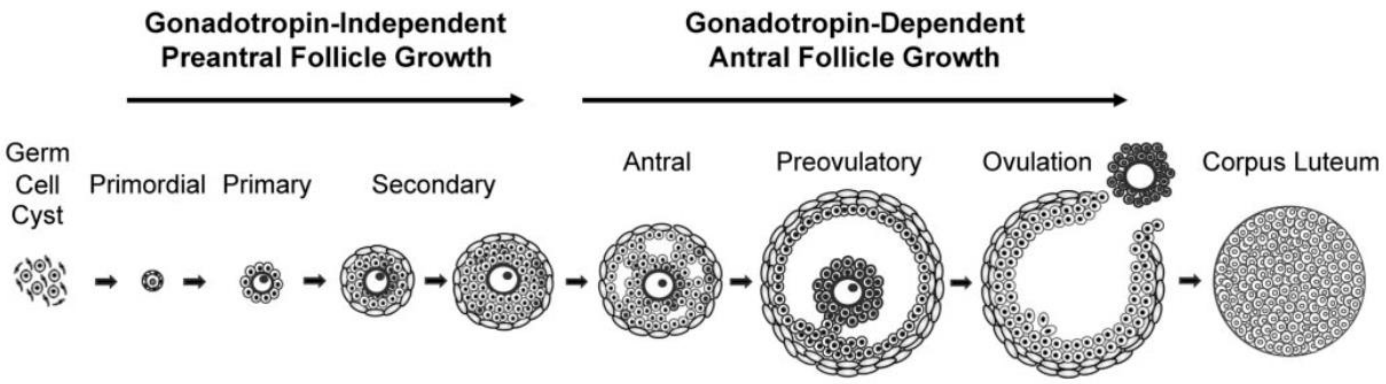

Figure 1. The process of folliculogenesis from germ cell cyst to the corpus luteum in humans. (Image adapted from Edson et al 2009)

Factors affecting oocyte quality

The first successful *in vitro* maturation (IVM) was performed 85 years ago for rabbit oocytes (Pincus and Enzmann, 1935). Further research led to the concept of maturation inhibition within the follicle as well as the connection between maturation and ovulation. In 1965, the first human IVM was reported (Edwards, 1965) and for the first decades it was mainly offered as an answer to high responders in order to prevent the ovarian hyperstimulation syndrome (Trounson *et al.*, 1994; Barnes *et al.*, 1995). In other cases, through IVM, surgically removed unstimulated ovaries become a source of oocytes for autologous infertility treatment or donation (Cha *et al.*, 1991; Cha and Chian, 1998).

Following studies used the term IVM for a broader range of practices, including oocytes derived from hormonally stimulated women or cumulus cell-free culture. These methodologies introduce variables that can affect meiotic fidelity and thus the term should not be used interchangeably (De Vos *et al.*, 2016). Cumulus-stripped oocytes derived from stimulated cycles demonstrated similar fertilization rates when compared to the *in vivo* group, while day 2 embryos divided improperly (Reichman *et al.*, 2010), which shows that the oocyte's developmental capacity is compromised. Another study focusing on the oocyte itself revealed differences in endoplasmic reticulum clusters, membrane potential and cortical actin thickness, offering an additional explanation to the reduced efficacy of *in vitro* cultured gametes that have already failed to mature *in vivo* after hormonal stimulation (Ferrer-Vaquer *et al.*, 2019). Additionally, only

a few case reports describe live births from ICSI of *in vitro* cultured germinal vesicle oocytes that failed to mature *in vivo* after hormonal stimulation (Nagy 1996).

It is important to clarify that the type of oocytes used in our study fall in the category of failed to mature *in vivo*/matured *in vitro* in the absence of cumulus cells. Thus, their developmental potential is expected to be compromised. The assessment of their spindle characteristics in terms of size, shape and post-translational modifications will reveal if *in vitro* culture affects the oocyte's development at the stages of spindle formation.

Ovarian hormonal stimulation results in the growth of multiple follicles leading to a heterogeneous pool of maturing oocytes. Stimulation was initially used to increase the yield of oocyte retrieval and potentially the IVF/ICSI success rates. Exogenous supraphysiologic FSH is administered daily in parallel with GnRH agonists or antagonists in order to control premature ovulation, which can occur after priming with hCG and the LH peak (ESHRE, 2019). However, adverse symptoms known as ovarian hyperstimulation syndrome manifested in patients and oocyte donors (5%). The syndrome is clinically classified in four types: mild, moderate, severe and critical. Its main pathophysiology is increased vascular permeability which can lead to fluid accumulation in third space compartments. Classical symptoms involve enlarged ovaries and abdominal distension, while severe case present thromboembolic phenomena (Claman *et al.*, 2011). The effect of hyperstimulation at

the organism level is currently under intense research. For example, no clear correlation with breast cancer has been shown apart from sporadic case studies in which the cause of the carcinoma cannot be confirmed (van den Belt-Dusebout *et al.*, 2016; Schneider *et al.*, 2017; Derks-Smeets *et al.*, 2018). Similar conclusions are drawn from a meta-analysis of data for ovarian, endometrial and cervical cancer (Siristatidis *et al.*, 2013). Regarding hyperstimulation, it is noteworthy that resulting mature oocytes would in all probability have remained dormant or have been recruited but become atretic within an unstimulated, natural, cycle.

Cryopreservation is a well established technique used for fertility preservation and oocyte donation. Evidence demonstrates that gamete freezing, either short- or long-term does not affect embryo development (Goldman *et al.*, 2015) while spindle structure is reformed within one hour of thawing (Cobo *et al.*, 2008; Bromfield *et al.*, 2009).

The human oocyte has higher levels of aneuploidy compared to other mammalian species, like ruminants and rodents (Albertini, 2014). A natural decline in oocyte quality is observed with advancing maternal age (>35 years) and correlates with genetic instability (Duncan *et al.*, 2012; Gruhn *et al.*, 2019), mitochondria deterioration and defects in cell cycle regulatory mechanisms. Furthermore, in human females, meiosis I is more error prone compared to meiosis II (Hassold and Hunt, 2001). Recent research has also shown that aged oocytes suffer from cohesion loss and centromere decompaction, leading to

incorrect kinetochore-microtubule attachments and aneuploidy (Zielinska *et al.*, 2019).

1.2) Sperm fitness

Spermatogenesis

During the fifth week of gestation, the sexually undifferentiated precursors of the germ line, called primordial germ cells (PGC), begin their migration towards the genital ridge. Their differentiation is initiated after colonization of the fetal gonads, and by 6 weeks, they reach the stage of gonocyte, and remain arrested until birth. After birth, their mitotic activity resumes and they differentiate into two types of spermatogonia: Type A and Type B. Type A spermatogonia have a developmental choice: they can either self-renew, or differentiate into Type B spermatogonia which become primed to enter meiosis and are then called spermatocytes (Fig. 2).

Throughout fetal life and until puberty, germ line meiosis appears to be inhibited by Sertoli cells (Bowles *et al.*, 2006; Feng *et al.*, 2014). At puberty, this inhibition is lifted and spermatocytes begin the process of meiosis. The organization of spermatogenesis within the seminiferous tubule is finely regulated. The diploid spermatocytes undergo the first and second meiotic divisions, thus forming the haploid spermatids. These cells accumulate in the epididymis, where they undergo spermiogenic differentiation to form spermatozoa (Bolcun-filas and Handel, 2018). The succession of all of these stages, from spermatogonia A to the spermatozoa, constitutes a cycle whose duration is approximately 42-76 days in humans.

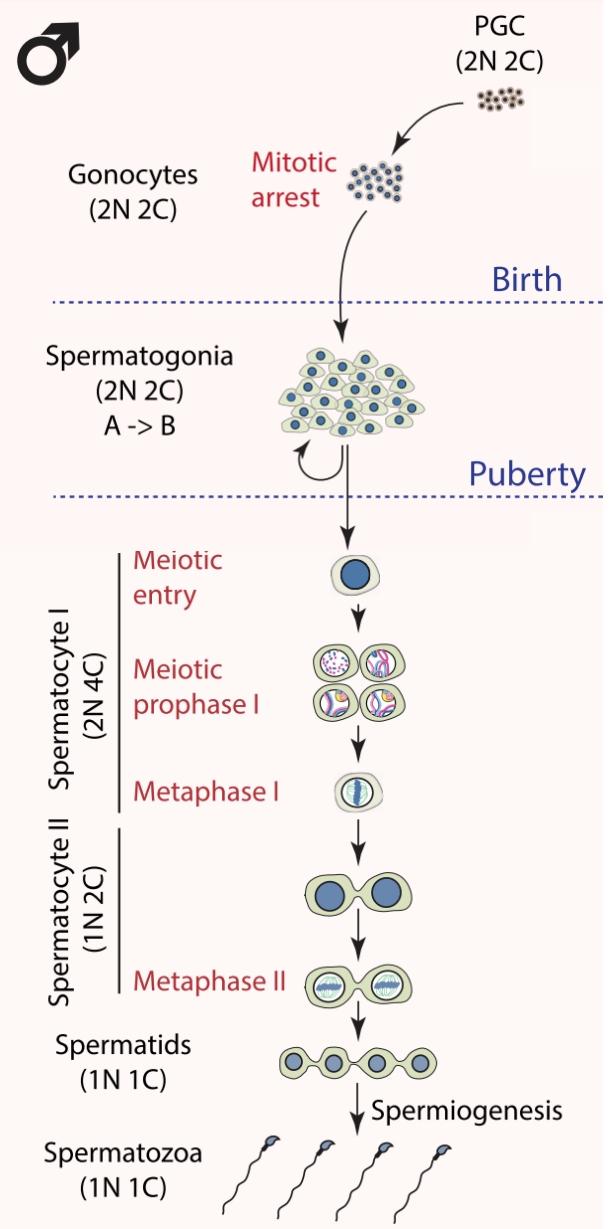

Figure 2. The process of spermatogenesis from the primordial germ cells (PGC) to spermatozoa. C value is for DNA content and N value is for the number of sets of chromosomes (ploidy). (image adapted from Bolcun-Filas and Handel, 2018)

Sperm fitness criteria

Sperm fitness is assessed based on semen volume, acidity and viscosity as well as spermatozoa number, motility and morphology. It is noteworthy that the measured parameters can vary greatly with time for the same individual (Castilla *et al.*, 2006). Sperm motility is categorized as progressive (linear or large circle movement), non-progressive (movement around itself) and immotility. Sperm morphology is evaluated based on the head, midpiece and tail characteristics. Disproportionate head size, amorphous shape, presence of vacuoles, decreased midpiece diameter, excess of residual cytoplasm and short, coiled or multiple tails are the main criteria for characterizing sperm as abnormal.

Based on the motility, the morphology and the quantity the sperm sample can be classified as normozoospermic, asthenozoospermic, teratozoospermic and oligozoospermic. The diagnosis of asthenozoospermia is made when progressive motility is less than 32% (WHO, 1999). Teratozoospermia is diagnosed when normal sperm are below 4%. In terms of spermatozoa quantity, the lower reference limits for spermatozoa concentration are $15x10^6$ cells/ml and $39x10^6$ cells per ejaculate (Cooper *et al.*, 2009). When this threshold is not reached the diagnosis is oligozoospermia.

2. Tubulin and human gametes

2.1) The tubulin family

Tubulin is the main protein constituent of microtubules, centrosomes, basal bodies and microtubule organizing centres. It consists of a superfamily formed by ten members (α through κ). α- and β- tubulin (55kDa each) form heterodimers through non-covalent bonds, polymerizing in linear polarized protofilaments which give rise to microtubules by lateral interactions (Bryan and Wilsont, 1971; Ludueńa *et al.*, 1977). The 450-residue-long peptides are 41% identical (Krauhs *et al.*, 1981; Ponstingl *et al.*, 1981). Protein conservation extends to all eukaryotic species with up to 60% homology (Wade, 2009), reaching 95% among vertebrate α- and β-tubulin genes (Sirajuddin *et al.*, 2014). The heterodimer's structure at 3.7-Å atomic resolution was first reported in 1998 by Nogales et al (Nogales *et al.*, 1998).

2.2) The multi-tubulin hypothesis

In 1976, Fulton and Simpson proposed the multi-tubulin hypothesis (Fulton and Simpson, 1976). The hypothesis states that tubulin gene diversity determines functional specification at the level of structure and interaction sites. The system complexity is established by the presence of multiple genes for each tubulin type, known as isotypes. They are found in almost all eukaryotes: animals and plants, some species of sea urchins as well as in certain protists and fungi (Wilson and Borisy, 1997). Extensive isotype characterization is available mainly for the alpha and beta tubulins (for detailed lists see (Ludueña and Banerjee, 2009)).

The multi-tubulin hypothesis is supported by several lines of evidence. Conservation of four chicken β-tubulin isotypes in humans and mouse that differ mainly in the carboxy-terminal tail. Interestingly, the fruit fly β3 isotype cannot fully replace the β2 in terms of spindle and nucleus shaping of spermatocytes (Hoyle and Raff, 1990). Furthemore, β1-isoform cannot generate axonemes in the absence of β2. Moreover, excess β1 led to axoneme abnormalities without affecting meiotic divisions and cytoplasmic microtubules of the precursor germ cells (Raff *et al.*, 2000). These observations support the hypothesis that different β-tubulin isotypes have distinct functional significance (Sullivan and Cleveland, 1986).

In the case of C. elegans, the mec-7 tubulin isotype is found only in microtubules of specific neuronal populations (touch neuron microtubules (Hamelin *et al.*, 1992)), accounting for the 15-protofilament cylinder formation structure typical of this cell type (four extra protofilaments compared to other cell types in this organism) (Savage *et al.*, 1994). Furthermore, incorporation of the moth β2 ortholog into a subset of Drosophila microtubules overrides their default protofilament number by adding three extra ones, supporting the notion that microtubule anatomy is isotype-dependent (Raff *et al.*, 1997). The same applies to the human β3 and β2B isotypes which quantitively alter lattice composition, polymerization dynamics and microtubule stability (Ti *et al.*, 2018).

The use of recombinant human β-tubulins with different isotypes, differing in their globular and carboxy-terminal domains showed the

catastrophe rate of the chimeric molecules was established by the tubulin core domain (Pamula *et al.*, 2016). Parker et al. reported that human βI and βIII isotype-specific carboxy-terminal tails differentially determine microtubule growth rate and interactions with depolymerizing protein mitotic centromere-associated kinesin (Parker *et al.*, 2018). Moreover, *in vitro* polymerization rate of unmodified α1B/βI+βIVb tubulin from an embryonic kidney cell line is faster than neuronal tubulin (which consists of different isotypes) (Vemu *et al.*, 2017). Microtubule growth and severing rates are major parameters of microtubule dynamics and are affected by tubulin genetic variability.

Conversely, multiple genes may not reflect functional differences but offer regulation platforms for the transcription machinery throughout differentiation pathways. Intra- and inter-species gene-swap experiments by various groups (in protists, yeast, fungi, chicken, mammalian cells and human cell-lines) revealed partial or complete redundancy. In these cases, expression levels and not individual role was the major determinant of microtubule fitness (Schatz *et al.*, 1986; May *et al.*, 1990; Ludueña, 1998). Furthermore, according to Kemphues *et al*, in Drosophila, spermatocyte-specific β2-tubulin has a dual function, being required for nuclear shaping as well as spindle and axoneme formation in the spermatocyte (Kemphues *et al.*, 1982). This implies functional versatility, as a single isotype can be used for different cellular stuctures in the same cell. However, the reason behind the tissue-specific expression of β2-tubulin remains to be discovered.

2.3) The human tubulin isotypes

Humans have nine isotypes for each of the α- and β-tubulins (Fig.3). (Roll-Mecak 2019).

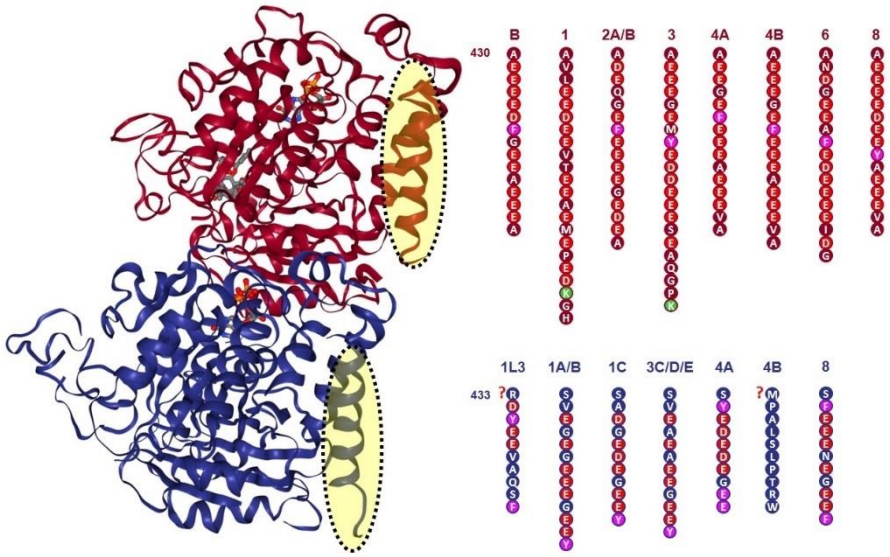

Figure 3. Tubulin heterodimer with β-tubulin shown in red and α-tubulin in blue. The sequences of the carboxytelic tails are given separately for each isotype (imaged adapted from Janke *et al* 2014).

Beta tubulin isotype expression patterns deviate in malignant cells and may correlate with treatment efficacy. For example, βIII-tubulin is differentially expressed in neuronal and non-neuronal tumors. Malignant pulmonary cells require βIII-tubulin overexpression to proliferate and survive under chemotherapeutic treatment. Clinical data demonstrate taxane resistance in breast and ovarian cancer or lung tumors impervious to paclitaxel when βIII levels are higher (D. Katsetos and Draber, 2012). Taxol resistance in ovarian epithelial

cancer is correlated with altered β-tubulin expression (Kavallaris *et al.*, 1997). Based on this, the isotype degree of expression may act as prognostic marker for treatment responsiveness in certain cancer types.

The carboxy terminal tails of soluble tubulin can block mitochondrial voltage-dependent anion channels in an isotype-specific manner. Homogeneous solutions of two types of recombinant tubulin, α1/β2 and α1/β3, differentially regulate pore permeability, severely affecting the mitochondrial energy load (Rostovtseva *et al.*, 2018). Human carboxyterminal tail sequences fused to yeast globular domain affect kinetics of human kinesin1 and kinesin2 motor proteins. The shorter βVI tail and the positively charged βIII tail decrease kinesin-1 velocity and processivity, respectively (Sirajuddin *et al.*, 2014).

A genetic screen on patients with oocyte meiosis I arrest led to the discovery of βVIII as the main isotype in primate oocytes (Feng *et al.*, 2016). Autosomal dominant mutations inherited paternally or appearing de novo may interfere with dimer assembly, stability, polymerization and interactions with motor and/or microtubule associated proteins. Affected oocytes may lack the spindle structure completely or form amorphous mesh-like spindles, as observed with polarized light and fluorescence microscopy. Over the last three years several mutations have been described accounting for phenotypes of different severity (Chen *et al.*, 2017, 2018; Wang *et al.*, 2017; Yuan *et al.*, 2018). The spindle was visible in two types of homozygous

mutations while polar body extrusion occurred in three cases with missense mutations. Exogenous expression of wild type and mutant βVIII tubulin in HeLa cells and mouse oocytes was in accordance with the mutation manifestation in the human oocytes.

2.4) Microtubule properties and polymerization cycle

Microtubules (hollow tubes with a diameter of 25nm and structural polarity) are found in the vast majority of eukaryotic cells regardless of their function, shape and developmental stage. They can be categorized as dynamic microtubules ($t_{1/2}$=5-10 min) or stable ones ($t_{1/2}$ up to hours). The tubulin chains, called protofilaments, are subsequently non-covalently combined in species- or cell-dependent numbers (11-15) leading to the formation of the microtubule lattice. In humans, microtubules have 13 protofilaments are found, although microtubules with 14 and 15 protofilaments have been observed in human blood platelets. For eukaryotes in general, the canonical microtubule consists of 13 protofilaments (Chaaban and Brouhard, 2017).

Microtubule building blocks, alpha and beta tubulin, dimerize and then polymerize in a self-assembly fashion.. Termed as dynamic instability, the phenomenon of bidirectional transition between elongation and shrinkage is mediated by GTP binding. α-tubulin maintains a GTP stable bond (N-site)(minus end) while the β-subunit facilitates the ligand hydrolysis and re-acquisition (E-site) (plus end) (Fig.4) (Alushin *et al.*, 2014; Severson *et al.*, 2016). Aside from GTP, tubulin polymerization also requires a temperature higher than 30° C

and magnesium ions (Wade, 2009). In the absence of the GTP-cap at the plus end, microtubules depolymerize. The balance between the two antagonistic reactions at a given tubulin concentration defines microtubule quantity, which fluctuates throughout a cell life cycle. Tubulin conformational cycle intrinsically modulates the growth-catastrophe rate through its GTPase activity.

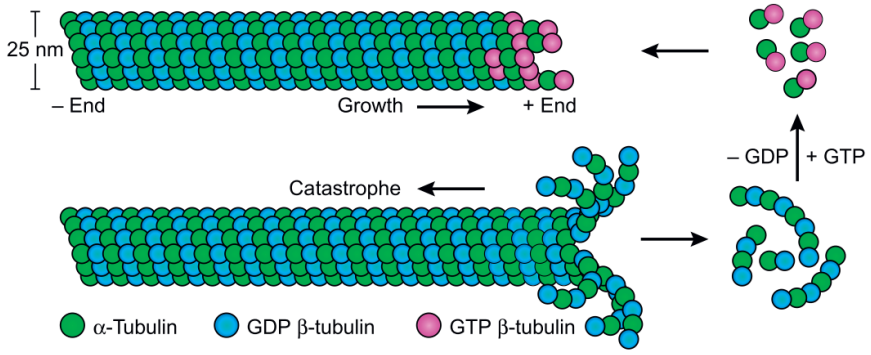

Figure 4. Microtubule dynamics (Image adapted from Severson *et al* 2016).

Microtubule dynamics regulation comes from a large variety of associated proteins including severing enzymes, whose activity localizes along the MT cylindrical surface and not the ends. Three *in vitro* MT severing enzymes are known: katanin (Mcnally and Vale, 1993), spastin (Evans *et al.*, 2005; Roll-Mecak and Vale, 2005) and fidgetin (Mukherjee *et al.*, 2012). They belong to the meiotic subfamily of AAA ATPases for depolymerization and severing. The only *in vivo* data come from overexpression of Katanin-like 1 in cells where MTs are disrupted. Paradoxically, microtubule content drops when severing activity is nullified. Research by Vemu et al demonstrated that spastin and katanin create MT cavities sealed by GTP-bound tubulins, resulting in the formation of GTP islands (Vemu *et al.*, 2018).

Microtubules main roles involve structural support, formation of cilia, propella-like movement of flagella, spindle formation and intra-cellular transport of molecules and vesicles. Tubulin mutations lead to impairments of the neuronal, muscular and reproductive system among others.

2.5) The oocyte meiotic spindle

Termed after the greek word μείωση (meiosi), meaning lessening, meiosis refers to the reductional asymmetric division of diploid cells to form haploid gametes. While it has most likely evolved from mitosis, meiosis is significantly more complex and its exact mechanisms remain among the hardest to solve (Wilkins and Holliday, 2009; Lenormand *et al.*, 2016). After germinal vesicle breakdown (dissolution of the nuclear membrane), the main meiotic stages include prophase I, metaphase I, anaphase I and telophase I followed by polar body extrusion and the second meiotic division which arrests at metaphase II until fertilization. During these steps, the meiotic spindle undergoes two cycles of assembly/disassembly.

The meiotic spindle consists of two microtubule focal points, known as poles, which consist of bundled microtubules anchored to the chromosomes centromeric regions (kinetochore MT or k-fibers) and interpolar microtubules (Maiato *et al.*, 2004). The preference of kinetochores for GTP bound MT and thus plus-ends is also demonstrated *in vitro* (Severin *et al.*, 1997). One major difference between the metazoan meiotic and the mitotic spindle is the absence

of centrioles and astral microtubules, which orientate towards the cortex side of the cell (Szollosi *et al.*, 1972; Gruss and J., 2018)
The most basic spindle characteristic is the poleward flux, "the poleward movement of MTs that is coupled to minus-end disassembly at the spindle pole"(Maddox *et al.*, 2003). The flux is responsible for chromosome migration while serving as a spindle length control mechanism (Rogers *et al.*, 2005). During metaphase the spindle length is maintained while plus-end tubulin addition and minus-end depolymerization occur at the same rate (treadmilling) (Mitchison *et al.*, 1986). The dynamics are altered at anaphase so that the k-fibers are shortened with disassembly happening at both MT ends (Mitchison and Salmon, 1992).

Abnormal chromosome distribution is naturally occurring at a rate of 10-30% in fertilized human oocytes leading either to miscarriages or genetically-caused disabilities. An important phenomenon in prophase I is that of homologous chromosome synapsis and recombination through the formation of chiasmata. Chromosomes then slide on the surface of the spindle forming end-on attachments by trial and error at the spindle equator when alignment occurs (Kitajima *et al.*, 2011). Homologous chromosomes are segregated in meiosis I while sister chromatids are segregated in meiosis II. Impaired MI segregation includes 'true' non-disjunction (paired homologues travel together to the same spindle pole), 'achiasmate' non-disjunction (failed to pair and/or recombine chromosomes travel independently towards the same pole) and premature separation of sister chromatids. Non-disjuction in meiosis II refers to failure of

sister chromatids to separate (Hassold and Hunt, 2001). A key mechanism for correct meiosis is the spindle assembly checkpoint (SAC) which delays anaphase until kinetochores are correctly bound to centromeres. Once SAC is inactivated and cohesion resolution is complete, chromosomes migrate towards the poles (Touati and Wassmann, 2016; Lane and Kauppi, 2018).

The inherent trend towards aneuploidy in oocytes can be partially explained by the large cytoplasmic volume of the oocytes, as it affects the diffusion of anaphase inhibitors and the convergence of microtubules to the poles (Kyogoku and Kitajima, 2017). Moreover, oocytes have no centrioles and therefore microtubule nucleation stabilization and organzisation is entirely controlled by the chromosomes through the small guanosine triphosphatase Ran. The process of spindle assembly is quite long (~16 h) with multipolar spindle intermediates, resulting in an inherent spindle instability which contributes to the intrinsic human oocyte aneuploidy (Holubcova *et al.*, 2015). A meta-analysis of live spindle visualization with polarized light microscopy has shown no predictive value when it comes to implantation rates and clinical pregnancy, although a correlation exists with increased fertilization and blastocyst rates (Petersen *et al.*, 2009).

2.6) The sperm flagellum

The spermatozoon consists of three parts. The sperm head, the midpiece and the flagellum. It is during the last steps of spermatogenesis (known as spermiogenesis) that remodelling occurs

to form the sperm tail of an average length of 50-60 μm in the human species. The axoneme derives from the basal body of the midpiece where mitochondria are also present. The sperm tail (flagellum) is composed by microtubules, outer dense fibers and fibrous sheaths (Fawcett, 1975). A central pair of microtubules is enclosed in nine doublets which are formed either by 13 protofilaments (A-tubule) or 10 protofilamets (B-tubule). The tail movement is mainly mediated by dynein which is a microtubule minus-end directed ATP-dependent motor (Lindemann and Lesich, 2010). The dynein structure is composed by an inner and outer arm complex which differentially interacts with the A- and B-tubules of the neighboring microtubule doublets. The forces exerted by the variations in the bond stability result in flagellum curvature (Nicastro *et al.*, 2006).

3. Tubulin post translational modifications

Soluble and polymerized alpha and beta tubulins undergo several post-translational modifications (PTM) that alter microtubule properties, converting them into mosaic structures (Fig. 5). Acetylation, detyrosination, (poly)glutamylation and (poly)glycylation are the most prevalent tubulin PTMs (McKean *et al.*, 2001). Phosphorylation, polyamination, methylation, ubiquitination, palmitoylation are also detected (Amargant *et al.*, 2018). Acetylation is the only PTM found in the lumen of microtubules while the rest appear in the outer surface of the tube. In particular, the carboxy-terminal tails of each tubulin heterodimer constitute PTM “hot spots”, located 4 nm apart longitudinally and

5nm laterally. Their negative charge and intrinsically disordered, flexible nature facilitate polymerization in cylindrical disposition (Ludueña, 2013). Proteolytic tail trimming affects interactions with motor proteins such as dynein, kinesin-1 and kinesin-2 (Roll-Mecak, 2015). Thus in addition to isotypes, PTMs introduce another level of microtubule regulation with a the dominant role of the tubulin carboxy-terminal tails, generating what is known as the tubulin code.

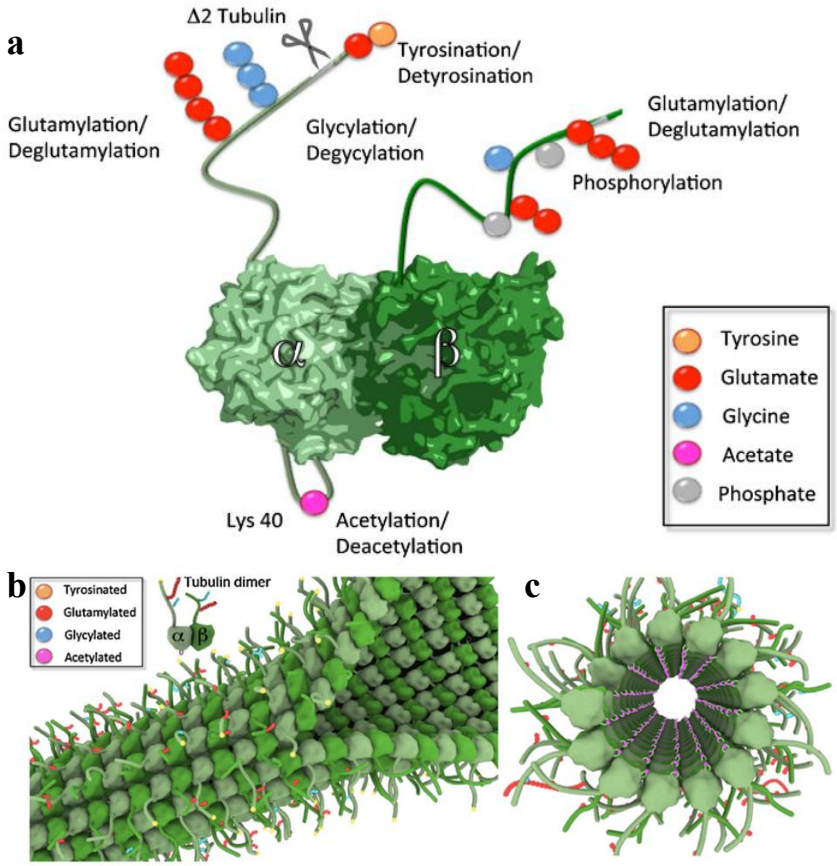

Figure 5. Tubulin post-translational modifications on the α-β tubulin heterodimer (a) and on the microtubules (b-c). (Image adapted from Roll-Mecak 2015 *Seminars in Cell and Dev Bio*)

3.1) Acetylation

Acetylation is the only modification targeted to the inner lumen of the microtubules, specifically at lysine 40 of all the alpha-tubulin isotypes (Choudhary *et al.*, 2009). It is found in long-lived microtubules, more likely at the middle or the minus-end (Song and Brady, 2015); its presence is associated with stability. The modification is conserved from protists to human and plants but not in yeast (Li and Yang, 2015). It was detected almost exclusively in flagella and not in soluble α-tubulin (L'Hernault and Rosenbaum, 1985), which led to the first characterization of acetylation biological function, the regulation of MT assembly (Maruta *et al.*, 1986; Perdiz *et al.*, 2011).

Along the phases of the cell-cycle in mouse oocytes, acetylation is found at the centrosomes in metaphase, followed by localization in the spindle during anaphase and the midbody during the telophase (Schatten *et al.*, 1988). In 1987, LeDizet and Piperno [10] identified the acetylation site as the Lysine 40 conserved ε-amino group of the N-terminal domain of α-tubulin (LeDizet and Piperno, 1987). A few years later they developed the most widely used specific monoclonal antibody (6-11B-1) for microtubule acetylation (LeDizet and Piperno, 1991). The use of cryo-electron microscopy revealed no effect of acetylation on microtubule architecture, such as protofilament distributions and microtubule helical lattice parameters, or tubulin conformation (Howes *et al.*, 2014).

Acetylation-Deacetylation enzymes

The enzymes responsible for the addition of the acetyl- group are αTAT1 (Akella *et al.*, 2010; Shida *et al.*, 2010) and NAA50, while SIRT2 (Inoue *et al.*, 2007) and HDAC6 (Hubbert, 2002) catalyze the removal of the modification. αTAT1 -/- mice lack acetylated microtubules demonstrating that this enzyme is indeed solely responsible for MT acetylation *in vivo*. The knockout phenotype involves brain and testis abnormalities without overall affecting the animal survival and fertility (Kim *et al.*, 2013). Overexpression of αTAT1 in a cell line destabilized microtubules independently of its enzymatic activity (Kalebic 2013), while RNAi inhibition had no effect on mitosis. Experiments done *in vitro* by the same researchers demonstrate that both active and inactive forms of mouse αTAT1 bind to MTs and destabilize them.

The rationale behind long-lived acetylated microtubules was the presence of the catalytic site in the filament lumen which allowed slow enzyme diffusion rate. However, recent study demonstrates that it is due to the slow catalytic rate of the αTAT1 in combination with its preference for microtubules instead of free tubulin (Kull and Sloboda, 2014; Szyk *et al.*, 2014). Acetylation of the β-tubulin subunit by NAA50 at lysine 242 is detected only in soluble heterodimers inhibiting their polymerization into microtubules (Chu *et al.*, 2011).

Overexpression of exogenous HDAC6 in mouse oocytes and zygotes, in which the enzyme is detected in the cytoplasmic area,

leads to premature chromatin condensation. The phenotype is attributed to the ubiquitin-binding property of the enzyme, which rescues the phenotype when mutated, while inhibition of the deacetylase activity maintains the overexpression phenotype (Verdel *et al.*, 2003). The presence of HDAC6 in mouse oocytes at the germinal vesicle stage has been confirmed (Zhou *et al.*, 2017). After GV breakdown and throughout the presence of the spindle, HDAC6 was detected in aggregates around the chromosomes and later on the spindle microtubules. Supplementation of the culture medium with tubastatin-A, a selective HDAC6 inhibitor, resulted to unsuccessful spindle migration and actin cap formation, thus revealing the importance of the enzyme for the completion of meiosis. On the other hand, HDAC6 inhibition has a stabilizing effect on MTs, which cannot be attributed to the increased acetylation levels (Zilberman *et al.*, 2009). Hyperacetylated tubulin found in HDAC6 KO mice supports its role as a tubulin deacetylase, however mice viability and development remains unaffected by HDAC6 absence (Zhang *et al.*, 2008). Overall, no causation can be found between MT acetylation and stability. An explanation for the observed correlation, however, lies in the substrate selectivity of the enzymes. HDAC6 binds only to soluble tubulin heterodimers, which are rapidly deacetylated. Their incorporation to newly generated MTs accounts for the deacetylated phenotype of the short-lived microtubules (Song and Brady, 2015).

SIRT2 is found in the cytoplasm, colocalizing with microtubules and occasionally with HDAC6 in an interactive manner (North *et al.*, 2003). SIRT2 inhibition in mouse oocytes caused spindle defects and

disorganized chromosome distribution with affected MT-kinetochore attachments, while overexpression of the enzyme compensated for meiotic defects in aged mouse oocytes (Zhang *et al.*, 2014). This finding was further supported by Qiu et al (Qiu *et al.*, 2017), who showed that the crucial Sirt2-deacetylated-substrate responsible for the age-related defects is BubR1 and not microtubules. SIRT2 is found in the spindle of mitotic cells, where acetylation is also detected. Nagai et al proposed a mechanism of SIRT2 inhibition by Furry in order to explain the simultaneous presence of acetylation and the deacetylase (Nagai *et al.*, 2013).

3.2) Detyrosination-Tyrosination cycle

Tyrosination refers to the addition of tyrosine as the last residue of the carboxy-terminus of α-tubulin which is primarily genomically encoded (TUBA4 and TUBA8 are the only exceptions) (Barra *et al.*, 1973). Cycles of detyrosination and ribosome independent tyrosination alter the tubulin tail and thus the microtubule characteristics. Detyrosinated MTs undergo slower turnover *in vivo*, hence the correlation of microtubule detyrosinated profile with microtubule longevity (Webster *et al.*, 1987). However, it should not be implied that detyrosination itself increases the microtubule intrinsic stability (Khawaja, 1988; Song and Brady, 2015). Tyrosination is indispensable for survival, as TTL knockout mice develop only until the perinatal stage due to neuronal defects (Erck *et al.*, 2005). Tyrosination and detyrosination coexist *in vivo* on

interphase and mitotic microtubules in a spatially-dependent manner (Gundersen *et al.*, 1984).

Metaphase II spindles in mouse oocytes contain acetylated and tyrosinated MT but detyrosination is not detected. Upon fertilization detyrosinated MT appear in the midbody, together with acetylation and tyrosination (de Pennart *et al.*, 1988). The importance of this modification in meiosis is demonstrated by the finding that CENP-E dependent transport of polar chromosomes towards the spindle equator is favoured by detyrosinated MT tracks (Barisic *et al.*, 2015). Increased tyrosination of the cortex side hemisphere of the metaphase I spindle in mouse oocytes is induced by GTPase cdc42 signaling. The resulting tyrosination gradient mediates the meiotic drive by altering the microtubule affinity to the selfish centromeres (Akera *et al.*, 2017).

Regarding interactions with other factors, kinesin-13 family members depolymerize MTs with tyrosine in the C-terminal tail (Peris *et al.*, 2009), a modification also required for the binding of CAP-Gly (cytoskeleton-associated protein Gly-rich) domain proteins, a subgroup of +TIPs (Peris *et al.*, 2006). On the contrary, kinesin-1 (KIF5) binding and motor activity is shown to be regulated by detyrosination (Kreitzer *et al.*, 1999; Dunn *et al.*, 2008).

Detyrosination-Tyrosination enzymes

The first PTM enzyme to be discovered was tubulin tyrosine ligase (TTL), the enzyme responsible for the addition of tyrosine (Hallak *et*

al., 1977). The substrate of TTL is not the polymerized protofilament, but rather the soluble heterodimer composed of α- and β-tubulin (Raybin and Flavin, 1977). The enzyme full sequence was deposited several years after its discovery (Ersfeld *et al.*, 1993). Two enzymes for the reverse reaction, vasohibins 1 and 2, were recently characterized as tyrosine carboxypeptidases by two independent groups (Aillaud *et al.*, 2017; Nieuwenhuis *et al.*, 2017).

TTL overexpression or RNA interference result in chromosomes retained at the spindle poles or performing random movements, respectively (Barisic and Maiato, 2016). This is in line with the observation that TTL overexpression inhibits MT polymerization (Szyk *et al.*, 2011).

3.3) Δ2-tubulin

Microtubules of mammalian cells and sea urchin flagella and cilia can be excluded from the tyrosination cycle after removal of the penultimate glutamate of the α-tubulin tail. This modification is irreversible and is known as Δ2-tubulin (Paturle-Lafanechere *et al.*, 1991; Mary *et al.*, 1996). Δ2-tubulin is most abundant in brain microtubules. To date it was found to occur during the first stages of neuronal differentiation of the rat cerebellum (Paturle-Lafanechère *et al.*, 1994).

Δ2-tubulin enzymes

The enzymes responsible for the removal of the glutamate exposed after detyrosination of the α-tubulin tail belong to the cytosolic carboxypeptidase family (CCP), which is composed of six members (Kalinina *et al.*, 2007; Rodriguez De La Vega *et al.*, 2007). CCP1, CCP4 and CCP6 are capable of catalyzing the formation of Δ2-tubulin (Rogowski *et al.*, 2010). CCP1 has been extensively studied as the lack of functional protein causes the pcd mouse phenotype (Purkinje cell degeneration). *In vitro* experiments with purified porcine brain tubulin and polymerized HEK293T microtubules are marked by an increase in Δ2-tubulin after addition of CCP1. *In vivo* overexpression and knock down assays in HEK293T cells modify Δ2-tubulin levels up to 5-fold (Berezniuk *et al.*, 2012).

3.4) Glutamylation- Glycylation

The addition of glutamic acid or glycine residues (from 1 to more than 20) can occur in glutamates of both α- and β-tubulin C-terminal tails. Polyglutamylation was first reported by Eddé et al in brain tubulin (Edde *et al.*, 1990). It is found in protists, plants and animals (Ludueña, 2013). While glycylation is mostly found in stable microtubules (axonemes and cilia) (Redeker *et al.*, 1994; Iftode *et al.*, 2000), glutamylation is not associated with microtubule stability. The glutamylated tubulin tails may differentially bind to microtubule associated proteins (MAP), thus creating a regulatory mechanism for MAP interactions (Bonnet *et al.*, 2001). In spermatozoa, differential pattern of glutamylation is detected between the middle and the

terminal piece in the peripheral and central doublets (Prigent *et al.*, 1996). The importance of microtubule glutamylation for motility is demonstrated through its interaction with the dynein arm (Kubo *et al.*, 2010, 2012).Throughout mitotic phases, glutamylated tubulin levels increase in polar and kinetochore microtubules but not in astral ones (Bobinnec *et al.*, 1998).

TTLL and CCP family enzymes

The tubulin tyrosine ligase-like (TTLL) family consists of 13 members that were discovered in three different organisms: mouse, *Tetrahymena thermophila* and zebrafish (Regnard *et al.*, 2003; Janke *et al.*, 2005; Pathak *et al.*, 2007). Their name derives from their structural similarity to the TTL domain (van Dijk *et al.*, 2007). TTLL members may have differential affinity for alpha or beta tubulin subunits, acting either independently or as part of a multi-protein complex (Janke *et al.*, 2005). TTLL7 is the most abundantly transcribed member of the family, mostly in the nervous system. Its affinity for β-tubulin was first observed when the enzyme was exogenously expressed in HEK293T cells (Ikegami *et al.*, 2006). The glutamylases TTLL4 and TTLL5 catalyze the addition of the branching glutamate which subsequently forms the substrate for the elongating glutamylases. TTLL4, 5, 6, 7, 11 and 13 can act individually while the activity of TTLL1, 2 and 9 is dependent on other proteins (Janke *et al.*, 2005; van Dijk *et al.*, 2007). TTLL10 is the enzyme responsible for tubulin polyglycylation, which is absent in humans due to a deleterious mutation (Rogowski *et al.*, 2009). Thus, only monoglycylated MTs are found in humans, catalyzed by

TTLL3 and TTLL8. The enzymes catalyzing the removal of glutamic residues are the cytosolic carboxypeptidases (CCPs) consisting of six members, while the ones for glycine removal have not yet been discovered.

4. Oocyte translational regulation

Oocyte maturation is a transcriptionally silent biological process (De La Fuente *et al.*, 2004). Most of the mRNA molecules that are necessary for the meiotic divisions are already present and translated, while another mRNA population remains inactive until embryo cleavage prior to embryonic genome activation. This system's dynamics demands accurate translational regulation, defining which mRNA molecules should be translated at the required levels at the precise time. A major regulatory hotspot for mRNA translation is the 3′ untranslated region (3′- UTR). In particular, the cytoplasmic-polyadenylation-element binding protein (CPEB) plays a central role in mRNA translation regulation throughout vertebrate oocyte maturation and early development. Its effect is manifested through interaction with the cytoplasmic polyadenylation element (CPE), a uridine-rich sequence (Gebauer and Hentze, 2004). This interaction can result in mRNA silencing prior to maturation or trigger cytoplasmic polyadenylation and translational activation upon resumption of meiosis. Pique et al have synthesized a translation prediction code based on CPE presence and configuration, initially studied in *Xenopus laevis* oocytes and verified for mammalian genes as well (Fig. 6) (Piqué *et al.*, 2008).

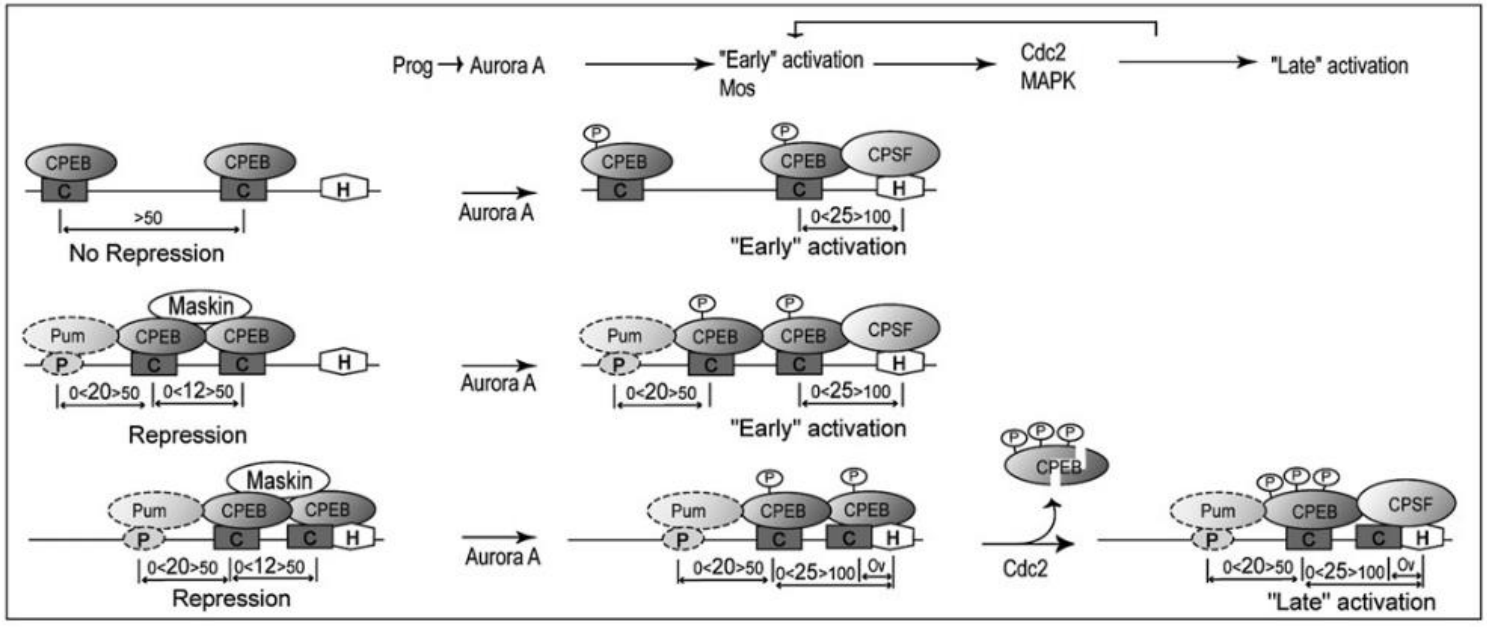

Figure 6. Schematic representation of the cis elements and trans-acting factors recruited, with their covalent modifications. The distances required to mediate translational repression and activation as well as the time of activation are indicated. Optional factors/elements are displayed with dotted lines. Pum: Pumilio, P: pumilio binding sequence, CPEB: cytoplasmic polyadenylation element binding protein, H: hexamer (polyadenylation signal), p: phosphoryl group, CPSF: cytoplasmic polyadenylation signal factor, Prog: progesterone (image from Pique et al 2008).

Overall, the thesis focuses on human gametes (both oocytes and spermatozoa) and the tubulin post translational modifications in addition to their enzymes. Previous characterization of tubulin PTM in human and animal somatic and mitotic cells has produced the existing body of knowledge regarding the role of PTM for microtubule properties and function within fully differentiated or dividing cells. Nevertheless, apart from some animal model studies (mice and sheep), no studies investigated the role of PTM in oocyte meiosis or the human flagellum. Adding some clinical value, no data exist regarding PTM presence in *in vivo* matured and *in vitro* cultured oocytes, as well as in sperm samples of different diagnosis.

5. Objectives

- Characterize MII spindle tubulin PTM of *in vivo* matured human oocytes in comparison to their *in vitro* cultured counterparts
- Determine the comparative transcript profiles of tubulin PTM enzymes in immature human oocytes, matured *in vivo*, cultured *in vitro* and failed to mature
- Determing whether the detected PTM enzyme transcripts are translated during maturation
- Characterize PTM pattern along the human sperm flagellum and correlate with motility pathologies

MATERIALS AND METHODS

MATERIALS AND METHODS

1.Ethical approvals

Approval to conduct these studies was obtained from the local Ethical Committee for Clinical Research. All procedures performed were in accordance with the ethical standards of the institutional research committees and with the 1964 Helsinki declaration of the Ethical principles for medical research involving human subjects, as revised in 2013 in Fortaleza (World Medical Association, 2013). Written informed consents to participate were obtained from all participants prior to their inclusions in the studies.

2. Oocyte collection and culture

Oocytes were retrieved from donors who underwent hormonal stimulation cycles. The cumulus oophorus was removed by hyaluronidase treatment which allows for morphological evaluation of the meiotic stage of the oocyte. For calculating duration of oocyte *in vitro* culture, time zero was set at oocyte retrieval from the ovary until the end point of metaphase II spindle formation. Oocytes at the GV stage were cultured for 33 hours in G2 PLUS medium .

2.1) Microscopy

Time-lapse microscopy (PrimoVision system) was used to accurately determine the timepoint of polar body for the specific sample type under the established culture conditions. The Oosight system was employed for oocyte live imaging to confirm the presence of the metaphase II spindle.

3. DNA-RNA molecular techniques

3.1) genomic and complementary DNA preparation

Genomic DNA was isolated from HEK293T cells through size exclusion column chromatography (QIAGEN, DNeasy Blood and Tissue kit). HEK293T cells ($2,5x10^6$) and BeWo cells (10^6) underwent guanidine-isothiocyanate lysis and RNA was recovered through silica-membrane purification (QIAGEN RNeasy Mini Kit, Cat No. 74106). cDNA was produced from HEK293T cell , BeWo cell, fetal brain (TaKaRa, Cat No. 636526) and testis (TaKaRa, Cat No. 636533) total RNA with the Invitrogen™ Cloned AMV First-Strand cDNA Synthesis Kit (Cat No. 12328032), as per manufacturer's instructions.

3.2) phusion polymerase PCR

MicroAmp™ 8-Tube Strip 0.2ml tubes were used for all PCR experiments with the Phusion High-Fidelity DNA Polymerase (2 U/μL, ThermoFisher, Cat No. F530L). Reactions were performed in a thermal cycler with the final volumes set at 20 μl or 50 μl. Reagents were prepared in a "master mix" solution which allowed for finalizing the 5X Phusion HF Buffer concentration to 1X upon separate addition of template. PCR amplicons were visualized by agarose gel between 1% to 1.5% depending on their size, stained with SYBR™ Safe DNA Gel Stain (Invitrogen, Cat No. S33102) alongside the GeneRuler 100 bp Plus DNA Ladder (Thermo Scientific, Cat No. SM0321).

3.3) single cell cDNA libraries

Individual oocytes from each group were subjected to pronase treatment (40 mg/ml, 1:20 for 3 min, 37 °C) for the dissolution of the zona pellucida. Subsequent incubation of each oocyte at 65 °C for 15 min in lysis buffer (20 mM DTT, 10 mM Tris.HCl pH 7.4, 0.5% SDS, 0.5µg/µl proteinase K) was followed by storage at -80 °C until further processing.

Total RNA isolation using magnetic beads, cDNA synthesis, library preparation and 24-cycle-amplification by random hexamer priming were performed according to the described protocol by Gonzalez-Roca et al 2010, followed by a cDNA purification step (PureLink Quick PCR Purification Kit, Invitrogen) (Gonzalez-Roca *et al.*, 2010).

3.4) quantitative PCR

qPCR reactions were performed with the SsoAdvanced™ Universal SYBR® Green Supermix (Bio-Rad, Cat No. 1725271) in the Bio-Rad CFX96 C1000 Touch thermal cycler system following the steps: 95 °C (30 sec), [95 °C (5 sec)- 60 °C (30 sec)]x40, 65 °C (5 min), 95 °C (5 min).

Sequences of the selected post translational modification enzymes´ primers are listed in Table 1.

3.5) DNA purification and Sanger sequencing

PCR products were purified through silica spin columns (QIAquick Gel Extraction t, Cat No. 28706). Sequencing was performed with the Sanger method.

PRIMER SEQUENCES

GENE	FORWARD(5´-3´)	REVERSE(5´-3´)	SIZE (bp)	E (%)	R^2
αTAT1	GGCGAGAACTCTTCCAGTAT	TTGTTCACCTGTGGGACT	139	101,5	>0,99
HDAC6	TTGCCAGTGGCCGCATTATC	CGCCAGTATCTGCGATGGAC	190	92,9	>0,99
SIRT2	CTGAAGGACAAGGGGCTACTC	CAGCTTAGCGGGTATTCGTG	161	98,4	>0,99
TTL	GCACCAAGCACCTCCCTTAC	GATGCCTTGGCACAGTTCTG	143	97,7	>0,99
TTLL1	GCCACCTAAGGAAGTCCTCG	TCTCCCCGAGTCTCTCGATC	142	96,3	>0,99
TTLL2	GGACCTGTGTTCCTCCACAC	TGCTTCCTGTAGCCTTGCTC	139	88	>0,99
TTLL3	GCTGATTGAGATCAACGCCAG	GCCCACATATTGAGGCACC	187	91,9	>0,99
TTLL4	GACGGTCCCACTTCAAAATC	CTGCATACGTGACAGGTTCC	176	98,4	>0,99
TTLL5	CGACCCATCATCAGTCCTAG	TAGCCTGGCTGTACACGTTG	154	97,8	0,989
TTLL6	CAATGAGAATTGGCACCCCAAC	CTCCATATCTGCTCCACGTTG	142	92	0,984
TTLL7	TTCCACGCATCTGGAAGGTG	CCACCTCCGGGCTTTTATTG	165	117,2	>0,99
TTLL9	GTAGGCTGAAGGACATCGTG	ATCACCAGCACATAGACACG	160	103,3	0,97
TTLL10	GTTTGACGTGCGCTCCTAC	GGGCTCTTCTTCTGCATGAAC	156	108,7	0,985
TTLL11	ACTTCTACCCTCGCTCATGG	CCTGACAACCACCATCAGGTT	129	102,4	>0,99
TTLL12	ACTTTGCCTACGGAGAGACG	ACGGGGTTGATGTCAAGTGG	169	101,3	>0,99
CCP1	GCAGTGAAGCGTTTACCCT	GCTGGGGCGATATGGCTC	188	108,3	0,989
CCP2	ACGTCTTCGAGAACCCCAAG	ATATTCTGGTTGAGGTGGAGC	139	95,8	>0,99
CCP3	ATCAGCTAGGGAGATGGGTG	AAAGGGGTTCCGTTTCTAAGC	195	91,9	0,986
CCP5	AGCTTTCCTTTTCATGGCAGTC	ACTAGTAGGAGCTGGGGATGG	183	94,5	0,985
CCP6	GACTCCTGGACCACACTTCC	CACGGGGTTCAGCCGATAAT	164	92,5	>0,99

Table 1. Primer sequences for qPCR amplification of PTM enzyme genes

PRIMER SEQUENCES

GENE	FORWARD (5´-3´)	REVERSE (5´-3´)	SIZE (bp)
aTAT1_204/206	gcata/GTTAAC/CCGCAG CCCCGTCAAACATC	gacct/GGATCC/TCTTGTGATAA AAATAAATACTTTTATTG	180
TTLL11_206tst1	ttatc/GTTAAC/CCCCTCC TGGAAGCCCAC	tccgg/GGATCC/TTTAATGAGGT AGATTCCATCACCCTGAC	73
CCP1_201tst2	ttcaa/AGATCT/GCCCGC TGCCATCTCTTG	gttag/GGATCC/TTTATTATCTTG AAACCAAACTGGCCC	147
CCP5_202	tgtcc/AGATCT/GCCTTTA TGTTCAAGCCCAGG	caagt/GGATCC/GATTTTTCCAA ACAACTTTTATTTCCTCAGAG	353
CCP6_204tst1	gcatg/GTTAAC/ACGGAG TCCTGGGAGGTCTTAT	ctacg/GGATCC/TTTAATTAAAC TACCGAGGAAATTGGG	642

Table 2. Primer sequences for PCR amplification of PTM enzyme alternative polyadenylation and splice variants that are detected in human oocytes. Lowercase letter are random nucleotides followed by the restriction enzyme sites used for subcloning to the luciferase vector.

3.6) statistical analysis

SPSS software was used for statistical analysis. For the comparison of the spindle morphometric parameters, non-parametric Kruskal–Wallis test was performed to compare continuous not-normally distributed values. For spindle pole distribution comparison was made according to Fisher test of exact count data. Transcript levels were compared according to the non-parametric Mann Whitney test. Luciferase UTR induced expression levels were compared with applying chi-square test. For all tests the level of significance was set at $p \leq 0.05$.

4. Molecular cloning

4.1) pJET

Ligation in the pJET1.2/blunt cloning vector was performed according to the manufacturer´s protocol (CloneJET PCR Cloning Kit, ThermoFisher, Cat No. K1231).

4.2) LUCassette constructs

The LUCassette (T7-luciferase-PTME_3´UTR) constructs were synthesized with PCR-based cloning. Primers were designed so that the 3´UTR of interest maintained its CPE sequences and the polyA signal, whose presence was verified with sequencing (primer sequences are found on Table 2.

4.3) Bacteria transformation

Transformation of One Shot™ TOP10 Chemically Competent *E.coli* cells (ThermoFisher, Cat No. 404010) was carried out with the following steps: incubation at 4 °C for 30min- heat shock at 42 °C for 45sec, 4 °C for 5min, LB addition and culture at 37 °C for 1h. Cells were subsequently spread on ampicillin-containing (100μg/ml) agar plates at three serial dilutions and placed at 37 °C O/N. Individual colonies were added in 3ml ampicillin-containing LB and bacteria were left to grow at 37 °C O/N. Their plasmid DNA was isolated with the QIAprep Spin Miniprep Kit (Cat No. 27106) as instructed by the accompanying protocol.

5. Immunocytochemistry (ICC)

5.1) Oocyte

Oocyte fixation was carried out in 4% w/v Pierce™ methanol-free formaldehyde (ThermoFisher, Cat No. 28906) in PBS and stored for a maximim of one month in 0.1% Tween20 PBS until ICH was performed. Permeabilization in 0.2 % TritonX-100 PBS lasted for 15 min with a subsequent 1-hour-incubation at room temperature in 0.2 % Tween20 2% BSA FBS PBS for blocking unspecific binding. All primary (1^o) and secondary (2^o) antibodies used are listed in Table 3, alongside the respective dilutions and incubation conditions. Incubation with the primary antibody for tubulin PTM preceded that of α- or β-tubulin unless mentioned otherwise in the results section. Primary antibodies were diluted in the blocking solution while secondary ones in 0.2 % Tween20 2% BSA PBS. Three to six 10-

min washing rounds were performed after each antibody incubation. DNA was stained by adding Hoechst dye (1:200) in the secondary antibody solution. The ZEISS confocal microscope LSM780 was used for image acquisition of samples either mounted in Vectashield or placed in a PBS droplet. Mounted samples with coverslips No 1 (0.13-0.16 mm) were visualized with the 63X glycerol plan-neofluar objective (80% glycerol as immersion liquid), while the 40X water c-apochromat objective was used for the free-in-droplet ones, adjusted for coverslip No 1.5 (0.17 mm). Images were analysed with FIJI software (version 2.0.0-rc-69/1.52i).

						INCUBATION CONDITIONS		
	ANTIBODIES	**HOST**	**CLONE**	**COMPANY**	**CAT No.**	**DILUTION**	**TEMPERATURE**	**DURATION (hours)**
1°	anti-α-tubulin	mouse	DM1A	Sigma-Aldrich	T6199	1:200	RT	2
	anti-β-tubulin	rabbit	polyclonal	abcam	ab6046	1:200	RT	2
	anti-acetylated tubulin	mouse	6-11B-1	Sigma-Aldrich	T7451	1:500	RT	2
	anti-Δ2-tubulin	rabbit	polyclonal	Millipore	AB3203	1:500	RT	2
	anti-tyrosinated tubulin	rat	YL1/2	Chemicon	MAB1864	1:500	RT	2
	anti-detyrosinated tubulin	rabbit	polyclonal	Millipore	AB3201	1:200	RT	2
	anti-polyglutamylated tubulin	mouse	GT335	AdipoGen	AG-20B-000B	1:500	RT	2
	anti-polyglutamylated tubulin	mouse	B3	Sigma-Aldrich	T9822	1:200	RT	2
2°	anti-mouse Alexa fluorophore 488	goat	polyclonal	ThermoFisher	A-11029	1:500	RT	1
	anti-rabbit Alexa fluorophore 488	goat	polyclonal	ThermoFisher	A-11008	1:500	RT	1
	anti-rat Alexa fluorophore 488	goat	polyclonal	ThermoFisher	A-11006	1:500	RT	1
	anti-mouse Alexa fluorophore 568	goat	polyclonal	ThermoFisher	A-10037	1:500	RT	1
	anti-rabbit Alexa fluorophore 568	goat	polyclonal	ThermoFisher	A-11036	1:500	RT	1

Table 3. Primary and secondary antibodies used for immunofluorescence experiments

5.2) Sperm

Circular coverslips with 12mm diameter were prepared by applying 100-150 µl of poly poly-L-lysine solution 0,1%w/v (in H_2O) [P(8920) SIGMA] and incubating for 40 min, followed by 3 washes of 10 min each. In the meantime, the frozen straws content was emptied in 1ml of PBS so as to dilute the cryopreservation agent for 5 min at 37 ºC. Three washing steps of 10 min in PBS were performed by centrifuging at 400g. Dilutions were prepared so as to adjust the final cell concentration at around 1500-3000 cells, out of which 30 µl were added on the coverslip leaving it for 40min to 1h to dry. Fixation was performed with PFA 4% for 1h at RT. After 3 x 10min washes, membrane permeabilization was performed with PBS 0,5 % Triton 100X for 15 min at RT. 5% BSA in PBS 1X was added for 1 h to block the unspecific binding sites, followed by 3 x 10min washes. The primary antibodies for tubulin modification and tubulin were diluted in 5% BSA in PBS 1 X and incubation lasted 1h at RT. Primary antibody dilutions were the following: acetylation (mouse, T7451) 1:1000, monoglycylation (mouse, MABS277) 1:200, GT335 (mouse, AG-20B-000B) 1:200, polyglutamylation (homemade) 1:200, α-tubulin clone DM1A (mouse, T6199) 1:1000, β-tubulin (rabbit, ab6046) 1:200. After 3 x 10min washes the secondary antibodies were also diluted in 5% BSA in PBS 1 X and incubation lasted 1h at RT. Primary antibody dilutions were the following: anti-mouse 488 (A-11029) 1:1000, anti-mouse 568 (A-10037) 1:1000, anti-rabbit 488 (A-11008) 1:100 and anti-rabbit 568 (A-11036) 1:1000. Finally, after 3 x 10min washes, the samples are mounted on

microscope slides with one drop of Fluorsave (CalBiochem, Cat No #345789).

Image acquisition was performed with a DMI-600 Leica wide-field fluorescent microscope (63X objective) and FIJI software (version 2.0.0-rc-69/1.52i) was used for the analysis. As tubulin was used for signal normalization, the final value corresponding to each point is the following ratio:

$(PTM_{tail}–PTM_{background})/(tubulin_{tail} – tubulin_{background})$

Applying the *Plot profile* command, the maximum intensity resolution is 0.1 μm. As each tail has different length, each tail was standardized to 1000 units and a mathematical equation of linear regression was applied to obtain an intensity value in every unit.

6. Luciferase assay

The circular plasmids with the luciferase coding region and the 3´UTR of cyclinB or the one of interest (TTLL11, CCP1, CCP5 and CCP6) were linearized with BamHI-HF while the restriction enzyme Ecl136II was used for the plasmid with the Renilla coding sequence for an incubation of 2h at 37 ºC. The reactions were terminated by the addition of 0,5M EDTA (1/20 vol.), 3M Na acetate (1/10 vol.) and EtOH (2 vol.) and 15 min incubation at -20 ºC. Removal of supernatant and resuspension in RNase free water was performed. *In vitro* transcription of 1μg of each linearized plasmid was performed for 2h using the mMessage RNA kit (AM1348) and subsequently purified with the MEGAclear kit (AM1908), eluted in 50 μl of elution solution, according to the manufacturer's protocols. The RNA

concentration was then brought to 100 ng/µl which is checked in a formaldehyde agarose gel (for 100 ml: 72 ml nuclease free water, 2g agarose, 10 ml MOPS 10X and 18 ml formaldehyde). For 500ml MOPS 10X, we mixed 20.93 g MOPS (200 mM), 4.1g sodium acetate (100 mM) and 10 ml EDTA 0.5M (10 mM) in distilled water and then adjusted to ph=7 with NaOH 10M. The gel was run at 130V for 15min prior to which the solution to be loaded was heated to 70 ºC for 5min and then placed in ice. Each luciferase RNA was mixed with an equal volume of Renilla RNA and water (which brought each RNA concentration at ≈33 ng/µl). A final dilution 1/66 (≈ 0,5 ng/µl) was performed on the day of injection in Xenopus eggs.

After harvesting the ovaries from the animals, the eggs at stage VI were separated and handled in 1X MBS buffer after addition of 280 µl of 2.5M $CaCl_2$ for every liter of buffer (40 oocytes per RNA mix). Using the microinjection system, we set the injected volume at 27 nl. For each RNA mix, 20 oocytes were left untreated and the other 20 were treated with progesterone for the induction of maturation within 4 hours (5µl 1000X in 5 ml of buffer). We selected 10 oocytes from each group and stored at -80 ºC. We continued with the Promega Dual-Luciferase™ Reporter (DLR™) Assay Systems protocol. The data were presented as a percentage of expression in reference to the cyclinB fold induction (positive control).

RESULTS

RESULTS

Chapter 1. Spindle PTM profile in cultured oocytes is similar to *in vivo* matured oocytes

Human oocytes matured *in vivo* and *in vitro* maintain similar spindle shape and size according to the literature (Combelles *et al.*, 2002; Coticchio *et al.*, 2013b). However, to the best of our knowledge, no characterization of the human oocyte spindle microtubule PTM profile and dynamics have been published to date. We conducted tubulin PTM characterization in the metaphase II meiotic spindle of fixed human oocytes using fluorescent-antibody staining. The modifications we examined were acetylation, detyrosination/ tyrosination, Δ2-tubulin and (poly)glutamylation. Our results showed the presence of tubulin PTM in human metaphase II spindles of oocytes matured *in vivo*. In addition, we expanded the analysis with a comparison of *in vivo* matured oocytes with their GV derived *in vitro* counterparts.

1.1) GVs reach metaphase II stage within 25-30h of *in vitro* culture

We first determined the optimal time of *in vitro* culture required for the GVs retrieved from hormonally stimulated donors to reach the MII stage of maturation, as defined by the time required for first polar body extrusion and spindle formation, determined by time-lapse and polarized light microscopy, respectively.

A total number of 45 GVs were cultured *in vitro* and videotaped in the PrimoVision incubator. The overall efficiency of maturation in culture was 44,4%, with 20/45 oocytes achieving first polar body extrusion at some point during the culture period. As shown in Fig 7., 40% of the mature oocytes (8/20) extruded a polar body between 21-23 hours. Another 20% (4/20) completed the first meiotic division between 23-25 hours while an equal number of GV required more than 25 hours. A polar body was visible for the remaining 20% at approximately 21 hours. In order to maximize the sample size, considering the limited availability of human GV oocytes, the duration of the *in vitro* culture was set at 30-33 hours. This time frame also allowed for progression to the metaphase II stage, which was confirmed by polarized light microscopy. We observed that only a percentage of the oocytes that extruded a polar body accomplished spindle assembly. After staining, spindles were categorized based on their microtubule configuration in the following groups: no metaphase plate, apolar and no microtubules.

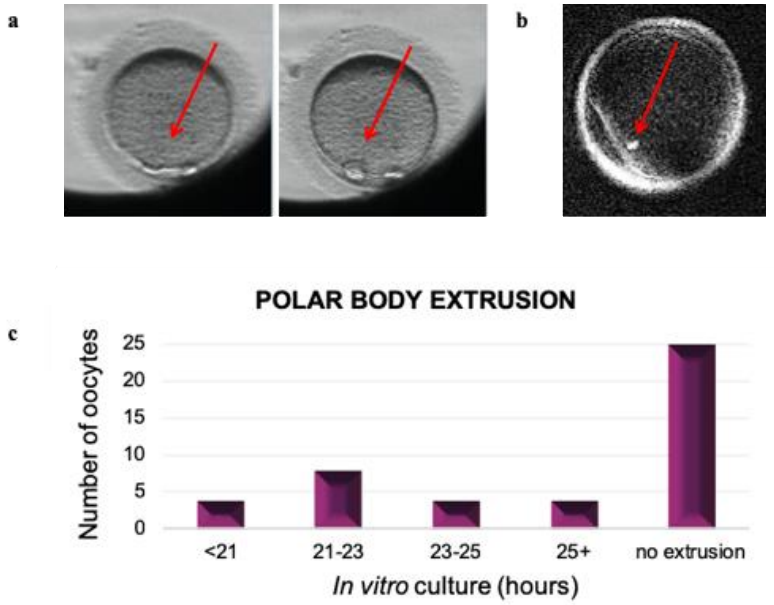

Figure 7. **a)** Time lapse oocyte microscopy for observing first polar body extrusion (red arrow). **b)** Metaphase II spindle structure as observed by polarized light microscopy (red arrow). **c)** *In vitro* culture duration in hours until first polar body extrusion among 45 oocytes.

1.2) Acetylated microtubule islands are present in metaphase II meiotic spindles

Microtubule acetylation was detected in metaphase II spindles of GV-derived oocytes (n=10). Two different staining protocols were used. One group of oocytes (n=7) was treated with pronase prior to fixation and permeabilization was performed after fixation (Fig. 8). For the second group, the zona pellucida (n=3) was kept intact, permeabilizing the oocytes shortly before fixation (Fig.9) which resulted in a lower antibody background signal. In both protocols, incubation with anti-tubulin antibody was followed by an incubation

with the anti-acetylation antibody. The PTM pattern observed was consistent following both methods.

We detected signal was symmetrical between the spindle hemispheres in terms of intensity. Along individual microtubule bundles, the signal was not continuous, suggesting the presence of acetylation islands. Inter-group comparison reveals differences in the distribution of acetylation, with cases of a uniform signal dispersion or higher concentration around the poles (Fig. 8). *In vivo* matured oocytes (n=5) had regions of acetylated spindle microtubules which were mainly found at the poles (Fig. 10). Quantitative comparison between spindles was impossible due to differences in exposure settings due to signal background variability. Chromosomes on the metaphase II plate were aligned in 4 out of the 15 spindles, with one or more misaligned chromatids in the rest. 3D reconstruction revealed the expected "homocentric rings" configuration in the equatorial transverse section of the spindle. Morphometric data of the DNA mass did not reveal any differences between the two groups, implying functional condensation mechanisms are occurring normally during *in vitro* culture. For a complete analysis, kinetochore staining would allow enumeration of chromosomes and greater detail in alignment evaluation.

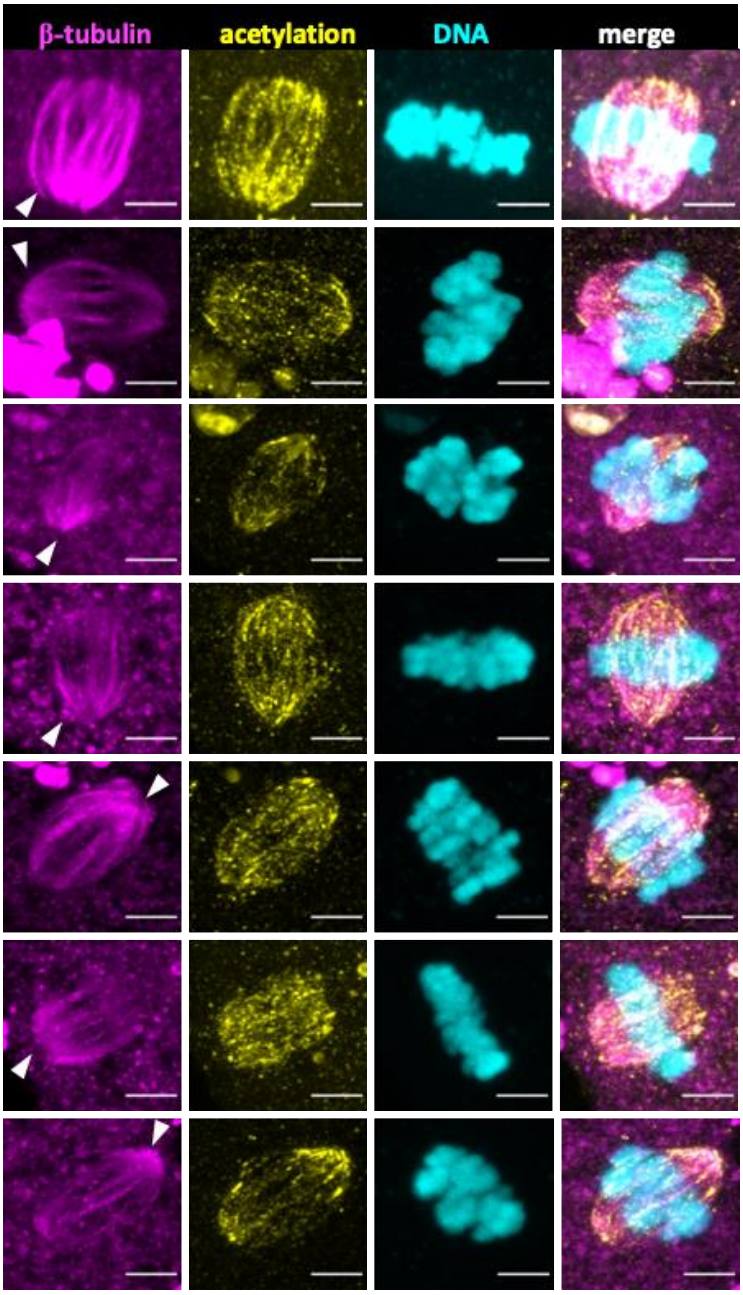

Figure 8. Acetylated microtubule islands are present in metaphase II meiotic spindles of *in vitro* cultured GV derived oocytes, stained for tubulin (magenta), tubulin acetylation (yellow) and DNA (cyan, Hoechst dye) after zona pellucida removal and post fixation permeabilization (n=7). White arrows point the cortex pole, each row corresponds to individual oocytes of the same of different donor origin. Scale bar 5 μm

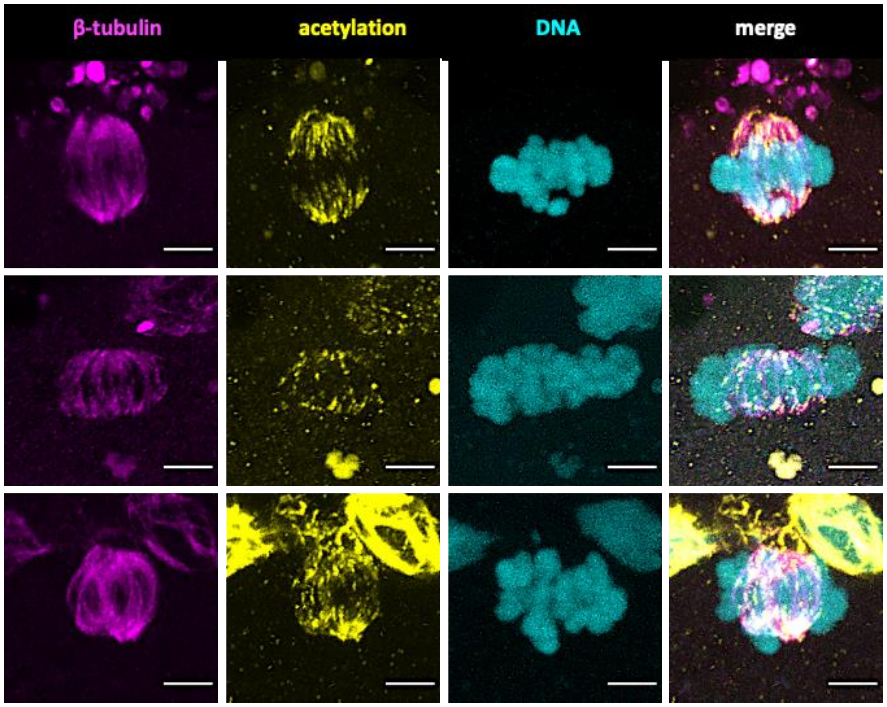

Figure 9. Acetylated microtubule islands are present in metaphase II meiotic spindles of *in vitro* cultured GV derived oocytes, stained for tubulin (magenta), tubulin acetylation (yellow) and DNA (cyan, Hoechst dye) with maintained zona pellucida and pre-fixation permeabilization (n=3). Each row corresponds to individual oocytes of the same of different donor origin. Scale bar 5 μm

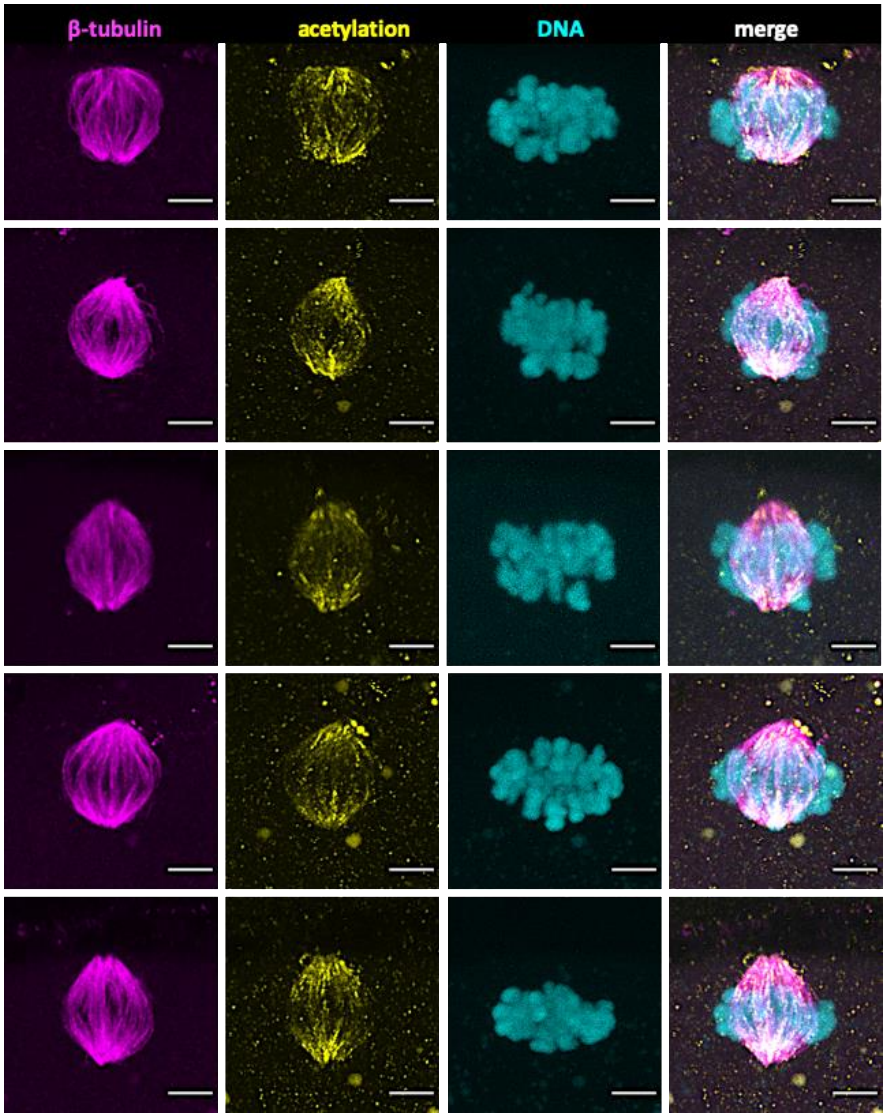

Figure 10. Acetylated microtubule islands are present in metaphase II meiotic spindles of *in vivo* matured oocytes (n=5), stained for tubulin (magenta), tubulin acetylation (yellow) and DNA (cyan, Hoechst dye). Each row corresponds to individual oocytes of the same of different donor origin. Scale bar 5 µm

1.3) Tyrosination- Detyrosination

Tyrosinated α-tubulin was detected in the MII spindles of *in vitro* cultured oocytes (n=8). In contrast to the interrupted occurrence observed with acetylation, tyrosination of microtubules showed a continuous pattern (Fig.11).

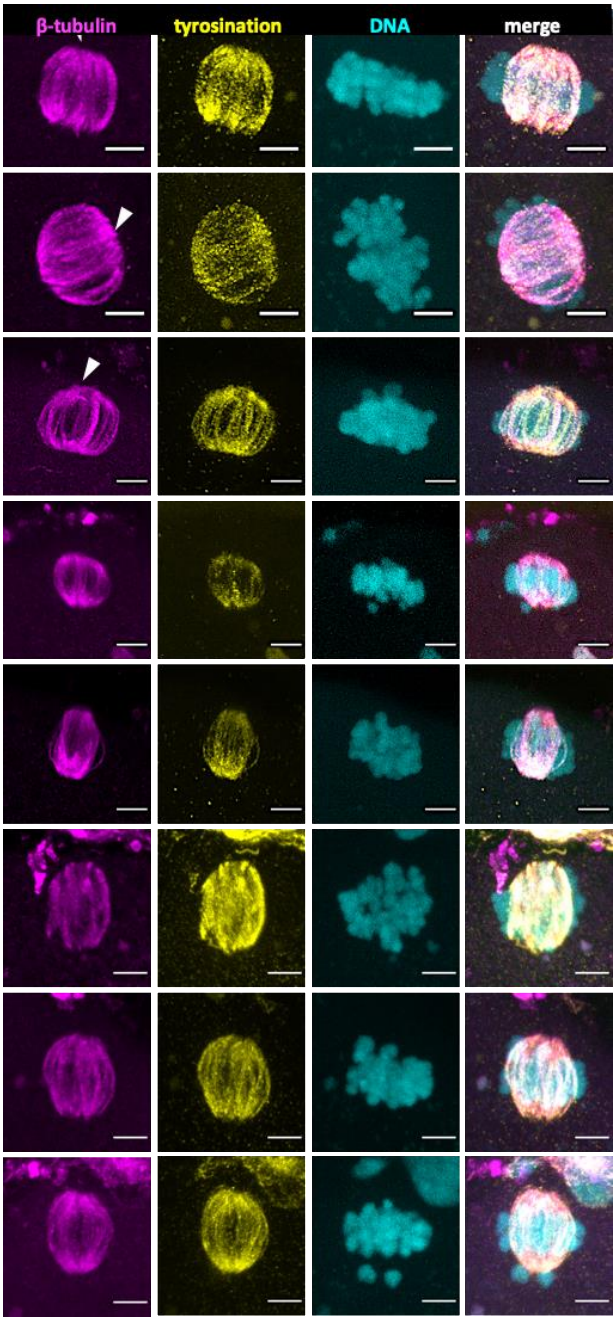

Figure 11. Tyrosinated microtubules are present in metaphase II meiotic spindles of *in vitro* cultured oocytes (n=8), stained for tubulin (magenta), tubulin tyrosination (yellow) and DNA (cyan, Hoechst dye). White arrows point the cortex pole, each row corresponds to individual oocytes of the same or different donor origin. Scale bar 5 μm

Tyrosination presence was also confirmed in *in vivo* matured oocytes (n=5). In three oocytes, signal intensity decreased from the cytosolic to the cortex pole (Fig. 12, rows 3-5), while one oocyte showed higher intensity in the cortex pole (Fig. 12, row 2).

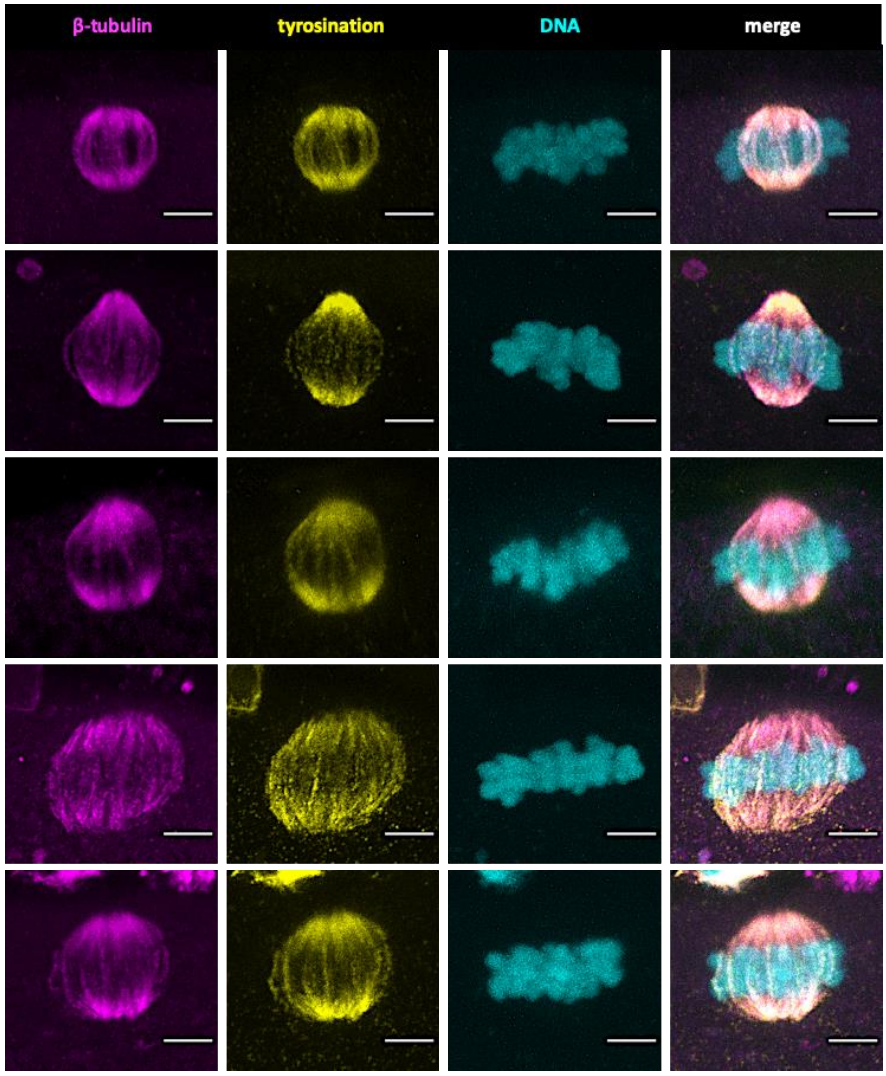

Figure 12. Tyrosinated microtubules are present in metaphase II meiotic spindles of *in vivo* matured oocytes (n=5), stained for tubulin (magenta), tubulin tyrosination (yellow) and DNA (cyan, Hoechst dye). Each row corresponds to individual oocytes of the same of different donor origin. Scale bar 5 μm

The reversible removal of tyrosine (detyrosination) was found solely in the *in vivo* matured oocytes (Fig. 13). The signal was barely detectable, even when using high concentrations of antibody. *In vitro* cultured oocytes showed complete absence of signal despite the presence of a well formed spindle and successful microtubule staining (Fig. 14).

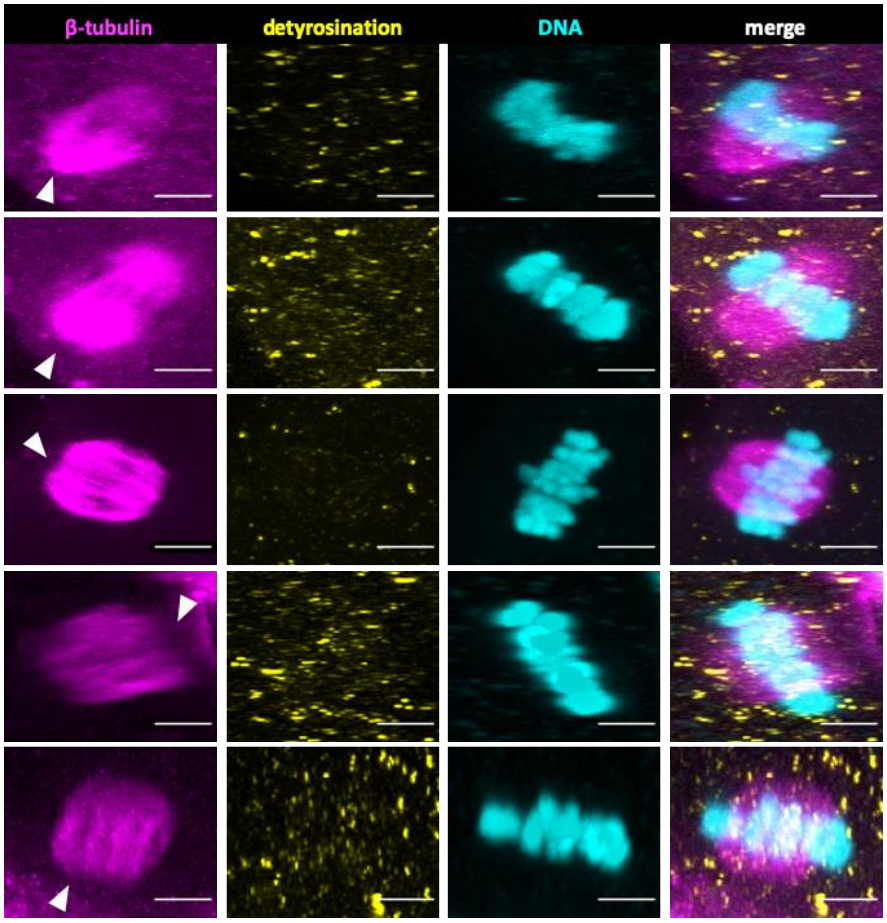

Figure 13. No detyrosinated microtubules are detected in metaphase II meiotic spindles of in vitro cultured oocytes (n=5), stained for tubulin (magenta), tubulin detyrosination (yellow) and DNA (cyan, Hoechst dye). White arrows point the cortex pole. Each row corresponds to individual oocytes of the same or different donor origin. Scale bar 5 μm

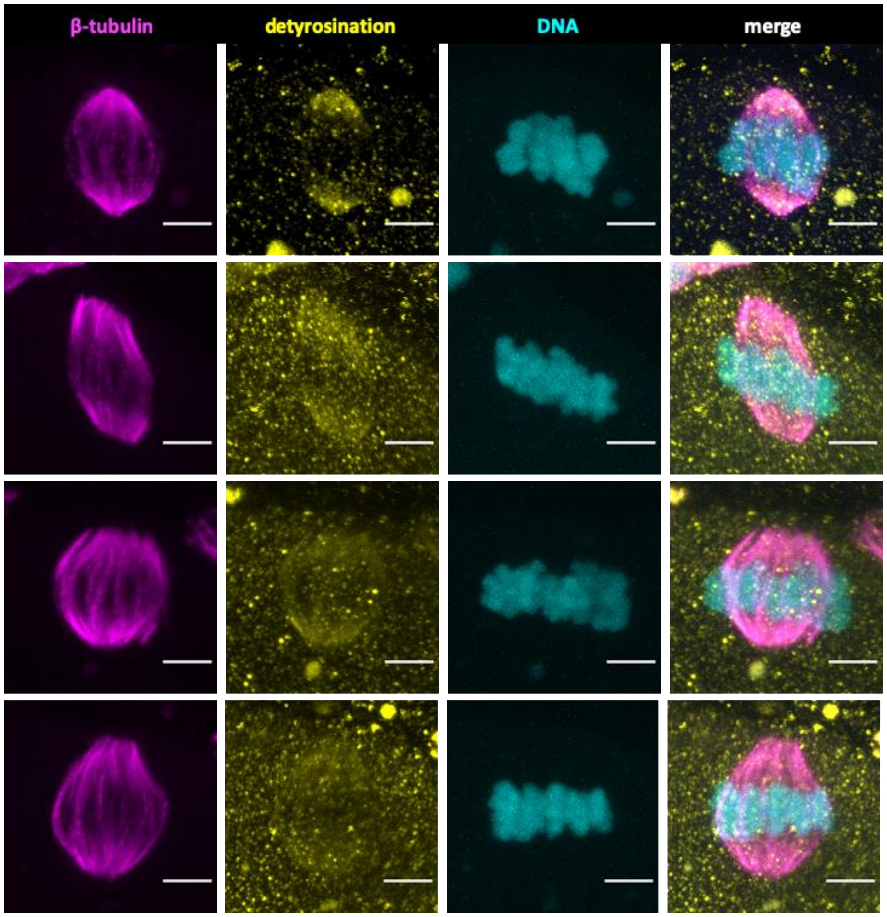

Figure 14. Low levels of detyrosinated microtubules are detected in metaphase II meiotic spindles of *in vivo* matured oocytes (n=4), stained for tubulin (magenta), tubulin detyrosination (yellow) and DNA (cyan, Hoechst dye). Each row corresponds to individual oocytes of the same of different donor origin. Scale bar 5 µm

1.4) Δ2- tubulin

Δ2-tubulin, the irreversibly modified form of α-tubulin, was detected in metaphase II meiotic spindles of human oocytes cultured *in vitro* (n=10) and matured *in vivo* (n=6). Overall, the signal covered all the spindle surface in both groups. In some samples within the *in vitro* cultured oocyte group, we observed higher intensity of signal localized in specific microtubule bundles (Fig. 15), which was not the case for the *in vivo* group. In both groups the signal for the modification was overlapping with that of α-tubulin. In the case of *in vivo* matured oocytes (Fig. 16), the pre-permeabilization protocol was followed, resulting in less background for the anti Δ2-tubulin antibody. The pre-permeabilization protocol introduced a step of short detergent exposure prior to fixation. As the detergent mainly affects the lipid membrane, we would not expect to have differences in primary antibody specificity. The observed phenotype of less background could be due to more efficient washing off of the excess antibody. Nevertheless, the different conditions render the signal comparison of the *in vitro* and the *in vivo* groups impossible.

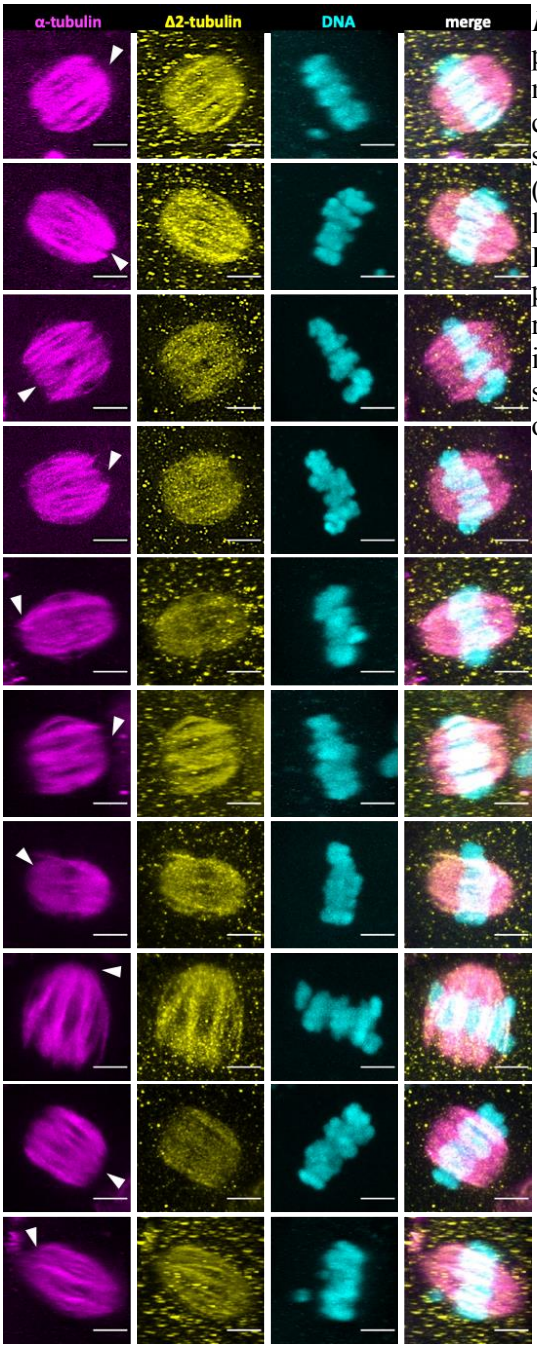

Figure 15. Δ2-tubulin is present in metaphase II meiotic spindles of *in vitro* cultured oocytes (n=10), stained for tubulin (magenta), Δ2-tubulin (yellow) and DNA (cyan, Hoechst dye). White arrows point the cortex pole, each row corresponds to individual oocytes of the same or different donor origin. Scale bar 5 µm

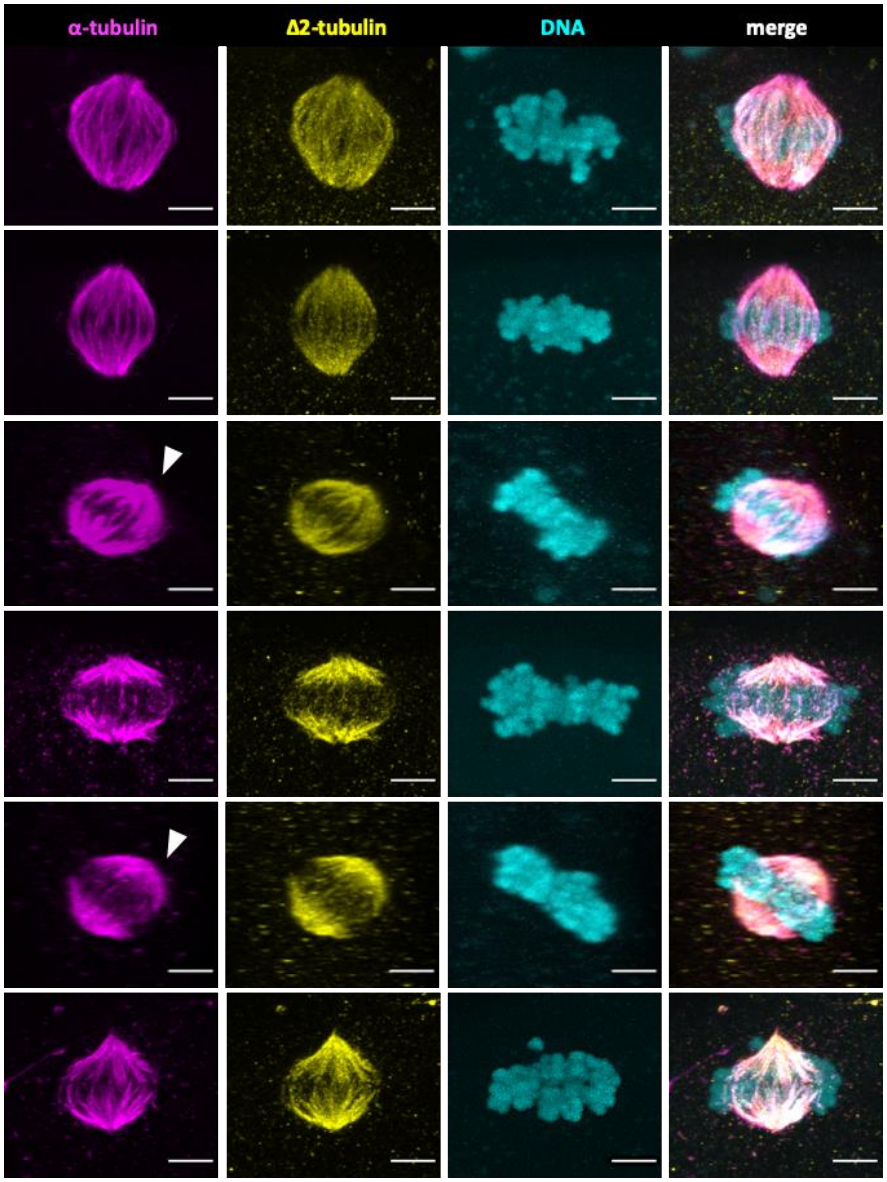

Figure 16. Δ2-tubulin is present in metaphase II meiotic spindles of *in vivo* matured oocytes (n=6), stained for tubulin (magenta), Δ2-tubulin (yellow) and DNA (cyan, Hoechst dye). White arrows point the cortex pole, each row corresponds to individual oocytes of the same or different donor origin. Scale bar 5 µm

1.5) (poly)Glutamylation

Incubation of human oocytes (n=5) with the commercial anti-glutamylation antibody GT335, which recognizes the branching point of the glutamate chain (one glutamate is enough to create the epitope) led to barely detectable signal (Fig. 17). Subsequent experiments with the anti-polyglutamylation antibody B3 revealed weak but distinctly visible signal suggesting the presence of the modification in the metaphase II spindles (n=8 for *in vitro* cultured oocytes and n=5 for *in vivo* matured oocytes, Fig. 18 and Fig. 19, respectively. The pattern of signal along the spindle seemed to spread on the microtubule surface with areas of higher concentration, but aggregates in the background make this conclusion tentative.

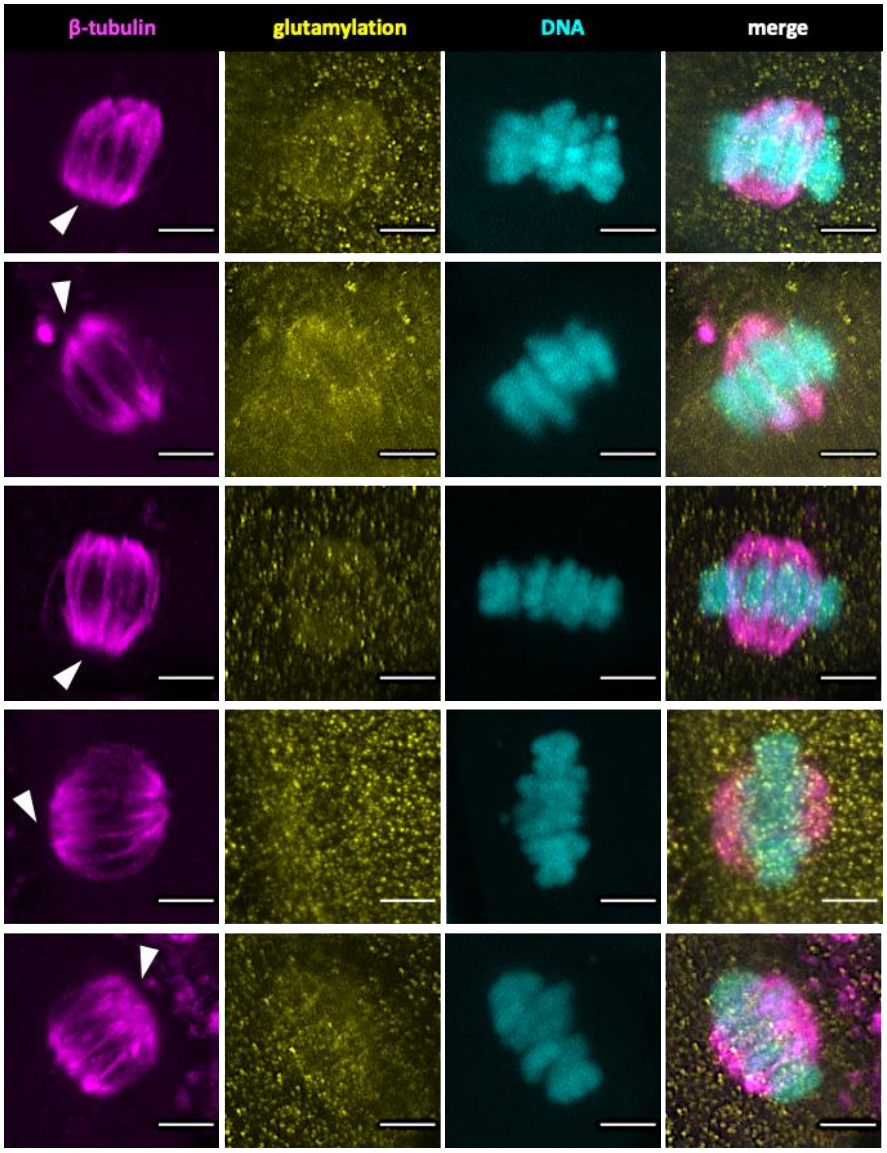

Figure 17. The glutamylation branching point is not detected in metaphase II meiotic spindles of *in vitro* matured oocytes (n=5), stained for tubulin (magenta), glutamylation (yellow) and DNA (cyan, Hoechst dye). White arrows point the cortex pole, each row corresponds to individual oocytes of the same or different donor origin. Scale bar 5 μm

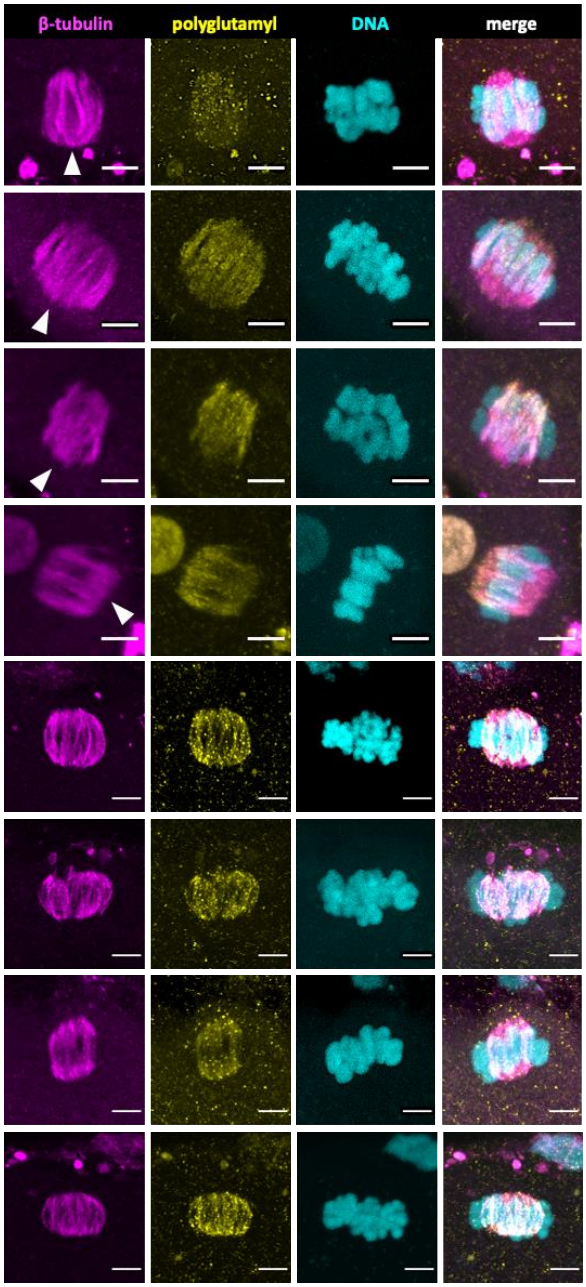

Figure 18. Polyglutamylated microtubules are present in metaphase II meiotic spindles of *in vitro* matured oocytes (n=8), stained for tubulin (magenta), polyglutamylation (yellow) and DNA (cyan, Hoechst dye). White arrows point the cortex pole, each row corresponds to individual oocytes of the same or different donor origin. Oocytes in rows 1-4 were not stained with the pre-permeabilization protocol. Scale bar 5 µm

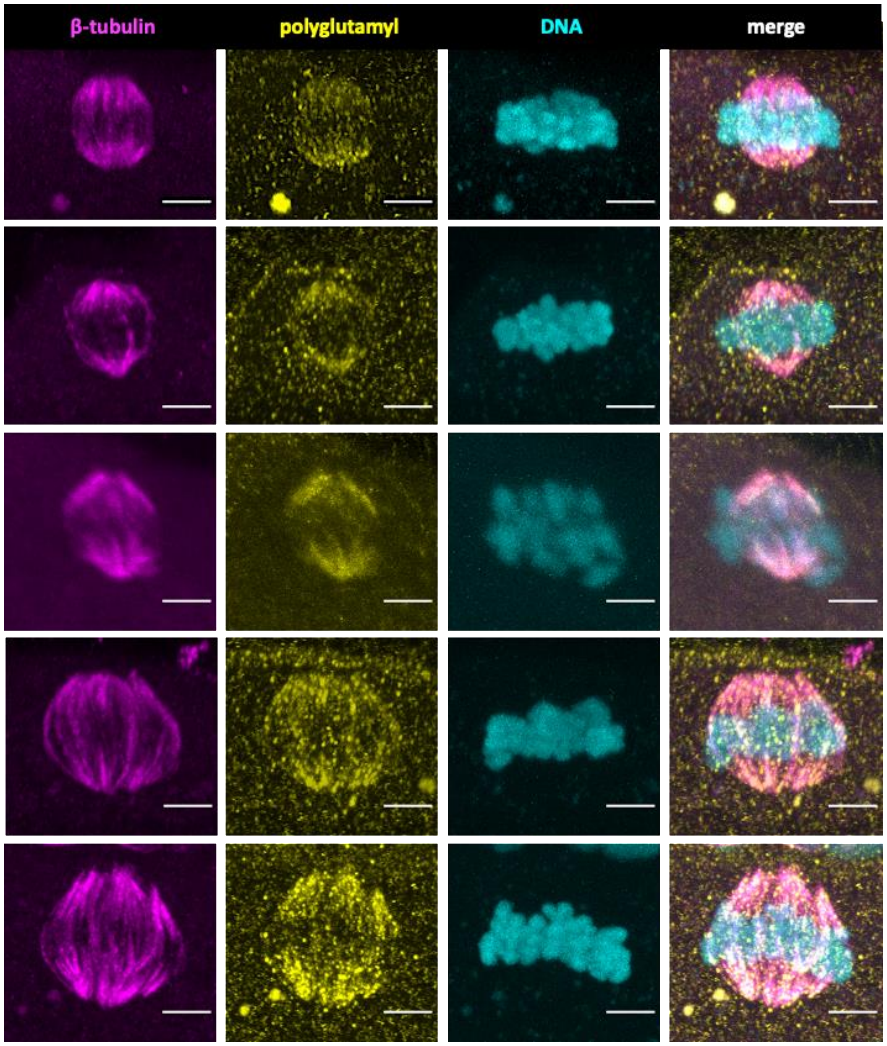

Figure 19. Polyglutamylated microtubules are present in metaphase II meiotic spindles of *in vivo* matured oocytes (n=8), stained for tubulin (magenta), polyglutamylation (yellow) and DNA (cyan, Hoechst dye). Each row corresponds to individual oocytes of the same or different donor origin. Scale bar 5 µm

1.6) Flat shaped spindle poles are prevalent in *in vitro* cultured oocytes

During determination of the PTM spindle profile we observed a prominent difference between the spindle pole shape of the IVO and the IVC groups. Following the nomenclature first used by Coticchio et al and Ferrer et al , the threshold for defining the pole as focused or flattened (blunt) was set at 2 μm (Coticchio *et al.*, 2013b; Ferrer-Vaquer *et al.*, 2019) (Fig. 20b). Pole diameter was measured solely in spindles whose major axis was orthogonally oriented to the objective. The four possible phenotypes were flattened-focused, focused-flattened, with the first word characterizing the cortex side, double flattened and double focused. As shown in Fig. 20a, MII spindles of oocytes cultured *in vitro* from the GV stage (IVC) have blunt-shaped poles compared to oocytes that had matured *in vivo* and were cryopreserved (IVO). Among the four possible phenotypes, 86% of the IVC oocytes had double flattened poles (25/29); only 7% had double focused spindles (2%) and two spindles bearing the flattened-focused and focused-flattened phenotypes (3.5% each). On the contrary, IVO oocytes maintained higher microtubule convergence in their poles (double focused) for 40.5% of oocytes (15/37), which was equal to the double flattened ones, while the focused flattened were found in 6 spindles (16.2%) compared to the one flattened focused (2.8%) (Fig 20c). As revealed in the exact measurements of the individual poles (Fig. 21), both the cortex and the cytosole pole diameters are significantly higher in the IVC compared to the IVO oocytes.

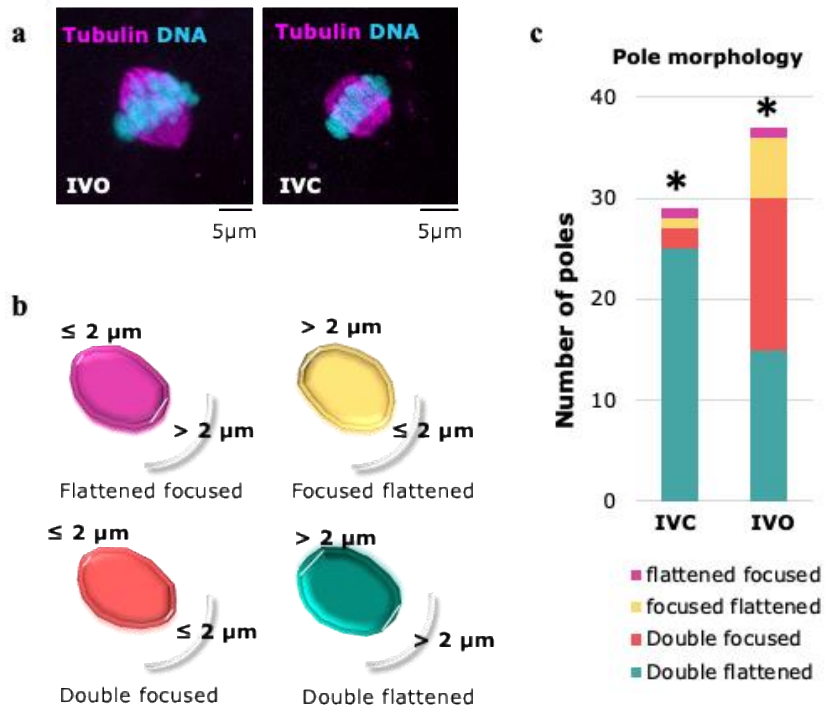

Figure 20. Tubulin staining (magenta) of MII spindles of human oocytes matured in vivo and cryopreserved (IVO, left) and cultured in vitro (IVC, right), with double focused and double flattened poles respectively. DNA is shown in cyan (Hoechst dye) b) The four possible phenotypes of the meiotic spindle pole shape with regard to their position towards the cortex (curved line). c) Proportion of spindle phenotypes in the IVC and the IVO groups: flattened focused (1,1), focused flattened (1,6), double focused (2,15) and double flattened (25,15). *p=0.0004 (Fisher's exact test)

Further morphometric analysis of the spindle size (maximum projection, major and minor axis length) and the metaphase plate position (proximal to distal ratio, angle) revealed decreased spindle size in the IVC group, which is in agreement with the observed shorter major axes of this group. All comparisons were made with the Kruskal- Wallis statistical test. (Fig.21).

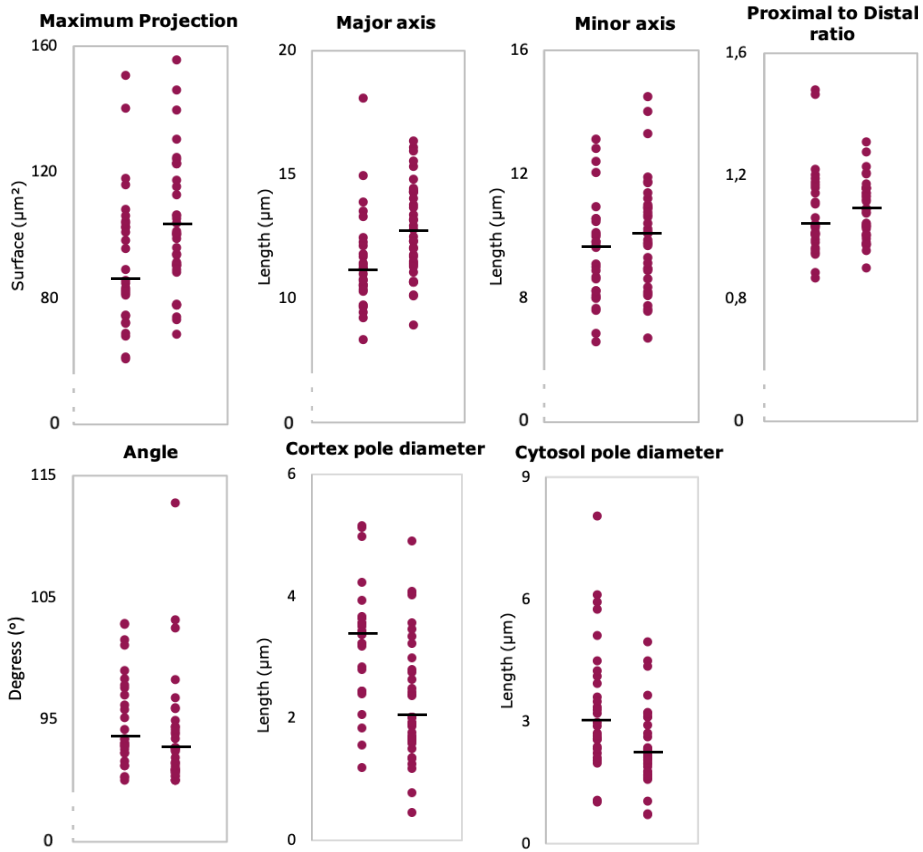

Figure 21. Morphometric analysis of meiotic spindles of *in vitro* cultured (IVC, n=29) and *in vivo* matured oocytes (IVO, n=37). Maximum projection of the spindle image in 2D corresponds to the area µm^2, which together with the major and minor axis length determine the spindle size. IVC oocytes have smaller spindles (p=0.019) which is attributed to shorter major axis (p= 000766). Proximal to distal axis ratio reveals the metaphase plate position with regard to the spindle equator. Angle in arc degree (°) is used to describe plate tilting. Spindle dimensions and DNA coordinates are comparable between the two groups. Cortex pole diameter is higher in the IVC group (p=0.000225) as well as cytosol pole diameter (p=0.000766) Bars show group medians and all comparisons were made using the Kruskal-Wallis test

Overall, oocytes that were cultured *in vitro* had similar spindle PTM pattern to *in vivo* matured oocytes. Acetylation signal appeared segmented along the MTs with higher inter-group variability in the signal distribution in the *in vitro* group. *In vivo* matured oocytes consistently presented increased acetylation signal at the spindle poles. Tyrosination was present in both groups, with three cases of signal decrease and one case of signal increase from the cytosol to the cortex pole in the *in vivo* matured oocytes. The *in vitro* group presented an overall uniform distribution. The detyrosination antibody was the only one resulting in complete signal absence in the *in vitro* versus the *in vivo* oocytes. The irreversible Δ2-tubulin modification was also detected in both groups without any particular signal distribution pattern along the microtubules. The last modification, glutamylation, was targeted with two different antibodies. GT335, which detects the glutamate chain branching point revealed barely detectable signal giving the initial impression that the modification is not present. Nevertheless, follow-up staining with the clone B3 anti-glutamylation antibody resulted in clearly detectable signal. However, due to high background, which could not be avoided even by altering certain staining parameters or briefly centrifuging the antibody solution, no clear modification pattern could be determined.

The morphometric analysis revealed clear differences between the two groups. *In vitro* cultured oocytes have smaller spindles due to their shorter major axis while their spindle poles have a trimmed-like

phenotype. Both the cytosol and the cortex side poles' diameters are higher in the *in vitro* group.

Chapter 2. PTM enzyme transcripts are present throughout human oocyte meiosis

The presence of the modifications of the transiently forming spindle in the transcriptionally quiescent oocyte suggested that PTM enzymes are present in the oocyte at the GV stage. The direct way of testing this would be to do immunofluorescence, but this approach is not feasible due to the low levels of enzyme present and the lack of suitable antibodies. A second approach would be proteomics of pools of oocytes. This approach is also not feasible, as proteomics requires microgram amounts of protein, which must be obtained by prohibitively high numbers of oocyte which were not available to us. Furthemore, single oocyte proteomics is not a currently well established technique.

As an alternative, we addressed this question by performing quantitative PCR analysis in four groups of oocytes: GV, *in vitro* cultured (IVC), *in vivo* matured after thawing and failed to mature both *in vivo* and *in vitro* (FTM).

2.1) Reference genes

As the human oocyte constitutes a distinct cell type, a reference gene selection process was introduced (Radonić et al., 2004). Ten putative reference genes were tested for their stability among the total number of oocytes across the groups for the normalization of the relative expression levels. Selection of the best reference genes was based on comparison between the algorithms BestKeeper (Pfaffl et al., 2004), NormFinder, GeNorm (Vandesompele et al., 2002) and the

comparative ΔCT method , following the method used by Barragan et al (2015). ACTB, RPLP1, GAPDH, DNMT1, SDHA and UBC demonstrated the highest stability value among the three groups and thus were chosen for the normalization of the expression values (Fig. 22).

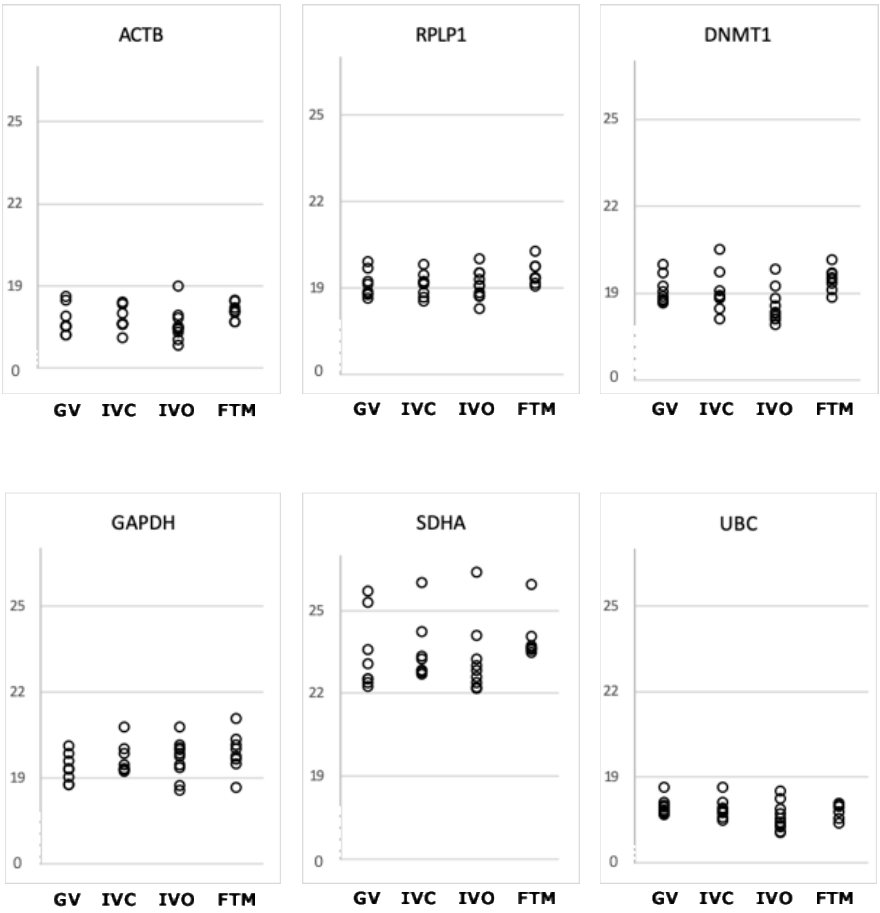

Figure 22. Cq values of the six reference genes for the study groups of human oocytes: GV (immature oocytes at the germinal vesicle stage, n=8), IVC (metaphase II oocytes cultured *in vitro* from the GV stage, n=8), IVO (metaphase II oocytes *in vivo* matured, n=10) and FTM (failed to mature oocytes after *in vitro* culture, n=8). Each point corresponds to an individual oocyte.

2.2) PTM enzyme genes overview

Primers were validated on several different cDNA sources: HEK293T cells, BeWo cells, human fetal brain tissue and human testis tissue with several primer combinations when necessary (up to four in some cases). All the primer pairs targeted the 3´end of the transcript. Primer pairs were designed to target different exons separated by an intron of around 1kb.

A total of 26 enzymes have been described in the literature for their ability to modify tubulin heterodimers in soluble or polymerized state. TTLL3, TTLL7, TTLL10, CCP2, CCP3, CCP4 and VASH2 were not detected among the groups of human oocytes tested (Fig. 23). Out of the 17 detected PTM enzymes, 7 were differentially expressed between two or more of the study groups (Table 4). In particular, GV had lower levels of NAA50 but higher TTLL4 when compared to failed to mature oocytes. The latter group had increased NAA50 and TTLL11 but lower TTLL12 transcript content when compared to the *in vitro* cultured MII oocytes, while NAA50 and CCP1 were significantly higher when compared to the *in vivo* matured oocytes. The comparison between GV and IVO oocytes revealed higher levels of TTLL6 and VASH1. Finally, the only difference between *in vitro* culture and *in vivo* maturation was the lower levels of TTLL12 and CCP1 for the latter group.

STUDY GROUPS	transcript
FTM > GV	NAA50
FTM > IVC	NAA50, TTLL11
FTM > IVO	NAA50, CCP1
FTM < GV	TTLL4
FTM < IVC	TTLL12
GV > IVO	TTLL6, VASH1
IVC > IVO	TTLL12, CCP1

Table 4. Overview of differentially expressed PTM enzymes at the transcript level. GV: immature oocytes at the germinal vesicle stage, IVC: metaphase II oocytes cultured *in vitro* from the GV stage, IVO: metaphase II oocytes *in vivo* matured and FTM: failed to mature oocytes after *in vitro* culture

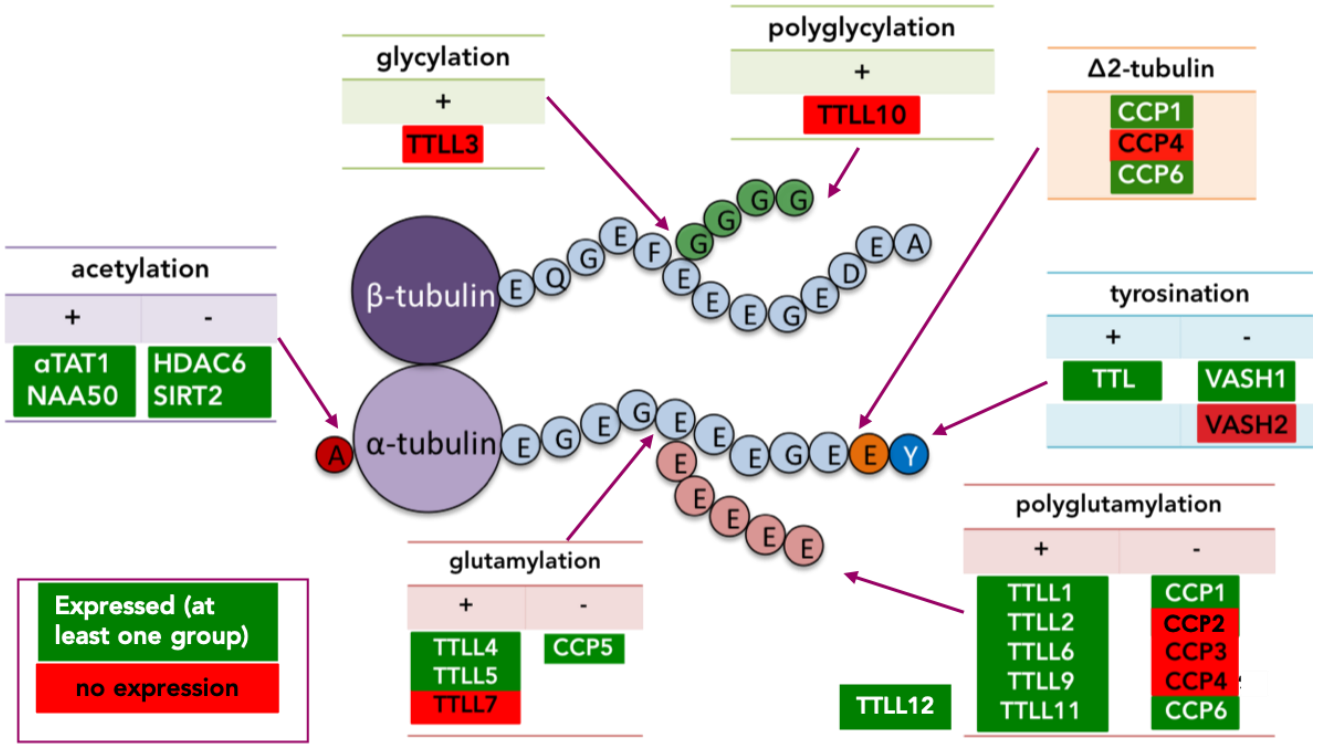

Figure 23. Overview of the presence of the PTM enzymes at the transcript level in at least one sample group (GV, IVC, IVO, FTM).

2.2) Acetylases-Deacetylases

All of the known PTM enzymes responsible for the acetylation and deacetylation of tubulin were present in human oocytes at the stage of immaturity (GV), metaphase II arrest (IVC, IVO) as well as in oocytes incompetent to resume meiosis even after *in vitro* culture (FTM). The levels of the a-tubulin acetyltransferase αTAT1 were stable among the groups with intragroup variability that is higher in the case of the mature oocytes (both IVC and IVO). The β-tubulin acetylase NAA50 reached the highest transcript levels in the FTM oocytes with a significant difference, albeit smaller (less than 2-fold) than that found in other groups. The deacetylases HDAC6 and SIRT2 were found at similar levels among the groups with an overall higher variability for the HDAC6 values (Fig. 24).

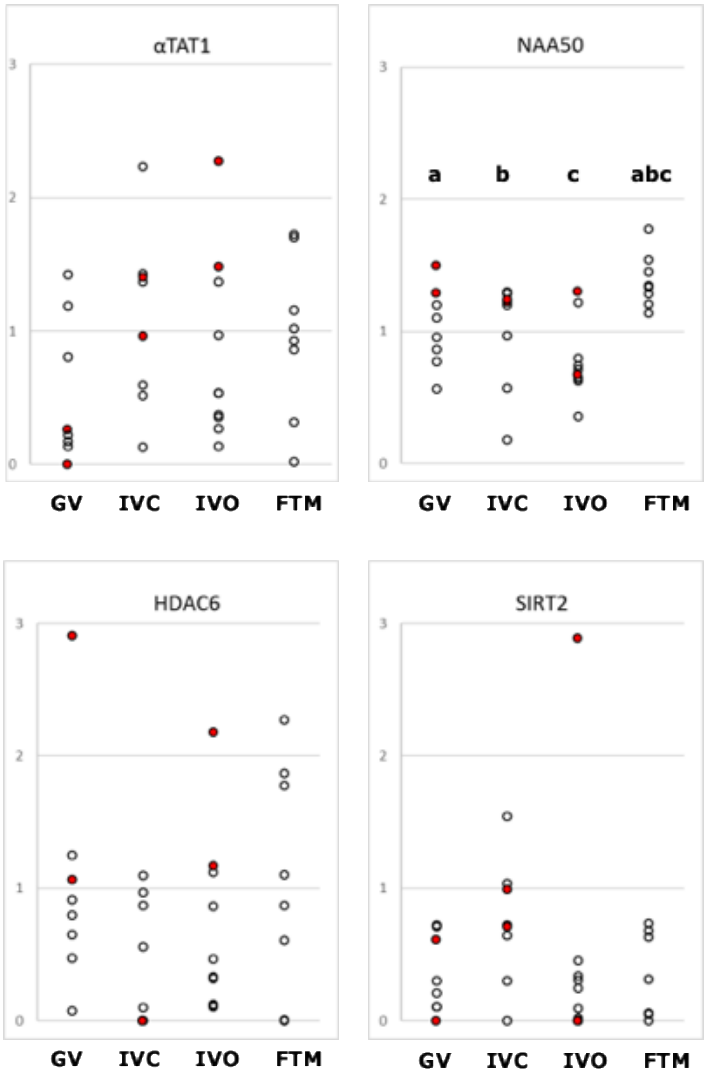

Figure 24. Scatter plots with average of expression values (arbitrary units) of the acetylases αTAT1, NAA50 and deacetylases HDAC6 and SIRT2. y axis: arbitrary normalized expression values, x axis: GV(germinal vesicle, n=6), IVC(metaphase II oocytes cultured in vitro from the GV stage, n=8), IVO(metaphase II oocytes in vivo matured, n=10) and FTM(failed to mature oocytes after in vitro culture, n=8). Each point corresponds to an individual oocyte. Red points show oocytes that were processed in the same picoprofiling batch with the FTM group. $p<0.05$ between same letter values

2.3) Tyrosinase-Detyrosinase

Tubulin tyrosine ligase (TTL) was present as a transcript in human oocytes at comparable levels between the studied groups (GV, IVC, IVO, FTM). Progression of meiosis did not affect the existing pool of transcripts while no difference was found in oocytes that failed to resume meiosis. In contrast, VASH1, one of the two characterized tubulin detyrosinases, was detected in only 3 GV and 1 FTM oocytes, with levels close to zero for the rest of the samples (Fig. 25). This suggests a higher proportion of tyrosinase compared to detyrosinase transcripts in the RNA pool of human oocytes.

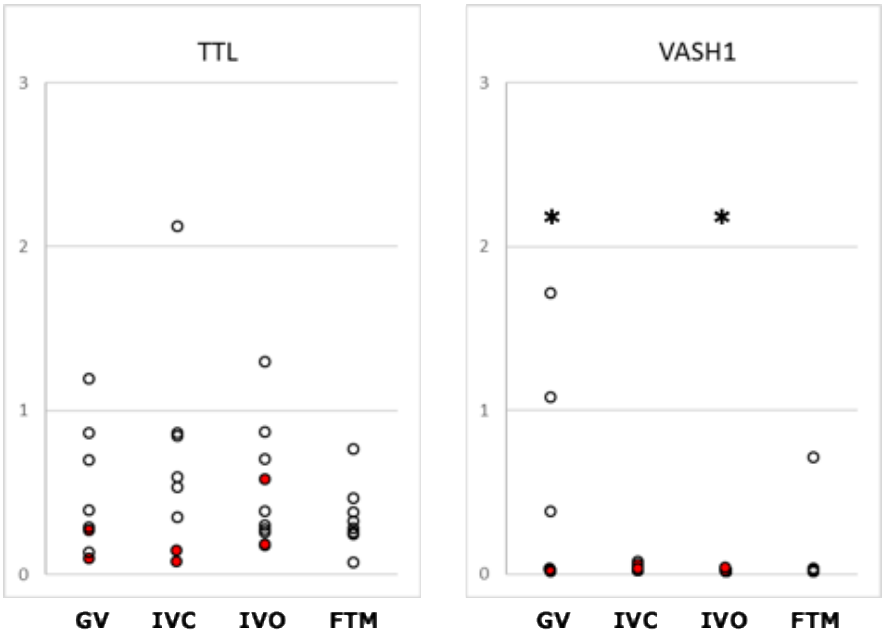

Figure 25. Scatter plots with average of expression values (arbitrary units) of the tyrosinase TTL and detyrosinase VASH1. y axis: arbitrary normalized expression values, x axis: GV(germinal vesicle, n=6), IVC(metaphase II oocytes cultured in vitro from the GV stage, n=8), IVO(metaphase II oocytes in vivo matured, n=10) and FTM(failed to mature oocytes after in vitro culture, n=8). Each point corresponds to an individual oocyte. Red points show oocytes that were processed in the same picoprofiling batch with the FTM group. *p<0.05

2.4) Monoglutamylases-Deglutamylase

The tubulin tyrosine ligase like family members 4 and 5 were detected in the four study groups of oocytes, with TTLL4 levels being overall higher compared to TTLL5. A slight but statistically significant difference was found between the GV and FTM group with the levels of TTLL4 being lower in the latter. The PTM enzyme catalyzing the reverse reaction, CCP5, was also detected in all the groups. CCP5 transcript levels were lower in the *in vitro* cultured oocytes, apart from one oocyte with a 10-fold higher expression value. This difference with the rest of the groups did not reach statistical significance, due to this oocyte with higher levels. *In vivo* matured oocytes have the highest intra-group variability for this particular transcript. Comparing the values of the monoglutamylases compared to the deglutamylase, it can be argued that the reaction of glutamylation is favored provided that the transcripts are translated into enzymatically functional protein molecules (Fig. 26).

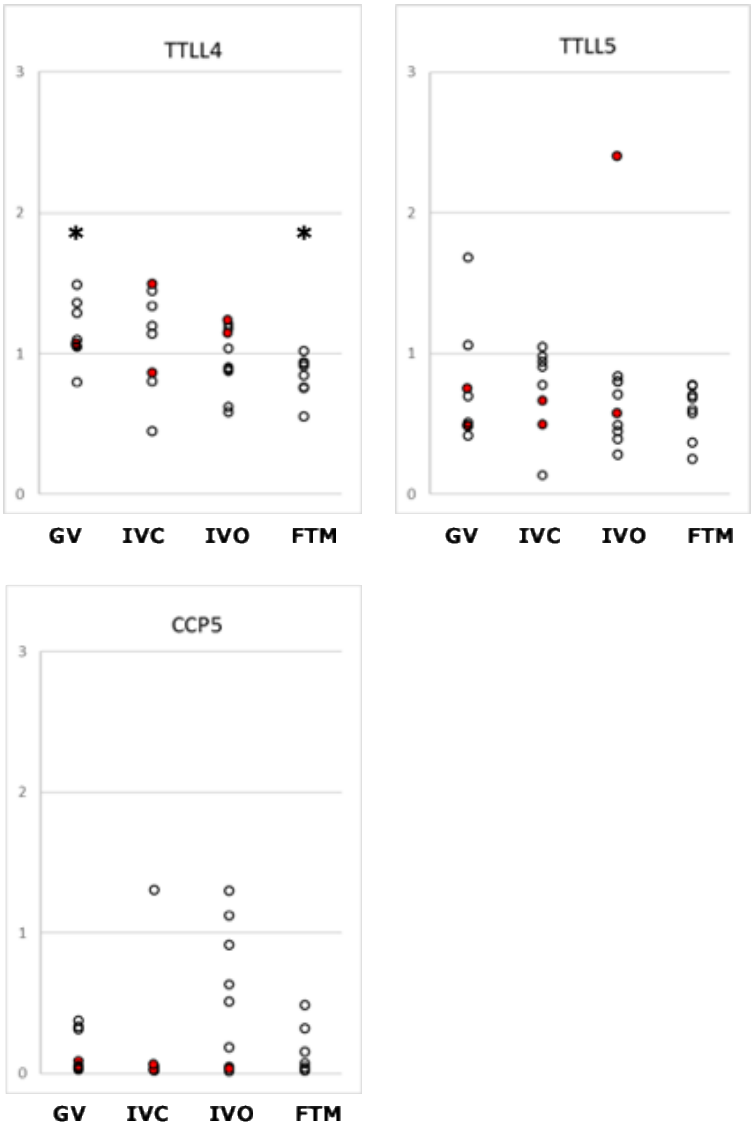

Figure 26. Scatter plots with average of expression values (arbitrary units) of the monoglutamylases TTL4, TTLL5 and first glutamate carboxypeptidase CCP5. y axis: arbitrary normalized expression values, x axis: GV(germinal vesicle, n=6), IVC(metaphase II oocytes cultured in vitro from the GV stage, n=8), IVO(metaphase II oocytes in vivo matured, n=10) and FTM(failed to mature oocytes after in vitro culture, n=8). Each point corresponds to an individual oocyte. Red points show oocytes that were processed in the same picoprofiling batch with the FTM group. *p<0.05

2.5) Polyglutamylases-Deglutamylases

Six members of the TTLL family were detected in oocytes, namely TTLL1, TTLL2, TTLL6, TTLL9, TTLL11 and TTLL12. TTLL12 is a pseudoenzyme, as it lacks its enzymatic activity; its role is yet unknown. Regarding the expression values, there was less intra-group variability in comparison to the majority of the other PTM enzymes. *In vitro* cultured oocytes were marked by higher expression levels compared to their *in vivo* counterparts and the failed to mature oocytes (Fig. 28). Among the enzymatically active TTLL members, TTLL6 and TTLL11 were found to be differentially expressed. TTLL6 was slightly higher in GV compared to IVO oocytes (Fig. 27), while TTLL11 was higher in the FTM oocytes compared to the IVC ones (Fig.28). TTLL1, TTLL2 and TTLL9 were detected in similar levels with relatively low intra-group variability (Fig. 27).

The CCP enzymes that were present in human oocytes at the transcript level were CCP1 and CCP6, responsible for the removal of the glutamic chain (but not the branching point). CCP1 levels at the GV, IVM and FTM were on average higher compared to the CCP6 ones. Inter-group comparison revealed lower levels of CCP1 in the *in vivo* matured oocytes compared to their *in vitro* counterparts and the failed to mature ones (Fig. 28).

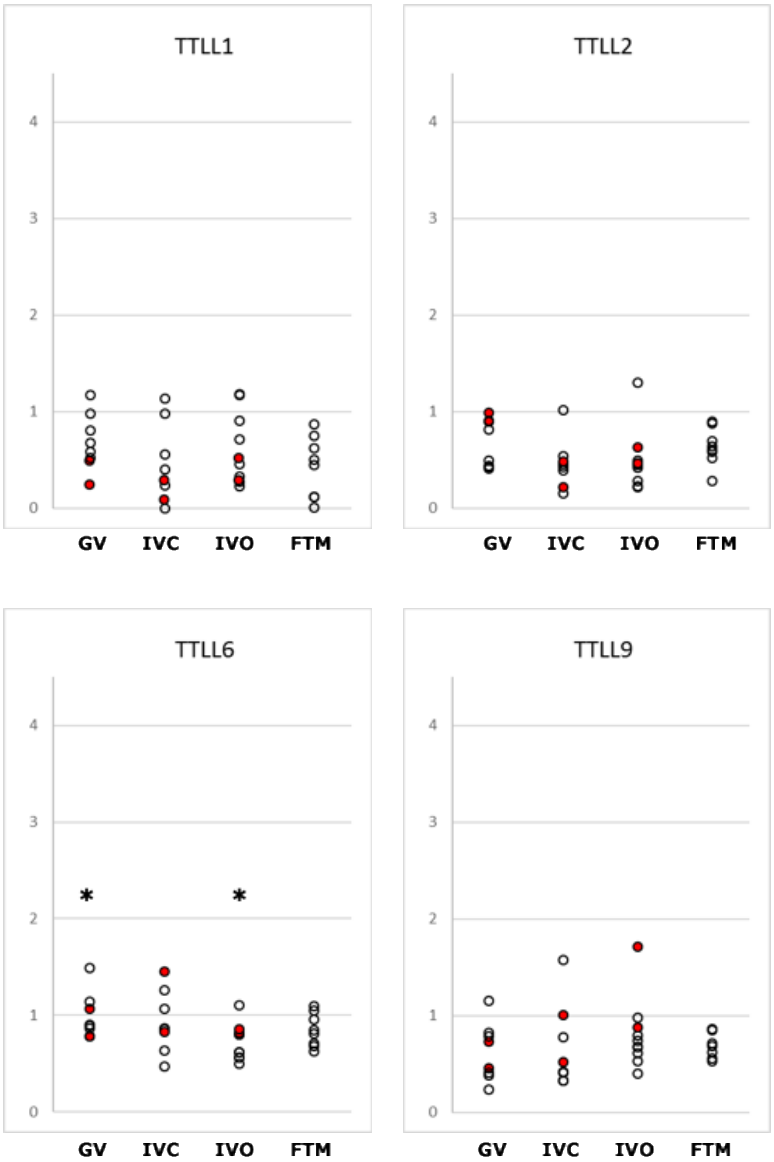

Figure 27. Scatter plots with average of expression values (arbitrary units) of the polyglutamylases TTL1, TTLL2, TTLL6, TTLL9. y axis: arbitrary normalized expression values, x axis: GV(germinal vesicle, n=6), IVC(metaphase II oocytes cultured in vitro from the GV stage, n=8), IVO(metaphase II oocytes in vivo matured, n=10) and FTM(failed to mature oocytes after in vitro culture, n=8). Each point corresponds to an individual oocyte. Red points show oocytes that were processed in the same picoprofiling batch with the FTM group. *p<0.05

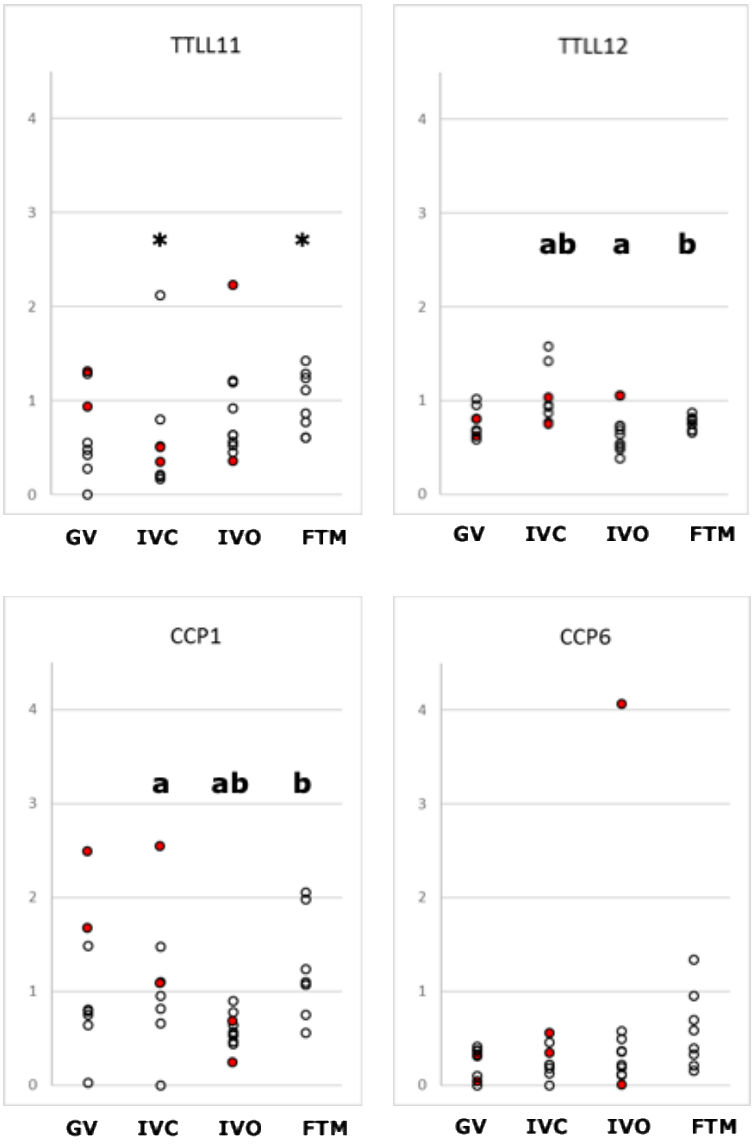

Figure 28. Scatter plots with average of expression values (arbitrary units) of the polyglutamylase TTLL11, the pseudoenzyme TTLL12 and the carboxypeptidases CCP1 and CCP6. y axis: arbitrary normalized expression values, x axis: GV(germinal vesicle, n=6), IVC(metaphase II oocytes cultured in vitro from the GV stage, n=8), IVO(metaphase II oocytes in vivo matured, n=10) and FTM(failed to mature oocytes after in vitro culture, n=8). Each point corresponds to an individual oocyte. Red points show oocytes that were processed in the same picoprofiling batch with the FTM group. $p<0.05$ between asterisk or same letter values

Chapter 3. Translational regulation of PTM enzymes in Xenopus oocytes

Given that direct detection of tubulin PTM proteins was not technically feasible, but tubulin PTM mRNA was detected, an indirect way to check for protein presence was by checking whether translation of the transcripts of interest was taking place. Oocyte maturation occurs in general absence of transcription, with spatial and temporal gene regulation of a specific subset of genes occurring at the level of translational control.

Because direct measurement of mRNA translation in oocytes is again not technically feasible, we sought to determine whether the 3'UTRs of specific tubulin PTM mRNAs contained elements involved in CPE-mediated regulation. In particular, the prediction of repression is given at the stage of germinal vesicle oocytes if two CPE are within a distance of 50bp between each other as this allows the interaction with the protein maskin. Upon progesterone exposure and resumption of the meiotic cycle the presence of CPE within 100 bp from the polyadenylation signal promotes binding of CPSF and thus the activation of translation (Fig.6 and Fig. 29).

3.1) Alternative splicing and polyadenylation variants of PTM enzymes in human oocytes

We produced a tubulin PTM enzyme transcript list containing 23 tubulin PTM enzymes using the Ensembl database (see Table 5). All of the enzymes had potential protein coding alternative splice

variants, while 15 transcripts had alternative polyadenylation signals. One or more transcripts of αTAT1, NAA50, TTLL11, CCP1, CCP2, CCP4, CCP5 and CCP6 had regulatory sequences for 3'UTR dependent translational control. All 3'UTR were screened with the software developed by Mendez group (http://genome.crg.es/CPE/server.html) for the detection of cytoplasmic polyadenylation elements (CPE). The presence and the configuration of the elements with respect to the polyadenylation signal is what defines the prediction for the expected type of translational regulation.

Bioinformatic analysis of all tubulin PTM mRNA 3'UTR variants revealed regulatory motifs for α-TAT1, NAA50, TTLL11, CCP1, CCP2, CCP4. CCP5 and CCP6. Out of the enzymes with CPE prediction, CCP2 and CCP4 were not detected in human oocytes, while NAA50 substrate is soluble β-tubulin and is not expected to be found in the spindle, thus, it was not analyzed further. Primers specific for the alternative polyadenylation variants allowed their detection in the oocyte RNA pool. In particular, αTAT1_204/206 was present in GV, IVC and IVO groups. TTLL11_206 transcript 1 as well as CCP1_201transcript 2 were found in all the oocyte templates tested. CCP5_202 was found only in GV oocytes, while CCP6_204 transcript1 was detected in only two IVC samples (Fig.29).

GENE	transcript	3´ UTR bp	HEXA	CPE prediction
aTAT1	**201/205**	**1664**	**1**	**no**
	206/204	**180**	**1**	**activation early weak**
	202/203	**1117**	**1**	**no**
NAA50	**201**	**5300**	**9**	**repression for largest**
		46	tst1	no
		909	tst2	no
		1177	tst3	no
		2070	tst4	repression
		2710	tst5	repression
		2748	tst6	repression
		2905	tst7	activation early strong, repression
		5075	tst8	repression
		5286	tst9	repression
	210	**2766**	**6**	**repression for largest**
		46	tst1	no
		909	tst2	no
		1177	tst3	no
		2070	tst4	repression
		2710	tst5	repression
		2748	tst6	repression
	203	**1445**	**3**	**no**
	209	**830**	**1**	**no**
	208	**331**	**1**	**no**
	206	**303**	**1**	**no**
	207	**104**	**1**	**no**
	204	**no utr**	**n/a**	**n/a**
HDAC6	**201**	**370**	**1**	**no**
	202	**1117**	**1**	**no**
	203	**364**	**1**	**no**
	204	**no utr**	**n/a**	**n/a**
	205	**no utr**	**n/a**	**n/a**
	206	**183**	**0**	**no**
	207	**364**	**1**	**no**

GENE	transcript	3´ UTR bp	HEXA	CPE prediction
	208	**no utr**	**n/a**	**n/a**
	209	**no utr**	**n/a**	**n/a**
	210	**70**	**0**	**no**
	211	**no utr**	**n/a**	**n/a**
	212	**249**	**2**	**no**
		125	tst1	no
		234	tst2	no
	213	**1271**	**2**	**no**
	214	**180**	**0**	**no**
	219	**558**	**0**	**no**
	232	**171**	**0**	**no**
	236	**no utr**	**n/a**	**n/a**
	237	**344**	**0**	**no**
	239	**346**	**1**	**no**
	240	**364**	**1**	**no**
	243	**no utr**	**n/a**	**n/a**
SIRT2	**201/204**	**598**	**1**	**no**
	202	**802**	**1**	**no**
	203	**no utr**	**n/a**	**n/a**
	205	**no utr**	**n/a**	**n/a**
	206	no utr	**n/a**	**n/a**
	209	no utr	**n/a**	**n/a**
	211	no utr	**n/a**	**n/a**
	219	no utr	**n/a**	**n/a**
TTLL1	**201**	**132**	**1**	**no**
	202	**no utr**	**n/a**	**n/a**
TTLL2	**201**	**208**	**1**	**no**
TTLL3	**201**	**no utr**	**n/a**	**n/a**
	202	**1494**	**1**	**no**
	203	**no utr**	**n/a**	**n/a**
	204	**no utr**	**n/a**	**n/a**
	205	**no utr**	**n/a**	**n/a**
	206	**no utr**	**n/a**	**n/a**
	207	**no utr**	**n/a**	**n/a**

GENE	transcript	3´ UTR bp	HEXA	CPE prediction
	208	**no utr**	**n/a**	**n/a**
	209	**no utr**	**n/a**	**n/a**
	212	**no utr**	**n/a**	**n/a**
	213	**433**	**0**	**no**
	216	**no utr**	**n/a**	**n/a**
	217	**no utr**	**n/a**	**n/a**
	218	**no utr**	**n/a**	**n/a**
	219	**no utr**	**n/a**	**n/a**
	220	**no utr**	**n/a**	**n/a**
	221	**517**	**0**	**no**
	224	**no utr**	**n/a**	**n/a**
TTLL4	**201/202**	**1027**	**1**	**no**
	203	**no utr**	**n/a**	**n/a**
	205	**113**	**0**	**no**
	206	**no utr**	**n/a**	**n/a**
	208	**no utr**	**n/a**	**n/a**
	209	**no utr**	**n/a**	**n/a**
	210	**304**	**0**	**no**
	211	**no utr**	**n/a**	**n/a**
	212	**390**	**0**	**no**
TTLL5	**201**	**580**	**0**	**no**
	202	**632**	**1**	**no**
	207	**177**	**0**	**no**
	211	**156**	**0**	**no**
	217	**547**	**1**	**no**
	219	**1327**	**6**	**no**
		644	tst1	**no**
		850	tst2	**no**
		1019	tst3	**no**
		1091	tst4	**no**
		1135	tst5	**no**
		1316	tst6	**no**
	221	**107**	**0**	**no**
TTLL6	**202**	**733**	**1**	**no**

GENE	transcript	3´ UTR bp	HEXA	CPE prediction
	205	**739**	**1**	**no**
TTLL7	**201**	**4934**	**22**	**no**
	214	**no utr**	**n/a**	**n/a**
TTLL8	**201**	**no utr**	**n/a**	**n/a**
	202	**no utr**	**n/a**	**n/a**
TTLL9	**205**	**1050**	**1**	**no**
	206	**1941**	**2**	**no**
	208	**470**	**0**	**no**
	211	**1942**	**2**	**no**
TTLL10	**201**	**722**	**0**	**no**
	202	**86**	**0**	**no**
	203	**88**	**0**	**no**
TTLL11	**201**	**659**	**0**	**no**
	202	**207**	**1**	**no**
	206	**838**	**2**	
		73	tst1	**activation early strong**
		820	tst2	**no**
TTLL12	**201**	**1386**	**1**	**no**
	204	**405**	**0**	**no**
TTLL13	**202**	**405**	**0**	**no**
	206	**no utr**	**n/a**	**n/a**
CCP1	**201**	**569**	**5**	
		36	tst1	**no**
		147	tst2	**activation early weak**
		543	tst3	**no**
		551	tst4	**no**
		563	tst5	**no**
	202	**567**	**5**	**see 201**
	205	**570**	**5**	**see 201**
	208	**438**	**2**	**see 201**
CCP2	**201**	**580**	**2**	
		393	tst1	**repression**
		567	tst2	**repression**

GENE	transcript	3´ UTR bp	HEXA	CPE prediction
	203	**582**	**2**	**see 201**
	205	**200**	**1**	**activation early weak**
	208	**no utr**	**n/a**	**n/a**
	210	**no utr**	**n/a**	**n/a**
	211	**no utr**	**n/a**	**n/a**
	213	**no utr**	**n/a**	**n/a**
CCP3	**202**	**146**	**1**	**no**
	203	**518**	**2**	**no**
	204	**no utr**	**n/a**	**n/a**
CCP4	**201**	**212**	**0**	**no**
	204	**8861**	**9**	
		811	tst1	**no**
		2399	tst2	**no**
		2595	tst3	**no**
		2764	tst4	**no**
		3002	tst5	**no**
		5501	tst6	**repression**
		5806	tst7	**repression**
		6416	tst8	**repression**
		6598	tst9	**repression**
	205	**no utr**	**n/a**	**n/a**
CCP5	**201**	**66**	**1**	**no**
	202	**357**	**1**	**activation early weak**
	203	**no utr**	**n/a**	**n/a**
	204	**no utr**	**n/a**	**n/a**
	205	**67**	**1**	**no**
	206	**no utr**	**n/a**	**n/a**
	207	**no utr**	**n/a**	**n/a**
	209	**616**	**1**	**Activation early weak**
CCP6	**201**	**no utr**	**n/a**	**n/a**
	202	**696**	**1**	**no**
	203	**272**	**0**	**no**
	204	**1318**	**4**	**repression**
		646	tst1	**repression**

GENE	transcript	3´ UTR bp	HEXA	CPE prediction
		856	tst2	**repression**
		1011	tst3	**repression**
	205	**3039**	**1**	**no**

Table 5. Alternative splice and polyadenylation variants of the PTM enzymes based on the Ensembl database. bp : base pairs, HEXA: hexamer that acts as polyadenylation signal, tst: transcript as defined by the alternative polyadenylation signals, CPE: cytoplasmic polyadenylation element.

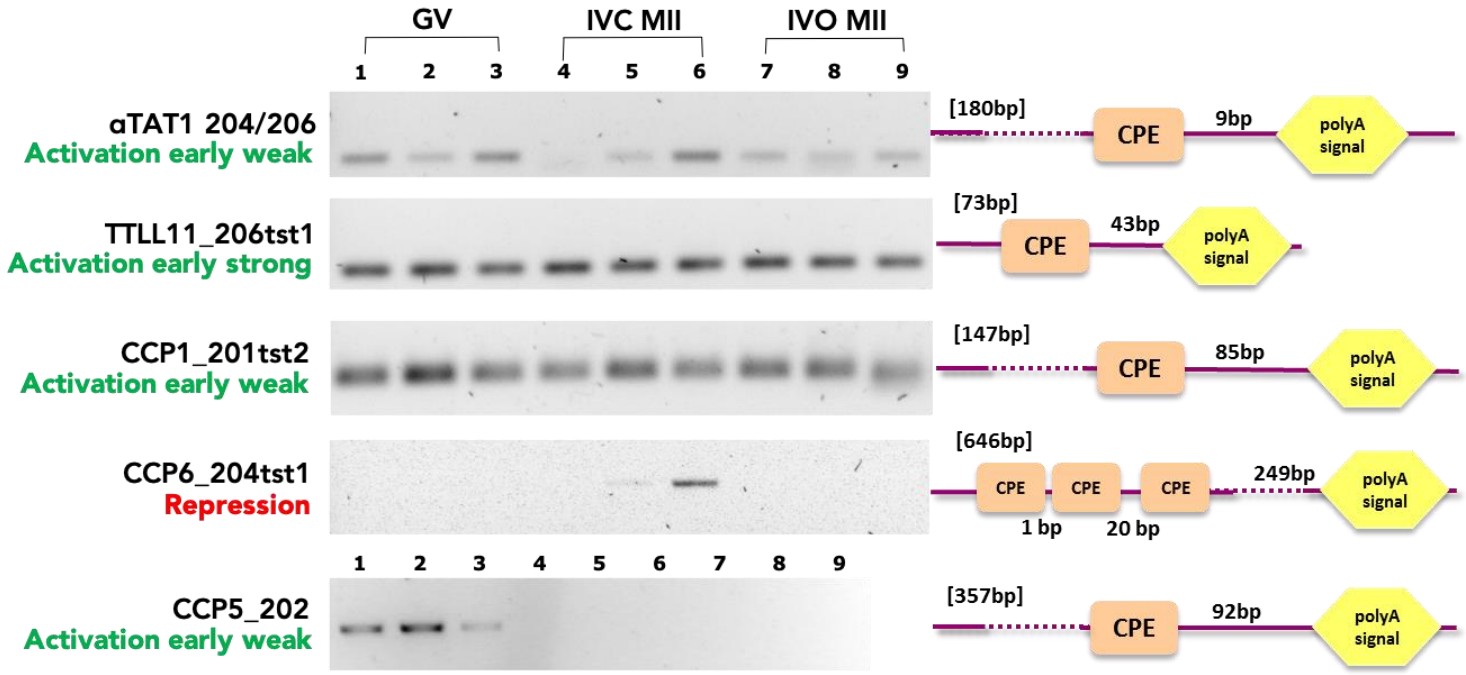

Figure 29. Agarose gel of 3'UTR amplicons as detected by PCR in three samples of GV oocytes (1-3), *in vitro* cultured MII (4-6) and *in vivo* matured MII (7-9). aTAT1_204/206, TTLL11_206transcript1, CCP1_201transcript2, CCP6_204transcript1 and CCP5_202 are shown with their CPE prediction given in green for activation and red for repression. Their 3' UTR configuration is shown in the right panel. bp: base pairs, CPE: cytoplasmic polyadenylation element

3.2) Translation of PTM enzyme transcripts is not regulated by their 3'UTR CPE code

In order to test whether the candidate 3'UTRs regulate translation, we used the following experimental strategy. The 3'UTR of TTLL_206tst1, CCP1_201tst2, CCP5_202 and CCP6_204tst1 were cloned downstream of the coding region of the luciferase gene (Fig.30a). This construct has a T7 promoter upstream of the luciferase ORF, allowing us to generate use in vitro transcription to generate mRNA.

After *in vitro* transcription, the RNA mix solutions (Fig. 30b) were injected in fully grown immature Xenopus oocytes at stage VI (no progesterone exposure) and oocytes that resumed meiosis (4 hours of progesterone exposure). Stage VI are post-vitellogenic oocytes characterized by the appearance of equatorial band. Progesterone is the natural trigger for amphibian ovulation causing germinal vesicle breakdown. The dual luciferase reporter assay revealed no differences in translational regulation throughout meiotic progression (30c).

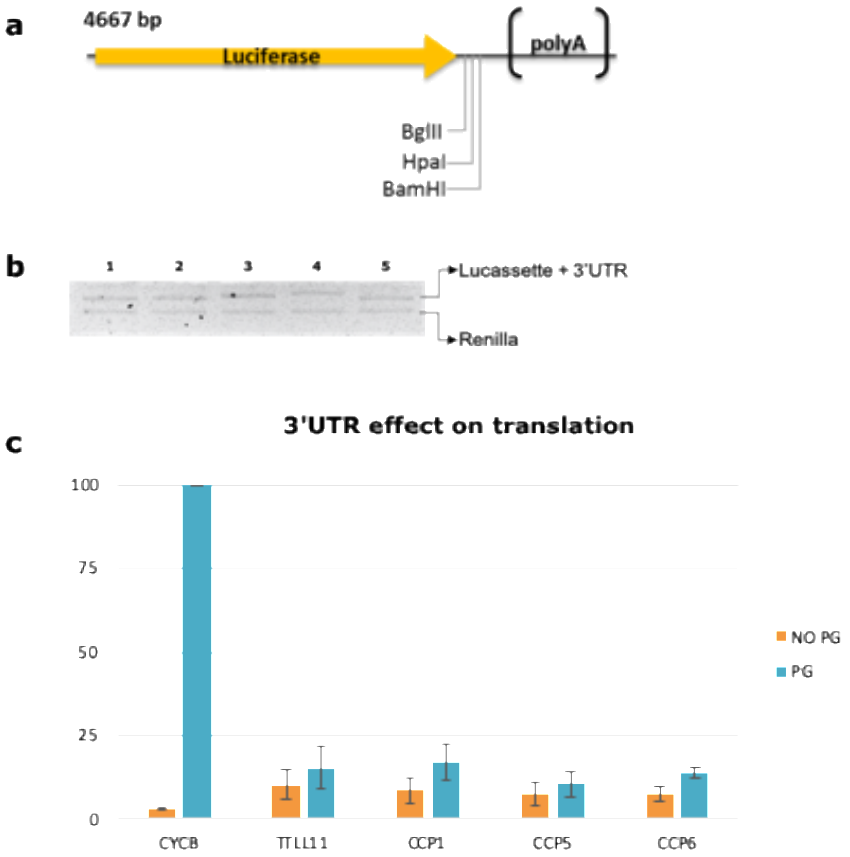

Figure 30. a) The map of the "Lucassette" plasmid featuring the luciferase coding region, the restriction enzyme sites and the polyA sequence. b) Agarose gel with equimolar mixture of Renilla vector RNA with the in vitro transcribed Lucassette recombined with the following 3'UTRs: (1)TTLL11, (2)CCP1, (3)CCP5, (4)CCP6 and (5) cyclinB. c) Normalized expression values of the luciferase transcript when combined with the 3'UTRs of TTLL11, CCP1, CCP5 and CCP6 under no exposure and exposure to progesterone (PG). Error bars ±SD. y'y axis shows expression percentage (UTR of interest/CYCB-PG)*100

Chapter 4. Comparative quantitative analysis of tubulin PTM pattern of the human sperm flagellum of normozoospermic, asthenozoospermic and teratozoospermic samples

The microtubules of the human sperm axoneme were expected to be post-translationally modified as is the case in other animal models (Fouquet *et al.*, 1996; Huitorel *et al.*, 2002; Bosc *et al.*, 2019) and other cell types with stable microtubules such as neurons. We were particularly interested in a potential correlation between PTM and sperm pathologies. Our first objective was to determine the PTM pattern in normozoospermic samples. Second, we sought to determine if there is a correlation between sperm tail tubulin PTM and particular sperm pathologies, namely, asthenozoospermia, in which flagellar movement is impaired, or teratozoospermia which shows abnormal tail morphology. Defining this potential association could offer a molecular explanation for the aberrant phenotypes.

The method of swim-up was previously applied so as to increase the sample homogeneity in terms of motility, as the upper fraction is enriched in motile spermatozoa and can be separated from the remaining less motile cells. However, as the main objective of our experiments became the establishment of the best immunofluorescence conditions for all type of sperm sample diagnosis (including asthenozoospermic) we omitted the step of gradient separation.

As the sperm tail is rich in tubulin and tubulin PTM, we needed to verify that the antibody concentrations applied do not saturate the tail, thus masking any differential PTM pattern along the flagellum (Fig. 33-36). We concluded that the best working antibody dilutions (as indicated by signal differences along the tail) for representing true PTM pattern were 1:1000 for acetylation, 1:200 for branching, 1:200 for polyglutamylation and 1:200 for monoglycylation.

We found the following tubulin modifications in the human flagellum: acetylation, monoglycylation and glutamylation. Their presence was shown with immunofluorescence experiments where co-staining of the tubulin and the modification is performed. There was a characteristic pattern of the signal along the tail for each modification (Fig. 31). Acetylation was marked by an increase in the first percentile of the tail, followed by steady levels which dropped in the last percentile. Monoglycylation had two peaks on the first and last percentile with consistent levels in between. In case of glutamylation, the antibody recognizing the first glutamate (branching) revealed a peak in the first percentile followed by a continuous decrease towards the end of the tail where higher variability and another increase were present. Polyglutamylation signal followed a smoother declining line along the flagellum length.

Preliminary experiments with normozoospermic, asthenozoospermic and teratozoospermic samples revealed overall similar patterns for acetylation and glutamylation between the groups (Fig.32). In particular, acetylation levels were slightly higher in the

normozoospermic sample, followed by the teratozoospermic and the asthenozoospermic. Moreover, the normozoospermic sample marked a steep increase and then decrease in the first part of the tail while the teratozoospermic had a milder curve. Levels were also higher in the normozoospeermic sample in the last part of the tail. For polyglutamylation, the signal pattern is maintained between the groups however normozoospermic tails seem to have lower levels overall. Finally, for branching, asthenozoospermia samples had the highest levels while normozoospermic and teratozoospermic tails were similar.

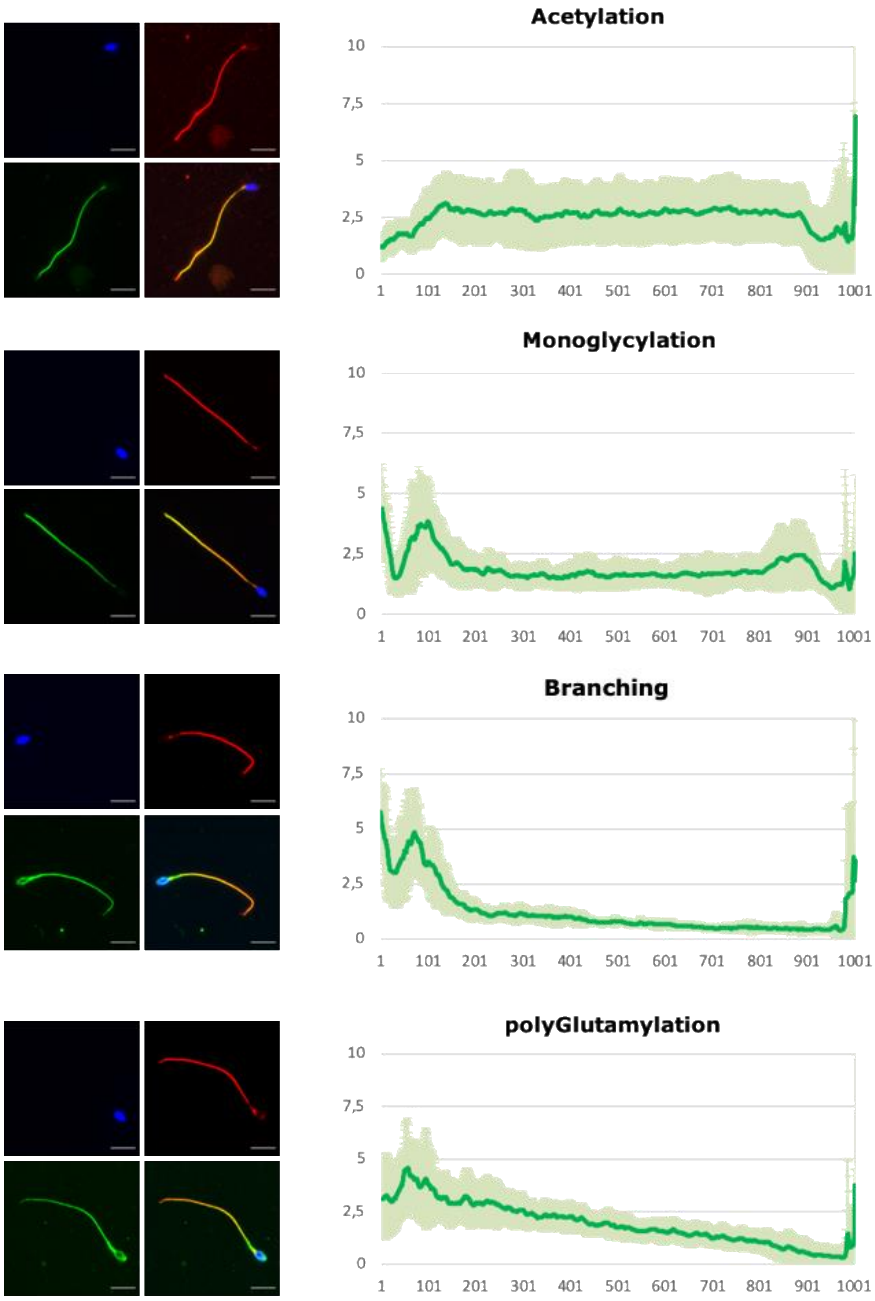

Figure 31. PTM presence and quantification along the sperm flagellum. The left panel shows the modification in green, tubulin in red, DNA in blue and the merged color image. The right panel shows the quantified signal normalized to tubulin. Scale bar 10 µm. x'x axis: tail length divided in 1000 bins

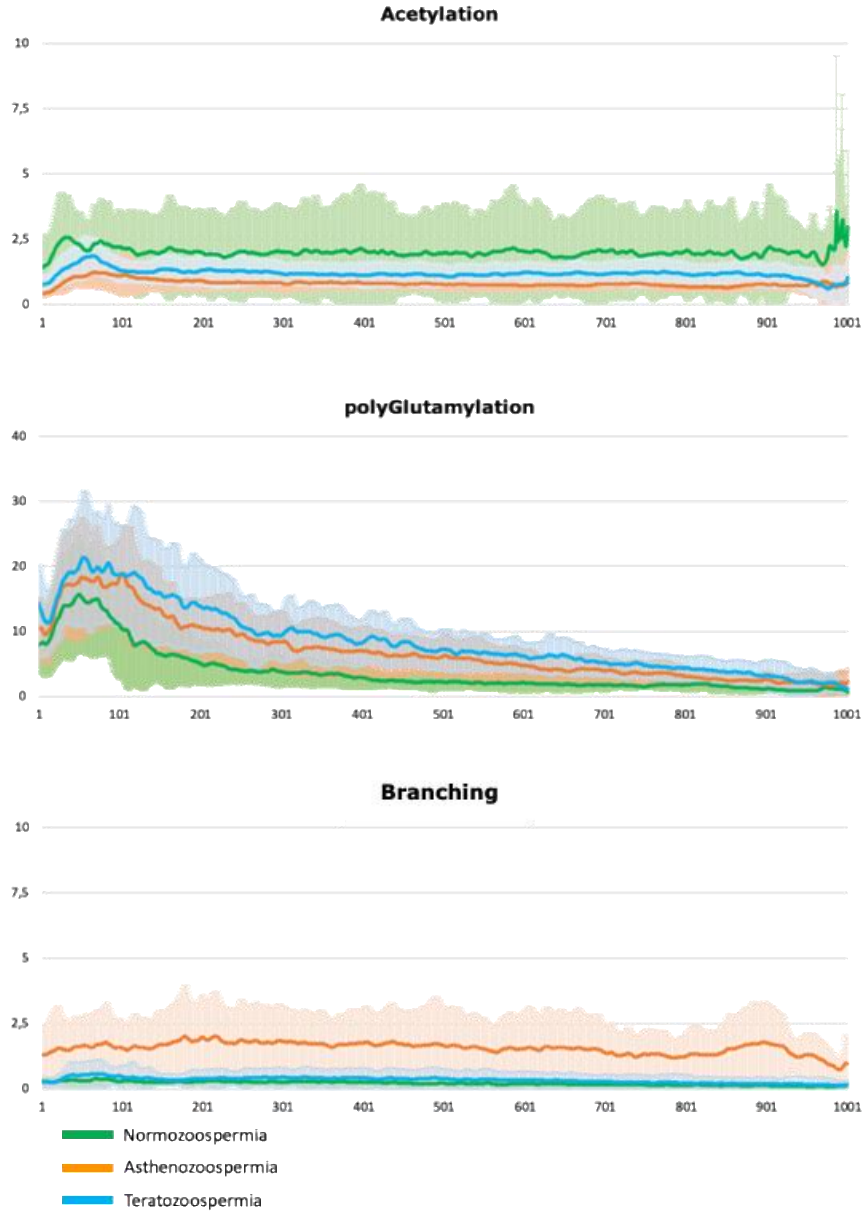

Figure 32. PTM signal of a single normozoospermic donor (n=10 tails measured), three pooled asthenozoospermic donors (n=10 tails measured) and a single teratozoospemic donor (n=10 tails measured). x'x axis: tail length divided in 1000 bins

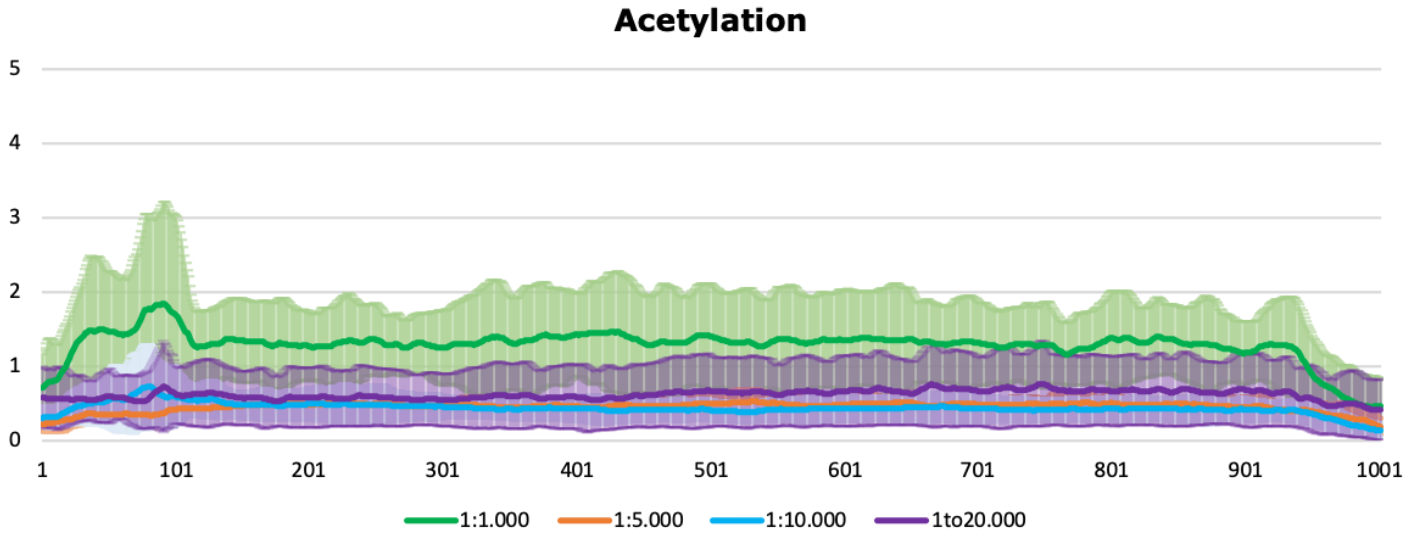

Figure 33. Acetylation antibody titration at dilutions of 1:1.000 (n=10 tails measured), 1:5.000 (n=10 tails measured), 1:10.000 (n=10 tails measured) and 1:20.000 (n=10 tails measured) of a single normozoospermic donor.

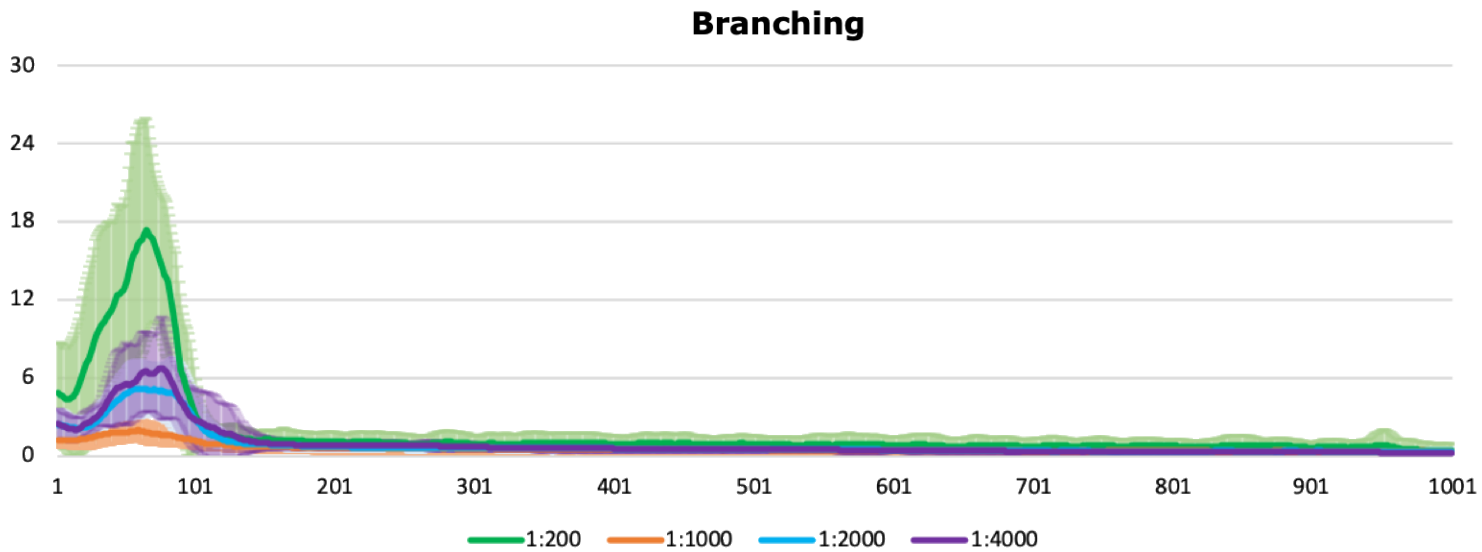

Figure 34. Branching antibody titration at dilutions of 1:200 (n=10 tails measured), 1:1.000 (n=10 tails measured), 1:2.000 (n=10 tails measured) and 1:4.000 (n=10 tails measured) of a single normozoospermic donor.

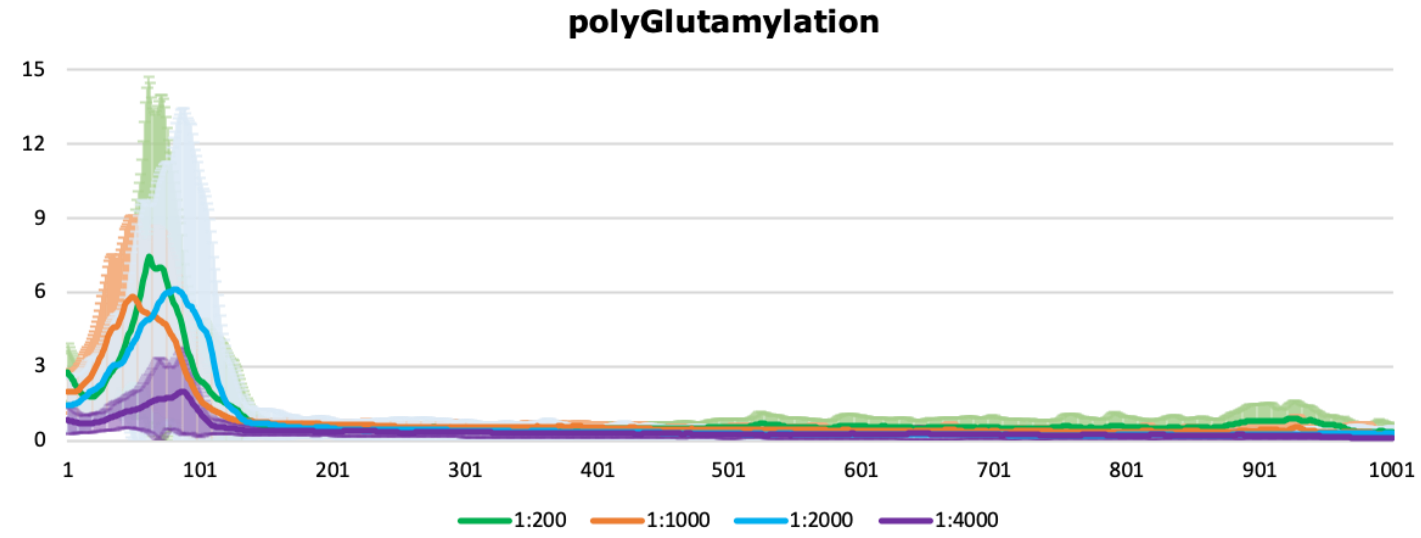

Figure 35. Polyglutamylation antibody titration at dilutions of 1:200 (n=10 tails measured), 1:1.000 (n=10 tails measured), 1:2.000 (n=10 tails measured) and 1:4.000 (n=10 tails measured) of a single normozoospermic donor.

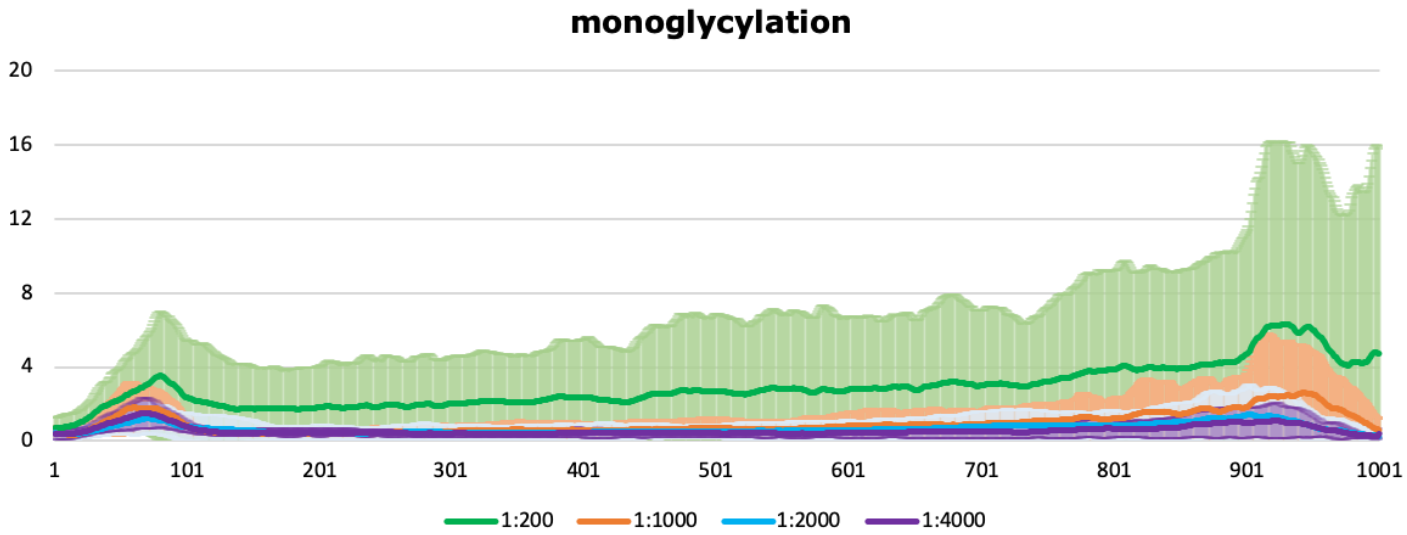

Figure 36. Monoglycylation antibody titration at dilutions of 1:200 (n=10 tails measured), 1:1.000 (n=10 tails measured), 1:2.000 (n=10 tails measured) and 1:4.000 (n=10 tails measured) of a single normozoospermic donor.

DISCUSSION

Discussion

1. Human gametes in basic research

1.1) Oocytes

Studies on human oocytes requires informed consent from the donor or patient. The only ethical limitation related to oocyte research is the inability to fertilize them and culture the resulting embryo for research purposes. In any case, this limitation is not relevant for the present study as all the endpoints in the human oocyte objectives were until the metaphase II arrest. Some technical challenges were met due to certain cellular parameters; transcriptional inactivity during the steps of maturation does not allow for gene editing experiments and low accumulative numbers prevent the use of oocytes for techniques such as western blot or artificial oocyte activation.

The ultimate measure of the oocyte developmental capacity is its ability to be fertilized and survive as an embryo, assuming quality of sperm and the receiving uterus are optimal. Restrictions on *in vitro* fertilization and embryo culture for research purposes allow only indirect study of the oocyte potential to give a healthy embryo. One method used to study the final stages of meiotic maturation is artificial oocyte activation (AOA). Short incubation steps with a calcium ionophore induce the necessary calcium oscillations for the resumption and completion of the second meiotic cycle. Therefore, if a sufficient number of activated MII stage oocytes could be obtained, the development of resulting parthenogenote embryos could be

monitored. This would require obtaining GVs, maturing these GVs to MII stage oocytes *in vitro*, performing AOA and culturing the activated oocytes to the blastocyst stage. However, the low efficiency of each of these steps (GV to MII, 45%; AOA, 5%) and the scarcity of GVs available to us precluded this approach.

COCs that have been removed from their follicular environment resume their meiotic division. Previous study with stimulated cycles reports rates of GV maturation, GV-derived MII fertilization and 2-cell stage cleavage at 67 %, 60% and 85% respectively (Kim *et al.*, 2000). However, arrest at the embryo stage may occur due to multinuclear blastomeres and aneuploidy (Nogueira *et al.*, 2000). Cumulus-stripped GV stage oocytes from stimulated ovaries that were cultured for a prolonged period of time (48h compared to the minimum necessary of 24h) have a lower rate of blastocyst development (Chian and Tan, 2002). Cumulus free partially matured oocytes will mature to the MII stage within 4-6 h of *in vitro* culture and can be fertilized and give rise to 2 cell stage embryos (61% per injected oocyte). The pregnancy rate of tranfer of embryos derived from *in vitro* cultured oocytes is 7.7% (Shu *et al.*, 2007). On the contrary, IVM after the use of endometrial priming in the presence of cumulus cells for 24-48 hours can result in up to 15-17% clinical pregnancy (Smith *et al.*, 2000; Child *et al.*, 2001; Yoon *et al.*, 2001). Acknowledging the low clinical potential of the *in vitro* cultured oocytes, the inclusion of this group in the study aimed at investigating differences related to levels of expression of tubulin PTM.

Our study groups consisted of oocytes with suboptimal characteristics: first, they did not undergo maturation in response to the stimulation signal to which they were exposed *in vivo*; second, *in vitro* culture was performed in the absence of cumulus cells. In the literature, the term '*in vitro* maturation' is used even for our type of samples, however the correct use of the term refers to oocytes that were not exposed to hormones and matured out of the follicle, within their cumulus surrounding cells. This is the reason behind naming our study group '*in vitro* cultured' and not '*in vitro* matured'. These oocytes are intrinsically compromised as they have failed to mature *in vivo*, in addition to potential effects due to the external manipulation process. The nature of their incompetency is attributed to suboptimal regulation of nuclear and cytoplasmic events, which need to be accurately fine-tuned throughout the meiotic stages.

1.2) Sperm

Access to donated sperm samples involves less ethical and technical limitations than the female gametes. As described in the introduction, the amount of spermatozoa per ejaculate on average is sufficient to perform the majority of biochemical and molecular biology techniques such as single cell immunofluorescence, western blot, proteomics analysis etc.

The study of individual sperm tails poses the question of how large should the sample size be to ensure sufficient representation of the population, which is the case in most experiments with cell lines

Another general experimental challenge that applies to sperm samples is that their parameters may also differ between different samples of the same individual due to biological variation (Castilla *et al.*, 2006). Overall, the restrictions of working with sperm samples are less tan the ones that refer to oocytes.

2. The spindles of *in vitro* cultured and *in vivo* matured human oocytes

2.1) Morphometric comparison

A number of studies have compared spindles of oocytes developed *in vivo* or cultured *in vitro*, both in animals and human (Combelles *et al.*, 2002; Albertini *et al.*, 2003; Coticchio *et al.*, 2013b; Ferrer-Vaquer *et al.*, 2019). The endpoint observations of these studies mainly include spindle shape, pole morphology, presence and distribution of MT organizing centres, chromosome alignment and kinetochore-microtubule binding. The initial stage of maturation (GV or non-GV oocytes) and the maturation media used can influence the presence of bipolar spindles with aligned chromosomes (Cekleniak *et al.*, 2001). We recorded the presence of apolar spindles (7%), complete absence of microtubules (9%) or misaligned chromosomes (20%) in *in vitro* cultured oocytes (n=59). These phenotypes were not observed in the *in vivo* matured oocytes (n=37). The proportion of spindle and chromosome aberrations is three times higher in *in vitro* cumulus cell-free culture of human GV oocytes compared to their *in vivo* counterparts (Li *et al.*, 2006). However, MII spindles derived from non-GV oocytes are comparable with those of *in vivo* matured oocytes independently of the *in vitro* culture medium used (Ferrer-Vaquer *et al.*, 2019).

Our observations and measurements indicate that the spindle dimensions are overall consistent apart from the major axis length and the spindle volume, while the double flattened pole phenotype

was more frequent in the *in vitro* cultured group. Our result does not agree with a previous study, which supports that the proportions of pole shape combinations remain stable among *in vivo* matured oocytes, *in vitro* matured ones (in the presence of cumulus cells) and *in vitro* cultured ones (in the absence of cumulus cells) (Coticchio *et al.*, 2013b). Moreover, this study reported a correlation between the double flattened phenotype and chromosomal misalignments as well as an association of single or double focused poles with correct metaphase plate formation. In our experiments, we came across occasional cases of chromosomal dispersion, with a "thicker" metaphase plate however there was no consistent link with the spindle pole phenotype. A possible reason behind the observed differences could the the age of each study population (25.3±4.2 years in our study versus 35.6±4.3 in Coticchio et al).

In vivo meiosis of mouse oocytes results in focused poles with clear γ-tubulin foci, while spindles of *in vitro* matured mouse oocytes present flattened poles with spread distribution of γ-tubulin (Sanfins *et al.*, 2003). This phenotype, combined with ectopic spindle formation far from the oocyte cortex, is observed in mouse oocytes cultured *in vitro* (Rossi *et al.*, 2006). Monkey oocytes have higher rates of asymmetric, tripolar and depolymerized spindles with displaced, lagging and disorganized chromosomes after *in vitro* culture (Yin *et al.*, 2006). Therefore, it is evident that *in vitro* culture somehow affects spindle formation, especially when the oocytes resume prophase I in the absence of their cumulus oophorus. The effect might be detrimental and lead to complete absence of the

structure, a disorganized microtubule mesh or abnormal pole number and/or shape. Spindle formation under both conditions do not seem to have major differences in terms of volume and dimensions, but further research is needed to eventually elucidate whether pole shape changes with *in vitro* culture and what this may mean for chromosome alignment.

Total time of *in vitro* culture was 30-33 h, based on time-lapse microscopy observation that most of the oocytes had extruded a polar body by 25h, which is in agreement with live imaging of human oocyte meiosis (Holubcova *et al.*, 2015). Although higher maturation rates can be achieved by prolongation of the *in vitro* culture, we avoided extending incubation times, as *in vitro* aging can interfere with spindle and chromosomal integrity (Bromfield *et al.*, 2009).

2.2) Tubulin PTM pattern comparison

All the modifications studied were present in human oocytes regardless of whether their meiotic maturation occurred *in vivo* or *in vitro*, with the exception of detyrosination, which was detected at very low levels in *in vivo* oocytes and not at all in *in vitro* cultured oocytes. Quantitative comparisons between signals obtained from different antibodies are not possible due to different binding affinities of each reagent. Signal comparison of the same antibody between individual oocytes is difficult, as the exposure settings differ due to background variability. Even under treatment conditions of the same permeabilization and fixation protocol, each oocyte presented a range of background levels for different antibodies.

Acetylation was overall present both in the *in vitro* cultured and the *in vivo* matured oocytes, suggesting that our *in vitro* culture conditions do not inhibit acetylation enzyme activity. The modification needs to occur during spindle assembly and cannot appear solely by pre-existing acetylated tubulin heterodimers, which implies the presence of catalytic activity. The differences seen in the modification pattern along the spindle microtubules could be due to insufficient (in the case of lack of signal) or unspecific binding (in the case of signal presence). The latter scenario is less likely as antibody specificity was maximized by performing sequential incubation, staining first with anti-tubulin followed by incubation with the antibody against the particular PTM. The antibodies used for all the experiments are commercial and validated for their specificity mainly in cell lines. However, we cannot exclude that various epitopes on the tubulin molecule could be recognized by the antibody in the case of human oocytes under our experimental conditions. The characteristic found in agreement among all oocytes is the segmented signal along the microtubules, which could correlate with specific types of MT fibers or modified tubulin loci.

As described in the introduction, acetylation is mostly found in long-lived (stable) microtubules. In the spindle, microtubules are in a constant polymerization-depolymerization cycle and are therefore in a state of dynamic instability. The metaphase II spindle is stable during meiotic arrest. This stability is required for future completion of the final meiotic division upon fertilization. However, the spindle preservation occurs through continuous microtubule elongation in

the plus-end and severing in the minus-end. In any case, these dynamically unstable microtubules appear to be stable enough for acetylation to occur.

Our results contradict those of Combelles et al 2002 who did an extensive analysis of acetylation throughout human oocyte meiosis under *in vitro* conditions and absence of cumulus cells (Combelles *et al.*, 2002). In this study, acetylation was not detected in the metaphase I nor in metaphase II spindle, but it did appear during anaphase I and on the midbody of telophase I. Metaphase II spindles of *in vivo* matured oocytes also lacked acetylation. One possible explanation might be technical. One apparent difference in the work of Combelles et al. and my work is the use of an initial step of taxol or DMSO incubation of the denuded oocytes in the protocol. Unfortunately, the anti-acetylation antibody clone they use is not described. Throughout their experiments, the specificity of their antibody staining is supported by the fact that signal is observed in anaphase I and telophase I, but is absent from the metaphase I and II spindles, functioning as a negative control. The continuous presence of signal in our oocytes calls into question the specificity of our chosen antibody in oocytes. Our antibody is commercial and has been validated in several cell types, although not oocytes. While the signal we observed is certainly not due to the secondary antibody used, we lack a specific negative control which would require eliminating acetylase activity in oocytes. This loss of function control is not feasible in oocytes. One argument against the results of Combelles *et al* is that the transient nature of the anaphase and telophase

microtubules is somewhat incompatible with the generally accepted correlation of acetylation with microtubule longevity (Howes *et al.*, 2014; Portran *et al.*, 2017). However, this correlation is not absolute. A study in mouse oocytes demonstrated the persistence of acetylation throughout the same meiotic stages of the Combelles *et al* study, while cold treatment experiments revealed the appearance of acetylation in newly formed microtubules (Schatten *et al.*, 1988). Thus, there can be exceptions to the association of acetylation with microtubule stability. Another study in ovine oocytes matured *in vitro* within the cumulus oophorus reports the presence of acetylation in the metaphase II spindle of sheep and lamb oocytes, both fresh (Serra *et al.*, 2018) and cryopreserved (Serra *et al.*, 2019). Overall, a comparative time-course analysis among different mammalian species using the same antibody and staining conditions would help clarify the contradictory findings.

What is the role of acetylation on meiotic spindle dynamics? The presence of acetylation in meiosis I kinetochore microtubules along their entire length, except for their plus end, has been proposed as a marker of poleward tubulin flux in crane-fly spermatocytes (Wilson and Forer, 1997). In the mouse model, metaphase I spindle hyperacetylation induced by knock down of kinesin Kif18a (mediated through its downregulating effect on the Sirt2 deacetylase) results in severe spindle abnormalities and obstruction of polar body extrusion (Tang *et al.*, 2018). Balanced acetylation levels seem to be important for meiosis completion. Therefore, an improvement of the current study would be enabled by quantitative immunofluorescence

analysis, allowing the comparison of acetylation levels between the *in vitro* and the *in vivo* group. As mentioned in the results, quantitative comparison of our data was not possible because exposure settings during imaging had to be altered to maximize the signal to background ratio in each oocyte. A study with higher sample size and simultaneous processing of the compared groups could allow for microscope settings standardization and thus inter- and intra-group comparisons.

As far as the tyrosination cycle is concerned, we observed complete absence of detyrosinated microtubules in *in vitro* oocytes and barely detectable levels in the *in vivo* group. The antibody functionality of the specific batch of antibody used was confirmed in sperm tail immunofluorescence. Moreover, tubulin staining was performed against the β subunit so as to avoid any steric inhibition between the primary antibodies. Thus, according to our verification steps, our result represents a true lack of detyrosinated microtubules and not an artifact. This suggests that all the microtubules remain tyrosinated, are rapidly re-tyrosinated or have exited the tyrosination cycle by forming Δ2-tubulin. Indeed, we do observe the reverse modification in both groups with the signal being more concentrated in the poles for the *in vivo* matured oocytes, compared to the in vitro matured oocytes. Three samples are also characterized by a slight signal intensity difference which decreases from the cytosol towards the cortex pole. However, as this pattern is not consistent within the group, a larger sample size is needed to confirm the observation. Ovine metaphase II spindles also consist of tyrosinated microtubules,

while detyrosinated microtubules are completely absent (Serra *et al.*, 2018).

Recent studies have reported interesting results regarding the role of tyrosination in chromosome interactions with microtubules. As described also in the introduction, in the case of mitotic cells, CENP-E mediated chromosome congression (the alignment of chromosomes in the equator) is dependent on detyrosinated microtubules (Barisic *et al.*, 2015). Our results suggest that a different molecular pathway, not based on microtubule detyrosination must be required to drive pole-proximal chromosomes towards the equator. The second study, also mentioned in the introduction, demonstrates that the tyrosination gradient in metaphase I mouse spindles guides the inheritance of selfish centromeres, a phenomenon known as meiotic drive (Akera *et al.*, 2017). It would be interesting to investigate whether such a gradient exists in metaphase I spindles of human oocytes, which can also present preferential segregation of dominant centromeres (Daniel, 2002).

Positive Δ2-tubulin staining suggests that detyrosination occurs during oocyte maturation as the C-terminus tyrosine removal is a prerequisite for the subsequent glutamic acid elimination. As this type of modification is irreversible, the tubulin cannot re-enter the tyrosination cycle, but can still undergo all other post-translational modifications. The ovine oocyte MII spindle screening for tubulin PTM reports conflicting findings, as no Δ2-tubulin is detected (Serra *et al.*, 2018). This is the second time that we observe contradicting

results when comparing the MII spindle modification profile between different organisms. Acetylation is absent in mouse oocytes but present in human and ovine ones, while Δ2-tubulin appears only in human and not in the ovine ones (no data are available for mouse). The detection of Δ2-tubulin was actually not expected as this modification is found in highly stable microtubules, like the axons of neurons, the centrosomes of fibroblasts, the cilia of the adrenal cortical cells and the axoneme of sperm flagella (Paturle-Lafanechère *et al.*, 1994). One possible explanation could be that the human MII spindle needs to maintain its stability for a long period of time until fertilization, which requires long-lived microtubules.

Finally, the results for microtubule glutamylation status were antibody dependent. Polyglutamylation signal was detected with the clone B3 antibody but the absence of branching signal (GT335 antibody) did not confirm the existence of glutamic chains. Even when the GT335 clone anti-glutamylation antibody was used individually (no previous staining for tubulin), no signal was detected. Thus, either the positive signal from clone B3 antibody is non-specific or for some unknown reason the clone GT335 antibody does not function under our conditions or for some reason cannot access its epitope. Upon comparison with the ovine MII spindles, polyglutamylation was not detected, even though the same antibody was used (clone B3) (Serra *et al.*, 2018). Such discrepancies highlight the need for more experiments, with additional negative controls, so as to draw stronger conclusions.

Glutamylation is the second modification that is found most commonly in brain tubulin. In mitotic spindles, centrosome-associated C1orf96/Centriole, Cilia and Spindle-Associated Protein (CSAP) is localized in glutamylated microtubules of mitotic spindles, promoting their stabilization (Ohta *et al.*, 2015). However, glutamylation is not exclusively linked to microtubule stability as it can promote shrinking through interactions with severing enzymes (Lacroix *et al.*, 2010; Valenstein *et al.*, 2016). Its presence in kinetochore microtubules of mitotic spindles (Barisic and Maiato, 2016) complies with the role it can play in severing, promoting the 'pacman-flux' mechanism for moving chromosomes (Zhang *et al.*, 2007). Thus, it could also act as a meiotic microtubule catastrophe mechanism by interacting with katanin, spastin or fidgetin, guiding the chromosomes to the opposite poles.

3. Tubulin PTM enzymes throughout oocyte maturation

The presence of modified microtubules indicates the presence of catalytic activity of PTM enzymes. As the microtubules form at the time of spindle assembly, the detected modifications cannot be all accumulated on the soluble tubulin prior to polymerization. The reason behind this is that some of the modifications are catalyzed by enzymes that preferentially bind to microtubules. Based on this premise, it is expected that the enzymes are present during oocyte meiosis. Direct demonstration of enzyme presence requires robust antibodies for the PTM enzymes, which are lacking. We sought to determine whether PTM enzymes are present at the transcript level. This approach has obvious limitations, as transcript presence does not guarantee protein presence or protein activity, while transcript absence is not proof of protein absence. This is especially true for the oocyte, which is known to be transcriptionally inactive with complex and strict regulatory mechanisms at the stage of protein translation. Many of the proteins necessary for maturation accumulate prior to germinal vesicle breakdown so that they can immediately be recruited during subsequent maturation, while the transcript pool can be maintained in a dormant state until the point of embryonic genome activation. Having this consensus view of oocyte RNA control, we can proceed to the interpretation of our results.

Transcript levels characterization in individual oocytes was performed by cDNA library creation and subsequent qPCR in four

study groups (GV, IVC, IVO, FTM). Our chosen method of cDNA library creation was based on magnetic bead total RNA isolation, known as Pico Profiling, initially optimized for 10 cells, (Gonzalez-Roca *et al.*, 2010) and subsequently applied for single oocytes (Vassena *et al.*, 2011; Barragán *et al.*, 2017). Expression profiling of individual oocytes poses the challenges of efficiency and accuracy due to stochastic events and increased chance of technical noise. The advantage of this method is the application of whole transcriptome amplification in a way that maintains the relative abundance of the initial transcript pool. It is also optimized for relative differences between samples. Technologies using logarithmic and linear amplification methods work efficiently with nanograms of RNA as starting quantity, while this scalable amplification can be performed with picograms of RNA.

As a limited number of oocytes were available throughout the project's duration, we wanted to extract as much information as possible and preserve the genetic variability among the samples, which is the reason behind processing the oocytes individually. The fact that the oocytes were retrieved from hormonally stimulated donors can affect the inter oocyte variability within the same group. In a natural cycle, a cohort of GVs enters a growth phase resulting to one, or less often two mature oocytes. However, this series of events is overruled resulting to greater heterogeneity between the oocytes (Steuerwald *et al.*, 2000; Barragán *et al.*, 2017).

Aiming to perform comparative analysis between all the study groups, it was necessary to find a set of reference genes that remain

stable throughout maturation *in vivo, in vitro* culture as well as maturation failure. The initial list was chosen based on a previous study on reference genes for spermatozoa which found that sample storage and the RNA extraction technique can influence gene stability (Barragán *et al.*, 2015). Therefore, our goal was to determine the optimal reference genes for our type of cells. The six genes (ACTB, RPLP1, GAPDH, DNMT1, SHDA, UBC) with the highest expression stability M<0.5 and coefficient of variation CV<0.25 according to the geNORM algorithm were used to normalize the expression values. The normalization error is higher when a single reference gene is used, while the inclusion of three or more genes increases the robustness of the normalization factor (Vandesompele *et al.*, 2002). It is noteworthy at this point that housekeeping gene stability may not only vary between tissues but between organisms as well. For example, ACTB is not consistently expressed throughout maturation in mouse, bovine and buffalo oocytes (Mamo *et al.*, 2007; Habermann-Macabelli *et al.*, 2014).

An immediate observation after the analysis of the expression profile is that GV transcript levels are never lower than those of the mature oocytes, which is in agreement with the repression of transcription during maturation. Representative enzymes are present for all the types of modifications, except for glycylation. As glycylation is a modification detected in cilia and flagella, never observed in spindle microtubules, this observation was expected.

The inclusion of failed to mature oocytes (both *in vivo* and *in vitro* culture) reveals differences with all the other groups. When comparing them to GV oocytes, it is important to keep in mind that each GV could also potentially be a failed to mature oocyte. The observed higher NAA50 levels and lower TTLL4 levels could have been as such from the GV stage, actively playing a role in the inhibition of maturation or be downstream targets of other factors that are accumulating within the apoptotic oocyte. In any case, this difference, although slight, is not observed in the mature oocytes, which keep comparable levels with the GV. Assuming that the increased levels of the NAA50 transcripts reflect higher levels of enzymatic activity, it can be argued that the increase of acetylated soluble β-tubulin is contributing to the phenotype by inhibiting microtubule polymerization (Chu *et al.*, 2011). Nevertheless, we collected only the oocytes that failed to mature at the initial stage of germinal vesicle breakdown, when microtubules are not playing an immediate role, so the effects, if any, must be indirect.

In the case of TTLL6, there is a decrease in the transcript levels as maturation progresses *in vivo* while this is not observed in the *in vitro* culture. The difference is slight so variations in glutamylation levels on the spindle microtubules of IVC and IVO oocytes would not be expected. Moreover, the redundancy of the TTLL enzymes' function might mask any difference in specific enzyme activity. Interestingly, out of the two detyrosinases that have been described so far, VASH1 and VASH2, only VASH1 was found in oocytes. Overall, its levels are minimal apart from some exceptions in the GV and the FTM group. In the spindle imaging experiments, we could not detect any

detyrosination, however the modification must happen if the Δ2-tubulin observation is valid.

The majority of the enzymes remains stable among the groups under study. As previously mentioned, we could not retrieve any information on protein presence. The dual luciferase reporter assay offered a verifiable method for determining the translational fate of our transcripts of interest. The limitation of the system is that it cannot detect protein presence per se, thus it is an indirect approach. Since the libraries were made of total RNA and the primers used for the qPCR experiments were not transcript specific we had to perform a thorough analysis of the described alternative spliced variants. The candidates under CPE regulation and human oocyte presence were subsequently tested in Xenopus oocytes. CPE-mediated regulation is maintained as a mechanism of translational control in Xenopus, mice and human samples (Dai *et al.*, 2018).

The PTM enzymes transcripts that we detected in at least one group of human oocytes were αTAT1_204/206, TTLL11_206transcript1, CCP1_201transcript2, CCP5_202 and CCP6_204. CCP5_202 was found only at the GV stage, which suggests that the transcript is eliminated from the detectable mRNA pool. Moreover, CCP6_204 was present in only two out of three *in vitro* cultured oocytes posing the question of how can the transcript appear selectively in the mature status of certain oocytes. The amplified band's specificity was verified through sequencing so it could be very low initials transcript levels in combination with the stochastic nature of PCR that led to

the observed results. We did not manage to clone αTAT1_204/206 so we proceeded with the rest of the candidates. Only CCP6_204 was predicted to be repressed in the germinal vesicle stage while the others had a prediction of activation as maturation occurs. The question generated is why the luciferase assays did not confirm the CPE prediction. Although the positive control, cyclin B, works efficiently, we did not include negative controls, such as the luciferase plasmid with a random sequence as a UTR or the CPE element mutated, as the initial objective was to check for the overall UTR sequence. The expected levels for activation would be at least 25% of the cyclin B control. CCP5_202 3' UTR could have some other regulatory region, which overrules the CPE effect, as its length is quite extended (~500 bp). Nevertheless, CCP1 and TTLL11 are not expected to have additional regulatory elements in their shorter sequences. As the recombined plasmids were sequenced and the RNA integrity was confirmed in a gel, it must be the downstream technical processing that somehow interfered with the activation of translation.

4. Sperm tail PTM patterns

Sperm evaluation is based on basic parameters such as concentration, morphology and motility, which has not changed in several decades. The etiologies of sperm pathologies may be found in the process of spermatogenesis, leading to oligozoospermia or even azoospermia or the last stage of spermatozoon formation affecting cell shape and movement. Although the sperm tail is not involved in zygote generation or embryo development, it is the spermatozoon motion engine needed to approach the oocyte. Our preliminary analysis involved a technique recently developed by a former colleague in the lab (Dr. F. Amargant) which, when fully developed, will allow quantification of tubulin PTM along the length of the sperm tail. This technique has the potential to elucidate basic molecular mechanisms underlying sperm tail defects as well as possibly find practical diagnostic applications.

We focused on acetylation, glutamylation and monoglycylation, as these are the modifications most prevalently found along the sperm tails (Fouquet *et al.*, 1994; Kann *et al.*, 1998). Only one previous study has shown the decrease of acetylation in asthenozoospermia (Bhagwat *et al.*, 2014). Our results are in agreement with this finding, as acetylation levels are the lowest (Fig.31). However further experiments need to be performed with the optimized antibody dilutions and proper statistical comparison.

Considering that the sperm tail microtubules are rich in tubulin PTM we performed the antibody titration experiments so as to test for signal saturation. The PTM pattern along the tail was maintained with the signal decreasing in higher dilutions, which was expected. The lowest antibody dilution resulted to signal with the highest variability in signal intensity. Nevertheless, for all antibodies tested, a loss of signal pattern was observed in higher dilutions. Thus we concluded that the initial dilutions were within a range that did not saturate the epitopes but was sufficient to reveal the signal intensity differences along the tail, corresponding to the modification sites distribution.

The optimization of the protocol performed with the titration experiments provides the conditions for performing quantitative analysis between samples of different diagnosis. Moreover, this technique allows for examination of the PTM along the different parts of the tail, where some PTM may be enriched. Acetylation, branching, polyglutamylation and monoglycylation can be compared among samples of normal and impaired morphology and motility. The statistical test for this type of series of data would need to be applied which will allow making quantitative correlations about the sperm tail tubulin PTM pattern and the tail properties.

Conclusions

1. This is the first study to show the presence of acetylation, Δ2-tubulin, tyrosination and polyglutamylation in the MII spindle of human oocytes cultured *in vitro* and matured *in vivo*.

2. Spindles of *in vitro* cultured oocytes differ from the ones of *in vivo* matured oocytes in pole shape (flattened poles) and size (smaller).

3. Absence of VASH1 mRNA in the matured oocytes is in agreement with the absence of detyrosinated microtubules. However, detyrosinase activity is required for Δ2-tubulin formation, suggesting the presence of VASH1 protein or other novel detyrosinase.

4. Seven PTM enzyme genes are differentially expressed at the transcript level, although the overall detected differences are small (< 2-fold).

5. PTM enzyme transcript 3´ UTRs with activation prediction only slightly increase the translation of luciferase (not statistically significant change, $p>0.05$).

6. PTM antibody concentrations have been standardized for sperm quantitative immunofluorescence experiments with preliminary results showing slightly different levels for polyglutamylation and branching in teratozoospermia and asthenozoospermia, respectively.

Bibliography

Adhikari D, Liu K. The regulation of maturation promoting factor during prophase I arrest and meiotic entry in mammalian oocytes. *Mol Cell Endocrinol* [Internet] 2014;**382**:480–487. Elsevier Ireland Ltd.

Aillaud C, Bosc C, Peris L, Bosson A, Heemeryck P, Dijk J Van, Friec J Le, Boulan B, Vossier F, Sanman LE, *et al.* Vasohibins/SVBP are tubulin carboxypeptidases (TCP) that regulate neuron differentiation. *Science (80-)* [Internet] 2017;**358**:1448–1453. American Association for the Advancement of Science.

Akella JS, Wloga D, Kim J, Starostina NG, Lyons-Abbott S, Morrissette NS, Dougan ST, Kipreos ET, Gaertig J. MEC-17 is an alpha-tubulin acetyltransferase. *Nature* [Internet] 2010;**467**:218–222. Nature Research.

Akera T, Chmátal L, Trimm E, Yang K, Aonbangkhen C, Chenoweth DM, Janke C, Schultz RM, Lampson MA. Spindle asymmetry drives non-Mendelian chromosome segragation. *Science (80-)* 2017;**358**:668–672.

Albertini DF. The Mammalian Oocyte. *Knobil Neill's Physiol Reprod Two-Volume Set* 2014;

Albertini DF, Sanfins A, Combelles CMH. Origins and manifestations of oocyte maturation competencies. *Reprod Biomed Online* 2003;**6**:410–415. Reproductive Healthcare Ltd.

Alushin GM, Lander GC, Kellogg EH, Zhang R, Baker D, Nogales E. High-Resolution microtubule structures reveal the structural transitions in αβ-tubulin upon GTP hydrolysis. *Cell* 2014;**157**:1117–1129. Cell Press.

Amargant F, Barragan M, Vassena R, Vernos I. Insights of the tubulin code in gametes and embryos: from basic research to potential clinical applications in humans†. *Biol Reprod* [Internet] 2018;**100**:575–589.

Baerwald AR, Adams GP, Pierson RA. Ovarian antral folliculogenesis during the human menstrual cycle: A review. *Hum Reprod Update* 2012;**18**:73–91.

Barisic M, Maiato H. The Tubulin Code: A Navigation System for Chromosomes during Mitosis. *Trends Cell Biol* [Internet] 2016;**26**:766–775. Elsevier Ltd.

Barisic M, Silva Sousa R, Tripathy SK, Magiera MM, Zaytsev A V, Pereira AL, Janke C, Grishchuk EL, Maiato H. Microtubule detyrosination guides chromosomes during mitosis. *Science (80-)* 2015;**348**:799–803.

Barnes FL, Crombie A, Gardner DK, Kausche A, Lacham-Kaplan O, Suikkari A-M, Tiglias J, Wood C, Trounson AO. *Blastocyst development and birth after in-vitro maturation of human primary oocytes, intracytoplasmic sperm injection and assisted hatching* [Internet]. *Hum Reprod* [Internet] 1995;**10**:.

Barra HS, Rodriguez JA, Arce CA, Caputto R. A soluble preparation from rat brain that incorporates into its own proteins arginine by a ribonuclease-sensitive system and tyrosine by a ribonuclease-insensitive system. *J Neurochem* 1973;**20**:97–108. Pergamon Press.

Barragán M, Martínez A, Llonch S, Pujol A, Vernaeve V, Vassena R. Effect of ribonucleic acid (RNA) isolation methods on putative reference genes messenger RNA abundance in human spermatozoa. *Andrology* 2015;**3**:797–804. Blackwell Publishing Ltd.

Barragán M, Pons J, Ferrer-Vaquer A, Cornet-Bartolomé D, Schweitzer A, Hubbard J, Auer H, Rodolosse A, Vassena R. The transcriptome of human oocytes is related to age and ovarian reserve. *Mol Hum Reprod* 2017;**23**:535–548. Oxford University Press.

Belt-Dusebout AW van den, Spaan M, Lambalk CB, Kortman M, Laven JSE, Santbrink EJP van, Westerlaken LAJ van der, Cohlen BJ, Braat DDM, Smeenk JMJ, *et al.* Ovarian Stimulation for In Vitro Fertilization and Long-term Risk of

Breast Cancer. *JAMA* [Internet] 2016;**316**:300. American Medical Association.

Berezniuk I, Vu HT, Lyons PJ, Sironi JJ, Xiao H, Burd B, Setou M, Angeletti RH, Ikegami K, Fricker LD. Cytosolic Carboxypeptidase 1 Is Involved In Processing α- and β-tubulin. *J Biol Chem* [Internet] 2012;**287**:6503–6517.

Bhagwat S, Dalvi V, Chandrasekhar D, Matthew T, Acharya K, Gajbhiye R, Kulkarni V, Sonawane S, Ghosalkar M, Parte P. Acetylated α-tubulin is reduced in individuals with poor sperm motility. *Fertil Steril* 2014;**101**:. Elsevier Inc.

Bobinnec Y, Moudjou M, Fouquet JP, Desbruyères E, Eddé B, Bornens M. Glutamylation of centriole and cytoplasmic tubulin in proliferating non-neuronal cells. *Cell Motil* [Internet] 1998;**39**:223–232. John Wiley & Sons, Ltd.

Bolcun-filas E, Handel MA. Meiosis : The Chromosomal Foundation of Reproduction. *Biol Reprod* 2018;**ioy021**:.

Bonnet C, Boucher D, Lazereg S, Pedrotti B, Islam K, Denoulet P, Larcher JC. Differential Binding Regulation of Microtubule-associated Proteins MAP1A, MAP1B, and MAP2 by Tubulin Polyglutamylation. *J Biol Chem* 2001;**276**:12839–12848.

Bosc C, Andrieux A, Janke C, Bieche I, Chemlali W, Martinez G, Straub J, Arnoult C, Geimer S, Giordano T, *et al.* Loss of the deglutamylase CCP5 perturbs multiple steps of spermatogenesis and leads to male infertility. *J Cell Sci* 2019;**132**:jcs226951.

Bowles J, Knight D, Smith C, Wilhelm D, Richman J, Mamiya S, Yashiro K, Chawengsaksophak K, Wilson MJ, Rossant J, *et al.* Retinoid signaling determines germ cell fate in mice. *Science (80-)* 2006;**312**:596–600.

Bromfield JJ, Coticchio G, Hutt K, Sciajno R, Borini A, Albertini DF. Meiotic spindle dynamics in human oocytes following slow-cooling cryopreservation. *Hum Reprod* 2009;**24**:2114–2123.

Bryan J, Wilsont L. Are Cytoplasmic Microtubules Heteropolymers?

Proc Natl Acad Sci [Internet] 1971;**8**:1762–1766.

Castilla JA, Álvarez C, Aguilar J, González-Varea C, Gonzalvo MC, Martínez L. Influence of analytical and biological variation on the clinical interpretation of seminal parameters. *Hum Reprod* 2006;**21**:847–851. Oxford University Press.

Cekleniak NA, Combelles CMH, Ganz DA, Fung J, Albertini DF, Racowsky C. A novel system for in vitro maturation of human oocytes. *Fertil Steril* 2001;**75**:1185–1193.

Cha K, Jung Jin Koo Md, Jae Ko J, Dong Hee Choi M, Yul Han S, Ki Yoon T. Pregnancy after in vitro fertilization of human follicular oocytes collected from nonstimulated cycles, their culture in vitro and their transfer in a donor oocyte program*. *Fertil Steril* [Internet] 1991;**55**:109–113.

Cha KY, Chian RC. Maturation in vitro of immature human oocytes for clinical use. *Hum Reprod Update* 1998;**4**:103–120.

Chaaban S, Brouhard GJ. A microtubule bestiary: structural diversity in tubulin polymers. *Mol Biol Cell* [Internet] 2017;**28**:2924–2931.

Chen B, Li B, Li D, Yan Z, Mao X, Xu Y, Mu J, Li Q, Jin L, He L, *et al.* Novel mutations and structural deletions in TUBB8: expanding mutational and phenotypic spectrum of patients with arrest in oocyte maturation, fertilization or early embryonic development. *Hum Reprod* [Internet] 2017;**32**:457–467.

Chen B, Wang W, Peng X, Jiang H, Zhang S, Li D, Li B, Fu J, Kuang Y, Sun X, *et al.* The comprehensive mutational and phenotypic spectrum of TUBB8 in female infertility. *Eur J Hum Genet* [Internet] 2018;Available from: http://www.nature.com/articles/s41431-018-0283-3.

Chen M, Heilbronn LK. The health outcomes of human offspring conceived by assisted reproductive technologies (ART). *Jounral Dev Orig Heal Dis* [Internet] 2017;**8**:388–402.

Chian RC, Tan SL. Maturational and developmental competence of cumulus-free immature human oocytes derived from stimulated

and intracytoplasmic sperm injection cycles. *Reprod Biomed Online* [Internet] 2002;**5**:125–132. Reproductive Healthcare Ltd, Duck End Farm, Dry Drayton, Cambridge CB23 8DB, UK.

Child TJ, Abdul-Jalil AK, Gulekli B, Lin Tan S. In vitro maturation and fertilization of oocytes from unstimulated normal ovaries, polycystic ovaries, and women with polycystic ovary syndrome. *Fertil Steril* [Internet] 2001;**76**:936–942. Elsevier.

Choudhary C, Kumar C, Gnad F, Nielsen ML, Rehman M, Walther TC, Olsen J V., Mann M. Lysine acetylation targets protein complexes and co-regulates major cellular functions. *Science* [Internet] 2009;**325**:834–840.

Chu C-W, Hou F, Zhang J, Phu L, Loktev A V, Kirkpatrick DS, Jackson PK, Zhao Y, Zou H. A novel acetylation of β-tubulin by San modulates microtubule polymerization via down-regulating tubulin incorporation. *Mol Biol Cell* [Internet] 2011;**22**:448–456.

Claman P, On O, Cheung AP, Goodrow GJ, On M, Hughes EG, On H, Min JK, On C, Roberts J, *et al. The Diagnosis and Management of Ovarian Hyperstimulation Syndrome*. 2011;

Cobo A, Pérez S, los Santos MJ De, Zulategui J, Domingo J, Remohí J. Effect of different cryopreservation protocols on the metaphase II spindle in human oocytes. *Reprod Biomed Online* [Internet] 2008;**17**:350–359. Reproductive Healthcare Ltd, Duck End Farm, Dry Drayton, Cambridge CB23 8DB, UK.

Combelles CMH, Cekleniak NA, Racowsky C, Albertini DF. Assessment of nuclear and cytoplasmic maturation in in-vitro matured human oocytes. *Hum Reprod* 2002;**17**:1006–1016.

Cooper TG, Noonan E, Eckardstein S von, Auger J, Baker HWG, Behre HM, Haugen TB, Kruger T, Wang C, Mbizvo MT, *et al.* World Health Organization reference values for human semen characteristics. *Hum Reprod Update* 2009;**16**:231–245.

Coticchio G, Albertini DF, Santis L De. *Oogenesis*. 2013a;. Springer: London.

Coticchio G, Guglielmo MC, Dal Canto M, Fadini R, Mignini Renzini M, Ponti E De, Brambillasca F, Albertini DF, Canto MD, Fadini R, *et al.* Mechanistic foundations of the metaphase II spindle of human oocytes matured in vivo and in vitro. *Hum Reprod* [Internet] 2013b;**28**:3271–3282.

D. Katsetos C, Draber P. Tubulins as Therapeutic Targets in Cancer: from Bench to Bedside. *Curr Pharm Des* 2012;**18**:2778–2792. Bentham Science Publishers Ltd.

Dai X-X, Jiang J-C, Sha Q-Q, Jiang Y, Ou X-H, Fan H-Y. A combinatorial code for mRNA 3′-UTR-mediated translational control in the mouse oocyte. *Nucleic Acids Res* [Internet] 2018;Available from: https://academic.oup.com/nar/advance-article/doi/10.1093/nar/gky971/5134329.

Daniel A. Distortion of female meiotic segregation and reduced male fertility in human Robertsonian translocations: Consistent with the centromere model of co-evolving centromere DNA/centromeric histone (CENP-A) [5]. *Am J Med Genet* 2002;**111**:450–452.

Derks-Smeets IAP, Schrijver LH, Die-Smulders CEM de, Tjan-Heijnen VCG, Golde RJT van, Smits LJ, Caanen B, Asperen CJ van, Ausems M, Collée M, *et al.* Ovarian stimulation for IVF and risk of primary breast cancer in BRCA1/2 mutation carriers. *Br J Cancer* 2018;**119**:357–363. Nature Publishing Group.

Dijk J van, Rogowski K, Miro J, Lacroix B, Eddé B, Janke C. A Targeted Multienzyme Mechanism for Selective Microtubule Polyglutamylation. *Mol Cell* 2007;**26**:437–448.

Duncan FE, Hornick JE, Lampson MA, Schultz RM, Shea LD, Woodruff TK. Chromosome cohesion decreases in human eggs with advanced maternal age. *Aging Cell* 2012;**11**:1121–1124.

Dunn S, Morisson EE, Liverpool TB, Molina-París C, Cross RA, Alonso MC, Peckham M. Differential trafficking of Kif5c on tyrosinated and detyrosinated microtubules in live cells. *J Cell Sci* 2008;**121**:1085–1095.

Edde B, Rossier J, Caer JP Le, Desbruyeres E, Gros F, Denoulet P,

Eddé B, Rossier J, Caer JP Le, Desbruyères E, *et al.* Posttranslational glutamylation of alpha-tubulin. *Science (80-)* [Internet] 1990;**247**:83 LP – 85.

Edson MA, Nagaraja AK, Matzuk MM. The mammalian ovary from genesis to revelation. *Endocr Rev* 2009;**30**:624–712.

Edwards RG. Maturation in vitro of Mouse, Sheep, Cow, Pig, Rhesus Monkey and Human Ovarian Oocytes. *Nature* [Internet] 1965;**208**:349–351. Nature Publishing Group.

Erck C, Peris L, Andrieux A, Meissirel C, Gruber AD, Vernet M, Schweitzer A, Saoudi Y, Pointu H, Bosc C, *et al.* A vital role of tubulin-tyrosine-ligase for neuronal organization. *Proc Natl Acad Sci U S A* 2005;**102**:7853–7858.

Ersfeld K, Web J, Plessmann U, Dodemont H, Gerke V, Weber K. Characterization of the Tubulin-Tyrosine Ligase. *J Cell Biol* 1993;**120**:725–732.

ESHRE. *OVARIAN STIMULATION FOR IVF/ICSI Guideline of the European Society of Human Reproduction and Embryology*. 2019;

Evans KJ, Gomes ER, Reisenweber SM, Gundersen GG, Lauring BP. Linking axonal degeneration to microtubule remodeling by Spastin-mediated microtubule severing. *J Cell Biol* 2005;**168**:599–606.

Farquhar CM, Bhattacharya S, Repping S, Mastenbroek S, Kamath MS, Marjoribanks J, Boivin J. Female subfertility. *Nat Rev Dis Prim* 2019;**5**:. Nature Publishing Group.

Fawcett DW. The mammalian spermatozoon. *Dev Biol* [Internet] 1975;**44**:394–436.

Feng CW, Bowles J, Koopman P. Control of mammalian germ cell entry into meiosis. *Mol Cell Endocrinol* 2014;**382**:488–497.

Feng R, Sang Q, Kuang Y, Sun X, Yan Z, Cowan NJ, Wang L. Mutations in TUBB8 and human oocyte meiotic arrest. *N Engl J Med* 2016;**374**:223–232.

Ferrer-Vaquer A, Barragán M, Rodríguez A, Vassena R. Altered cytoplasmic maturation in rescued in vitro matured oocytes. *Hum Reprod* [Internet] 2019;1–11Available from: https://academic.oup.com/humrep/advance-article-abstract/doi/10.1093/humrep/dez052/5497424.

Fouquet J-P, Kann M-L, Edde B, Wolff A, Desbruyeres E, Denoulet P. Differential distribution of glutamylated tubulin during spermatogenesis in mammalian testis. *Cell Motil* [Internet] 1994;**27**:49–58. John Wiley & Sons, Ltd.

Fouquet J-P, Prigent Y, Kann M-L. Comparative immunogold analysis of tubulin isoforms in the mouse sperm flagellum: Unique distribution of glutamylated tubulin. *Mol Reprod Dev* [Internet] 1996;**43**:358–365. John Wiley & Sons, Ltd.

Fulton C, Simpson PA. Selective synthesis and utilisation of flagellar tubulin. The multi-tubulin hypothesis. *Cold Spring Harb Lab Press* 1976;**3**:987–1005.

Gebauer F, Hentze MW. Molecular mechanisms of translational control. *Nat Rev Mol Cell Biol* [Internet] 2004;**5**:827–835.

Goldman KN, Kramer Y, Hodes-Wertz B, Noyes N, McCaffrey C, Grifo JA. Long-term cryopreservation of human oocytes does not increase embryonic aneuploidy. *Fertil Steril* 2015;**103**:, p. 662–668. Elsevier Inc.

Gonzalez-Roca E, Garcia-Albéniz X, Rodriguez-Mulero S, Gomis RR, Kornacker K, Auer H. Accurate expression profiling of very small cell populations. *PLoS One* 2010;**5**:14418–14429.

Gruhn JR, Zielinska AP, Shukla V, Blanshard R, Capalbo A, Cimadomo D, Nikiforov D, Chan AC-H, Newnham LJ, Vogel I, *et al.* Chromosome errors in human eggs shape natural fertility over reproductive life span. *Science (80-)* [Internet] 2019;**365**:1466–1469.

Gruss O, J. O. Animal Female Meiosis: The Challenges of Eliminating Centrosomes. *Cells* [Internet] 2018;**7**:73. Multidisciplinary Digital Publishing Institute.

Gundersen GG, Kalnoski MH, Bulinski JC. Distinct populations of microtubules: Tyrosinated and nontyrosinated alpha tubulin are distributed differently in vivo. *Cell* 1984;**38**:779–789.

Habermann-Macabelli C, Ferreira RM, Gimenes LU, Carvalho NAT De, Soares JG, Ayres H, Ferraz ML, Watanabe YF, Watanabe OY, Sangalli JR, *et al.* Reference gene selection for gene expression analysis of oocytes collected from dairy cattle and buffaloes during winter and summer. *PLoS One* 2014;**9**:13–21.

Hallak ME, Rodriguez JA, Barra HS, Caputto R. Release of tyrosine from tyrosinated tubulin. Some common factors that affect this process and the assembly of tubulin. *FEBS Lett* [Internet] 1977;**73**:147–150.

Hamelin M, Scott IM, Way JC, Culotti JG. *The mec-7 f-tubulin gene of Caenorhabditis elegans is expressed primarily in the touch receptor neurons* [Internet]. *EMBO J* [Internet] 1992;**1**:.

Hassold T, Hunt P. To err (meiotically) is human: The genesis of human aneuploidy. *Nat Rev Genet* 2001;**2**:281–291.

Holubcova Z, Blayney M, Elder K, Schuh M. Error-prone chromosome-mediated spindle assembly favors chromosome segragation defects in human oocytes. *Sci Reports* 2015;**348**:1143–1147.

Howes SC, Alushin GM, Shida T, Nachury M V, Nogales E. Effects of tubulin acetylation and tubulin acetyltransferase binding on microtubule structure. *Mol Biol Cell* [Internet] 2014;**25**:257–266.

Hoyle HD, Raff EC. Two Drosophila Beta Tubulin Isoforms Are Not Functionally Equivalent. *J Cell Biol* [Internet] 1990;1009–1026Available from: http://doi.org/10.1083/jcb.111.3.1009.

Hubbert C. HDAC6 is a microtubule-associated deacetylase. *Nat Lett* 2002;**417**:455–458.

Huitorel P, White D, Fouquet J-P, Kann M-L, Cosson J, Gagnon C. Differential distribution of glutamylated tubulin isoforms along the sea urchin sperm axoneme. *Mol Reprod Dev* [Internet]

2002;**62**:139–148. John Wiley & Sons, Ltd.

Iftode F, Clérot JC, Levilliers N, Bré MH. Tubulin polyglycylation: A morphogenetic marker in ciliates. *Biol Cell* 2000;**92**:615–628.

Ikegami K, Mukai M, Tsuchida JI, Heier RL, MacGregor GR, Setou M. TTLL7 is a mammalian β-tubulin polyglutamylase required for growth of MAP2-positive neurites. *J Biol Chem* 2006;**281**:30707–30716.

Inhorn MC, Patrizio P. Infertility around the globe: New thinking on gender, reproductive technologies and global movements in the 21st century. *Hum Reprod Update* 2014;**21**:411–426. Oxford University Press.

Inoue T, Hiratsuka M, Osaki M, Oshimura M. The molecular biology of mammalian SIRT proteins: SIRT2 in cell cycle regulation. *Cell Cycle* 2007;**6**:1011–1018.

Janke C, Rogowski K, Wloga D, Regnard C, Kajava A V., Strub J-M, Temurak N, Dijk J van, Boucher D, Dorsselaer A van, *et al.* Tubulin polyglutamylase enzymes are members of the TTL domain protein family. *Science* [Internet] 2005;**308**:1758–1762.

Kalinina E, Biswas R, Berezniuk I, Hermoso A, Aviles FX, Fricker LD. A novel subfamily of mouse cytosolic carboxypeptidases. *FASEB J* 2007;**21**:836–850.

Kann M-L, Prigent Y, Levilliers N, Bré M-H, Fouquet J-P. Expression of glycylated tubulin during the differentiation of spermatozoa in mammals. *Cell Motil* [Internet] 1998;**41**:341–352. John Wiley & Sons, Ltd.

Kavallaris M, Kuo DY, Burkhart CA, Regl DL, Norris MD, Haber M, Horwitz SB. Taxol-resistant epithelial ovarian tumors are associated with altered expression of specific beta-tubulin isotypes. *J Clin Invest* [Internet] 1997;**100**:1282–1293.

Kemphues KJ, Kaufman TC, Raff RA, Raff EC. *The Testis-Specific P-Tubulin Subunit in Drosophila melanogaster Has Multiple Functions in Spermatogenesis* [Internet]. *Cell* [Internet] 1982;**31**:.

Kempisty B, Zawierucha P, Ciesiolka S, Piotrowska H, Antosik P, Bukowska D, Jeseta M, Nowicki M, Brussow KP, Zabel M. Developmental competence of mammalian oocytes-insights into molecular research and the promise of microfluidic technology: A review. *Vet Med (Praha)* 2015;**60**:663–674.

Khawaja S. Enhanced stability of microtubules enriched in detyrosinated tubulin is not a direct function of detyrosination level. *J Cell Biol* [Internet] 1988;**106**:141–149.

Kim BK, Lee SC, Kim KJ, Han CH, Kim JH. In vitro maturation, fertilization, and development of human germinal vesicle oocytes collected from stimulated cycles. *Fertil Steril* 2000;**74**:1153–1158.

Kim GW, Li L, Gorbani M, You L, Yang XJ. Mice lacking α-tubulin acetyltransferase 1 are viable but display α-tubulin acetylation deficiency and dentate gyrus distortion. *J Biol Chem* 2013;**288**:20334–20350.

Kitajima TS, Ohsugi M, Ellenberg J. Complete kinetochore tracking reveals error-prone homologous chromosome biorientation in mammalian oocytes. *Cell* [Internet] 2011;**146**:568–581. Elsevier Inc.

Krauhs E, Little M, Kempf T, Hofer-Warbinek R, Ade W, Ponstingl H. *Complete amino acid sequence of β-tubulin from porcine brain (sequence microheterogeneity/similarity to a-tubulin, troponin T, and nucleotide binding proteins)* [Internet]. *Biochemistry* [Internet] 1981;**78**:.

Kreitzer G, Liao G, Gundersen GG. *Detyrosination of Tubulin Regulates the Interaction of Intermediate Filaments with Microtubules In Vivo via a Kinesin-dependent Mechanism*. *Mol Biol Cell* 1999;**10**:.

Kubo T, Yagi T, Kamiya R. Tubulin polyglutamylation regulates flagellar motility by controlling a specific inner-arm dynein that interacts with the dynein regulatory complex. *Cytoskeleton* [Internet] 2012;**69**:1059–1068. John Wiley & Sons, Ltd.

Kubo T, Yanagisawa H aki, Yagi T, Hirono M, Kamiya R. Tubulin

Polyglutamylation Regulates Axonemal Motility by Modulating Activities of Inner-Arm Dyneins. *Curr Biol* 2010;**20**:.

Kull FJ, Sloboda RD. A slow dance for microtubule acetylation. *Cell* [Internet] 2014;**157**:1255–1256. Elsevier.

Kyogoku H, Kitajima TS. Large Cytoplasm Is Linked to the Error-Prone Nature of Oocytes. *Dev Cell* 2017;**41**:287–298.

L'Hernault SW, Rosenbaum JL. Chlamydomonas α-tubulin is posttranslationally modified by acetylation on the ε-amino group of a lysine. *Biochemistry* [Internet] 1985;**24**:473–478. American Chemical Society.

La Fuente R De, Viveiros MM, Burns KH, Adashi EY, Matzuk MM, Eppig JJ. Major chromatin remodeling in the germinal vesicle (GV) of mammalian oocytes is dispensable for global transcriptional silencing but required for centromeric heterochromatin function. *Dev Biol* [Internet] 2004;**275**:447–458.

Lacroix B, Dijk J Van, Gold ND, Guizetti J, Aldrian-Herrada G, Rogowski K, Gerlich DW, Janke C. Tubulin polyglutamylation stimulates spastin-mediated microtubule severing. *J Cell Biol* 2010;**189**:945–954.

Lane S, Kauppi L. Meiotic spindle assembly checkpoint and aneuploidy in males versus females. *Cell Mol Life Sci* [Internet] 2018;Available from: https://doi.org/10.1007/s00018-018-2986-6.

LeDizet M, Piperno G. Identification of an acetylation site of Chlamydomonas a-tubulin (posttranslational acetylation/epitope mapping/a-tubulin isoforms/microtubule stability). *Biochemistry* 1987;**84**:5720–5724.

LeDizet M, Piperno G. Detection of Acetylated α-Tubulin by Specific Antibodies. *Methods Enzymol* 1991;**196**:264–274.

Lenormand T, Engelstädter J, Johnston SE, Wijnker E, Christoph R. Evolutionary mysteries in meiosis. *R Soc Publ* 2016;**371**:20160001.

Li L, Yang XJ. Tubulin acetylation: Responsible enzymes, biological functions and human diseases. *Cell Mol Life Sci* 2015;**72**:4237–4255. Springer Basel.

Li Y, Feng HL, Cao YJ, Zheng GJ, Yang Y, Mullen S, Critser JK, Chen ZJ. Confocal microscopic analysis of the spindle and chromosome configurations of human oocytes matured in vitro. *Fertil Steril* 2006;**85**:827–832.

Lindemann CB, Lesich KA. Flagellar and ciliary beating: the proven and the possible. *J Cell Sci* [Internet] 2010;**123**:519–528.

Ludueña RF. Multiple Forms of Tubulin: Different Gene Products and Covalent Modifications. *Int Rev Cytol* [Internet] 1998;**178**:207–275.

Ludueña RF. A Hypothesis on the Origin and Evolution of Tubulin. *Int Rev Cell Mol Biol* [Internet] 2013;**302**:, p. 41–185. Elsevier.

Ludueña RF, Banerjee A. The Isotypes of Tubulin. *Role Microtubules Cell Biol Neurobiol Oncol* 2009;, p. 123–175. Humana Press.

Ludueńa RF, Shooter EM, Wilson L. Structure of the tubulin dimer. *J Biol Chem* [Internet] 1977;**252**:7006–7014.

Maddox P, Straight A, Coughlin P, Mitchison TJ, Salmon ED. Direct observation of microtubule dynamics at kinetochores in Xenopus extract spindles: Implications for spindle mechanics. *J Cell Biol* 2003;**162**:377–382.

Maiato H, DeLuca J, Salmon ED, Earnshaw WC. The dynamic kinetochore-microtubule interface. *J Cell Sci* 2004;**117**:5461–5477.

Mamo S, Gal AB, Bodo S, Dinnyes A. Quantitative evaluation and selection of reference genes in mouse oocytes and embryos cultured in vivo and in vitro. *BMC Dev Biol* [Internet] 2007;**7**:14.

Maruta H, Greer K, Rosenbaum JL. *The Acetylation of Alpha-Tubulin and Its Relationship to the Assembly and Disassembly*

of Microtubules. *J Cell Biol* 1986;**103**:.

Mary J, Redeker V, Caer J-P Le, Rossier J, Schmitter J-M, Mary J, Klotz C, Redeker V, Caer J-P Le, Rossier J, *et al. Posttranslational Modifications in the C-terminal Tail of Axonemal Tubulin from Sea Urchin Sperm Downloaded from* [Internet]. *J Biol Chem* [Internet] 1996;**271**:.

May GS, Waring RB, Morris NR. Increasing tubC β-tubulin synthesis by placing it under the control of a benA β-Tubulin upstream sequence causes a reduction in benA β-tubulin level but has no effect on microtubule function. *Cell Motil* [Internet] 1990;**16**:214–220. John Wiley & Sons, Ltd.

McKean PG, Vaughan S, Gull K. The extended tubulin Superfamily. *J Cell Sci* 2001;**15**:2723–2733.

Mcnally FJ, Vale RD. *Identification of Katanin, an ATPase That Severs and Disassembles Stable Microtubules*. *Cell* 1993;**75**:.

Mitchison T, Evans L, Schulze E, Kirschner M. Sites of microtubule assembly and disassembly in the mitotic spindle. *Cell* [Internet] 1986;**45**:515–527. Elsevier.

Mitchison TJ, Salmon ED. Poleward Kinetochore Fiber Movement Occurs during Both Metaphase and Anaphase-A in Newt Lung Cell Mitosis. *J Cell Biol* 1992;**119**:569–582.

Mukherjee S, Diaz Valencia JD, Stewman S, Metz J, Monnier S, Rath U, Asenjo AB, Charafeddine RA, Sosa HJ, Ross JL, *et al.* Human fidgetin is a microtubule severing enzyme and minus-end depolymerase that regulates mitosis. *Cell Cycle* 2012;**11**:2359–2366. Taylor and Francis Inc.

Nagai T, Ikeda M, Chiba S, Kanno S-I, Mizuno K. Furry promotes acetylation of microtubules in the mitotic spindle by inhibition of SIRT2 tubulin deacetylase. *J Cell Sci* [Internet] 2013;**126**:4369–4380.

Nicastro D, Schwartz C, Pierson J, Gaudette R, Porter ME, Mcintosh JR. The Molecular Architecture of Axonemes Revealed by Cryoelectron Tomography. *Science (80-)* [Internet]

2006;**313**:944–948.

Nieuwenhuis J, Adamopoulos A, Bleijerveld OB, Mazouzi A, Stickel E, Celie P, Altelaar M, Knipscheer P, Perrakis A, Blomen VA, *et al.* Vasohibins encode tubulin detyrosinating activity. *Science (80-)* 2017;**5676**:1–9.

Nogales E, Wolf SG, Downing KH. Structure of the tubulin dimer by electron crystallography. *Nature* [Internet] 1998;**391**:199–203.

Nogueira D, Staessen C, Velde H Van de, Steirteghem A Van. Nuclear status and cytogenetics of embryos derived from in vitro-matured oocytes. *Fertil Steril* 2000;**74**:295–298.

North BJ, Marshall BL, Borra MT, Denu JM, Verdin E. The human Sir2 ortholog, SIRT2, is an NAD+-dependent tubulin deacetylase. *Mol Cell* 2003;**11**:437–444.

Ohta S, Hamada M, Sato N, Toramoto I. Polyglutamylated tubulin binding protein C1orf96/CSAP is involved in microtubule stabilization in mitotic spindles. *PLoS One* 2015;

Pamula M, Ti S-C, Kapoor T. The structured core of human β tubulin confers isotype-specific polymerization properties. *J Cell Biol* [Internet] 2016;**213**:425–433.

Parker AL, Teo WS, Pandzic E, Vicente JJ, Mccarroll JA, Wordeman L, Kavallaris M. β-Tubulin carboxy-terminal tails exhibit isotype-specific effects on microtubule dynamics in human gene-edited cells. *Life Sci Alliance* [Internet] 2018;**1**:1–16.

Pathak N, Obara T, Mangos S, Liu Y, Drummond IA. The Zebrafish fleer Gene Encodes an Essential Regulator of Cilia Tubulin Polyglutamylation □ D □ V. *Mol Biol Cell* [Internet] 2007;**18**:4353–4364.

Paturle-Lafanechere L, Edde B, Denoulet P, Dorsselaer A Van, Mazarguil H, Caer JP Le, Wehland J, Job D. Characterization of a major brain tubulin variant which cannot be tyrosinated. *Biochemistry* [Internet] 1991;**30**:10523–10528. American Chemical Society.

Paturle-Lafanechère L, Manier M, Trigault N, Pirollet F, Mazarguil H, Job D. Accumulation of delta 2-tubulin, a major tubulin variant that cannot be tyrosinated, in neuronal tissues and in stable microtubule assemblies. *J Cell Sci* [Internet] 1994;**107**:1529–1543.

Pennart H de, Houliston E, Maro B. Post-translational modifications of tubulin and the dynamics of microtubules in mouse oocytes and zygotes. *Biol Cell* 1988;**64**:375–378.

Perdiz D, Mackeh R, Poüs C, Baillet A. The ins and outs of tubulin acetylation: More than just a post-translational modification? *Cell Signal* 2011;**23**:763–771.

Peris L, Thery M, Fauré J, Saoudi Y, Lafanechère L, Chilton JK, Gordon-Weeks P, Galjart N, Bornens M, Wordeman L, *et al.* Tubulin tyrosination is a major factor affecting the recruitment of CAP-Gly proteins at microtubule plus ends. *J Cell Biol* 2006;**174**:839–849.

Peris L, Wagenbach M, Lafanechère L, Brocard J, Moore AT, Kozielski F, Job D, Wordeman L, Andrieux A. Motor-dependent microtubule disassembly driven by tubulin tyrosination. *J Cell Biol* [Internet] 2009;**185**:1159–1166.

Petersen CG, Oliveira JBA, Mauri AL, Massaro FC, Baruffi RLR, Pontes A, Franco JG. Relationship between visualization of meiotic spindle in human oocytes and ICSI outcomes: A meta-analysis. *Reprod Biomed Online* 2009;**18**:235–243. Reproductive Healthcare Ltd.

Pincus G, Enzmann E V. The comparative behaviour of mammalian eggs in vivo and in vitro. *J Exp Med* 1935;**62**:665–675.

Piqué M, López JM, Foissac S, Guigó R, Méndez R. A Combinatorial Code for CPE-Mediated Translational Control. *Cell* 2008;

Ponstingl H, Krauhs E, Little M, Kempf T. *Complete amino acid sequence of a-tubulin from porcine brain (sequence microheterogeneity/homology with muscle proteins)* [Internet]. *Biochemistry* [Internet] 1981;**78**:.

Portran D, Schaedel L, Xu Z, Théry M, Nachury M V. Tubulin acetylation protects long-lived microtubules against mechanical ageing. *Nat Cell Biol* [Internet] 2017;**19**:391–398.

Prigent Y, Kann ML, Lach-Gar H, Pechart I, Fouquet JP. *Glutamylated tubulin as a marker of microtubule heterogeneity in the human sperm flagellum* [Internet]. *Mol Hum Reprod* [Internet] 1996;**2**:.

Qiu D, Hou X, Han L, Li X, Ge J, Wang Q. Sirt2-BubR1 acetylation pathway mediates the effects of advanced maternal age on oocyte quality. *Aging Cell* 2017;

Raff EC, Fackenthal JD, Hutchens JA, Hoyle HD, Rudolf Turner F. *Microtubule Architecture Specified by a β-Tubulin Isoform* [Internet]. *Science (80-)* [Internet] 1997;**275**:.

Raff EC, Hutchens JA, Hoyle HD, Nielsen MG, Turner FR. Conserved axoneme symmetry altered by a component β-tubulin. *Curr Biol* [Internet] 2000;**10**:1391–1394.

Raybin D, Flavin M. Enzyme which specifically adds tyrosine to the α chain of tubulin. *Biochemistry* [Internet] 1977;**16**:2189–2194. American Chemical Society.

Redeker V, Levilliers N, Schmitter JM, Caer JP Le, Rossier J, Adoutte A, Bré MH. Polyglycylation of tubulin: a posttranslational modification in axonemal microtubules. *Science (80-)* 1994;**266**:1688–1691.

Regnard C, Fesquet D, Janke C, Boucher D, Desbruyères E, Koulakoff A, Insina C, Travo P, Eddé B. Characterisation of PGs1, a subunit of a protein complex co-purifying with tubulin polyglutamylase. *J Cell Sci* [Internet] 2003;**116**:4181–4190.

Reichman DE, Politch J, Ginsburg ES, Racowsky C. Extended in vitro maturation of immature oocytes from stimulated cycles: An analysis of fertilization potential, embryo development, and reproductive outcomes. *J Assist Reprod Genet* 2010;**27**:347–356.

Rodriguez De La Vega M, Sevilla RG, Hermoso A, Lorenzo J, Tanco

S, Diez A, Fricker LD, Bautista JM, Avilés FX. Nna1-like proteins are active metallocarboxypeptidases of a new and diverse M14 subfamily. *FASEB J* 2007;**21**:851–865.

Rogers GC, Rogers SL, Sharp DJ. Spindle microtubules in flux. *J Cell Sci* 2005;**118**:1105–1116.

Rogowski K, Dijk J van, Magiera MM, Bosc C, Deloulme JC, Bosson A, Peris L, Gold ND, Lacroix B, Grau MB, *et al.* A family of protein-deglutamylating enzymes associated with neurodegeneration. *Cell* 2010;**143**:564–578.

Rogowski K, Juge F, Dijk J van, Wloga D, Strub JM, Levilliers N, Thomas D, Bré MH, Dorsselaer A Van, Gaertig J, *et al.* Evolutionary Divergence of Enzymatic Mechanisms for Posttranslational Polyglycylation. *Cell* 2009;**137**:1076–1087.

Roll-Mecak A. Intrinsically disordered tubulin tails: Complex tuners of microtubule functions? *Semin Cell Dev Biol* [Internet] 2015;**37**:11–19. Elsevier Ltd.

Roll-Mecak A, Vale RD. The Drosophila homologue of the hereditary spastic paraplegia protein, spastin, severs and disassembles microtubules. *Curr Biol* 2005;**15**:650–655. Cell Press.

Rossi G, Macchiarelli G, Palmerini MG, Canipari R, Cecconi S. Meiotic spindle configuration is differentially influenced by FSH and epidermal growth factor during in vitro maturation of mouse oocytes. *Hum Reprod* [Internet] 2006;**21**:1765–1770.

Rostovtseva TK, Gurnev PA, Hoogerheide DP, Rovini A, Sirajuddin M, Bezrukov SM. Sequence diversity of tubulin isotypes in regulation of the mitochondrial voltage-dependent anion channel. *J Biol Chem* [Internet] 2018;**293**:10949–10962.

Sanfins A, Lee GY, Plancha CE, Overstrom EW, Albertini DF. Distinctions in Meiotic Spindle Structure and Assembly During In Vitro and In Vivo Maturation of Mouse Oocytes. *Biol Reprod* 2003;**69**:2059–2067.

Savage C, Xue Y, Mitani S, Hall D, Zakhary R, Chalfie M. Mutations

in the Caenorhabditis elegansβ-tubulin gene mec-7 : effects on microtubule assembly and stability and on tubulin autoregulation. *J Cell Sci* 1994;**107**:2165–2175.

Schatten G, Simerly C, Asai DJ, Szuke E, Cooke P, Schatten H. Acetylated α-Tubulin in Microtubules during Mouse Fertilization and Early Development. *Dev Biol* 1988;**130**:74–86.

Schatz F, Solomon PJ, Botsteinl D. Genetically Essential and Nonessential ot-Tubulin Genes Specify Functionally Interchangeable Proteins. *Mol Cell Biol* [Internet] 1986;**6**:3722–3733.

Schneider J, Lahl J, Kramer W. Long-term breast cancer risk following ovarian stimulation in young egg donors: a call for follow-up, research and informed consent. *Reprod Biomed Online* [Internet] 2017;**34**:480–485.

Serra E, Gadau SD, Berlinguer F, Naitana S, Succu S. Morphological features and microtubular changes in vitrified ovine oocytes. *Theriogenology* [Internet] 2019; Elsevier Inc.Available from: https://linkinghub.elsevier.com/retrieve/pii/S0093691X19305072.

Serra E, Succu S, Berlinguer F, Porcu C, Leoni GG, Naitana S, Gadau SD. Tubulin posttranslational modifications in in vitro matured prepubertal and adult ovine oocytes. *Theriogenology* [Internet] 2018;**114**:237–243. Elsevier Inc.

Severin FF, Sorger PK, Hyman AA. *Kinetochores distinguish GTP from GDP forms of the microtubule lattice*. 1997;

Severson AF, Dassow G von, Bowerman B. Oocyte Meiotic Spindle Assembly and Function. *Curr Top Dev Biol* 2016;**116**:, p. 65–98. Elsevier Inc.

Shida T, Cueva JG, Xu Z, Goodman MB, Nachury M V, Kathryn Anderson by V. The major α-tubulin K40 acetyltransferase αTAT1 promotes rapid ciliogenesis and efficient mechanosensation. *Proc Natl Acad Sci U S A* 2010;**107**:21517–21522.

Shu Y, Gebhardt J, Watt J, Lyon J, Dasig D, Behr B. Fertilization, embryo development, and clinical outcome of immature oocytes from stimulated intracytoplasmic sperm injection cycles. *Fertil Steril* 2007;**87**:1022–1027.

Sirajuddin M, Rice LM, Vale RD. Regulation of microtubule motors by tubulin isotypes and post-translational modifications. *Nat Cell Biol* 2014;**16**:335–344.

Siristatidis C, Sergentanis TN, Kanavidis P, Trivella M, Sotiraki M, Mavromatis I, Psaltopoulou T, Skalkidou A, Petridou ET. Controlled ovarian hyperstimulation for IVF: Impact on ovarian, endometrial and cervical cancer-A systematic review and meta-analysis. *Hum Reprod Update* 2013;**19**:105–123.

Smith SD, Mikkelsen AL, Lindenberg S. Development of human oocytes matured in vitro for 28 or 36 hours. *Fertil Steril* 2000;**73**:541–544.

Song Y, Brady ST. Post-translational modifications of tubulin: pathways to functional diversity of microtubules. *Trends Cell Biol* [Internet] 2015;**25**:125–136.

Steuerwald N, Cohen J, Herrera RJ, Brenner CA. Quantification of mRNA in single oocytes and embryos by real-time rapid cycle fluorescence monitored RT-PCR. *Mol Hum Reprod* 2000;**5**:1034–1039.

Sullivan KF, Cleveland DW. Identification of conserved isotype-defining variable region sequences for four vertebrate f8 tubulin polypeptide classes. *Cell Biol* [Internet] 1986;**83**:4327–4331.

Szollosi D, Calarco P, Donaheu RP. Absence of Centrioles in the First and Second Meiotic Spindles of Mouse Oocytes. *J Cell Sci* 1972;**11**:521–541.

Szyk A, Deaconescu AM, Piszczek G, Roll-Mecak A. Tubulin tyrosine ligase structure reveals adaptation of an ancient fold to bind and modify tubulin. *Nat Struct Mol Biol* 2011;**18**:1250–1259.

Szyk A, Deaconescu AM, Spector J, Goodman B, Valenstein ML,

Ziolkowska NE, Kormendi V, Grigorieff N, Roll-Mecak A. Molecular basis for age-dependent microtubule acetylation by tubulin acetyltransferase. *Cell* [Internet] 2014;**157**:1405–1415. Elsevier Inc.

Tang F, Pan M-H, Wan X, Lu Y, Zhang Y, Sun S-C. Kif18a regulates Sirt2-mediated tubulin acetylation for spindle organization during mouse oocyte meiosis. *Cell Div* [Internet] 2018;**13**:1–9.

Ti SC, Alushin GM, Kapoor TM. Human β-Tubulin Isotypes Can Regulate Microtubule Protofilament Number and Stability. *Dev Cell* 2018;**47**:175–190.

Touati SA, Wassmann K. How oocytes try to get it right: spindle checkpoint control in meiosis. *Chromosoma* [Internet] 2016;**125**:321–335. Chromosoma.

Trounson A, Wood C, Kausche A. In vitro maturation and the fertilization and developmental competence of oocytes recovered from untreated polycystic ovarian patients. *Fertil Steril* [Internet] 1994;**62**:353–362.

Valenstein ML, Roll-Mecak A, Abstract G. Graded Control of Microtubule Severing by Tubulin Glutamylation. *Cell* [Internet] 2016;**164**:911–921. Elsevier Inc.

Vandesompele J, Preter K De, Pattyn F, Poppe B, Roy N Van, Paepe A De, Speleman F. Accurate normalization of real-time quantitative RT-PCR data by geometric averaging of multiple internal control genes. *Genome Biol* [Internet] 2002;**3**:RESEARCH0034.

Vassena R, Boué S, González-Roca E, Aran B, Auer H, Veiga A, Izpisua Belmonte JC. Waves of early transcriptional activation and pluripotency program initiation during human preimplantation development. *Development* [Internet] 2011;**138**:3699–3709.

Vemu A, Atherton J, Spector JO, Moores CA, Roll-Mecak A. Tubulin isoform composition tunes microtubule dynamics. *Mol Biol Cell* [Internet] 2017;**28**:3564–3572.

Vemu A, Szczesna E, Zehr EA, Spector JO, Grigorieff N, Deaconescu AM, Roll-Mecak A. Severing enzymes amplify microtubule arrays through lattice GTP-tubulin incorporation. *Science (80-)* 2018;**361**:eaau1504.

Verdel A, Seigneurin-Berny D, Faure AK, Eddahbi M, Khochbin S, Nonchev S. HDAC6-induced premature chromatin compaction in mouse oocytes and fertilised eggs. *Zygote* [Internet] 2003;**11**:323–328.

Verlhac M-H, Terret M-E. Oocyte Maturation and Development. *F1000Research* [Internet] 2016;**5**:1–8.

Vos M De, Smitz J, Thompson JG, Gilchrist RB. The definition of IVM is clear - Variations need defining. *Hum Reprod* 2016;**31**:2411–2415.

Wade R. On and around microtubules: an overview. *Mol Biotechnol* [Internet] 2009;**43**:177–191.

Wang A-C, Zhang Y-S, Wang B-S, Zhao X-Y, Wu F-X, Zhai X-H, Sun J-X, Mei S-Y. Mutation analysis of the TUBB8 gene in nine infertile women with oocyte maturation arrest. *Reprod Biomed Online* [Internet] 2017;**35**:305–310. Informa UK Ltd.

Webster DR, Gundersen GG, Bulinski JC, Borisy GG. Differential turnover of tyrosinated and detyrosinated microtubules. *Proc Natl Acad Sci* [Internet] 1987;**84**:9040–9044.

WHO. *WHO laboratory manual for the examination of human semen and sperm-cervical mucus interaction*. 1999; Cambridge university press.

Wilkins AS, Holliday R. The evolution of meiosis from mitosis. *Genetics* [Internet] 2009;**181**:3–12. Genetics.

Wilson PG, Borisy GG. Evolution of the multi-tubulin hypothesis. *BioEssays* [Internet] 1997;**19**:451–454.

Wilson PJ, Forer A. Effects of Nanomolar taxol on crane-fly spermatocyte spindles indicate that acetylation of kinetochore microtubules can be used as a marker of poleward tubulin flux.

Cell Motil Cytoskeleton 1997;**37**:20–32. Wiley Online Library.

World Medical Association. *Declaration of Helsinki: ethical principles for medical research involving human subjects. Adopted by the 18th WMA General Assembly, Helsinki, Finland, June 1964, and last amended by the 64th WMA General Assembly, Fortaleza, Brail, October 2013*. 2013;

Yin H, Duffy DM, Gosden RG. Comparative maturation of cynomolgus monkey oocytes in vivo and in vitro. *Reprod Biol Endocrinol* [Internet] 2006;**4**:14.

Yoon HG, Yoon SH, Son WY, Lee SW, Park SP, Im KS, Lim JH. Pregnancies resulting from in vitro matured oocytes collected from women with regular menstrual cycle. *J Assist Reprod Genet* 2001;**18**:325–329.

Yuan P, Zheng L, Liang H, Li Y, Zhao H, Li R, Lai L, Zhang Q. A novel mutation in the TUBB8 gene is associated with complete cleavage failure in fertilized eggs. *J Assist Reprod Genet* 2018;

Zegers-Hochschild F, Adamson GD, Dyer S, Racowsky C, Mouzon J de, Sokol R, Rienzi L, Sunde A, Schmidt L, Cooke ID, *et al.* The International Glossary on Infertility and Fertility Care, 2017. *Fertil Steril* 2017;**108**:393–406. Elsevier Inc.

Zhang D, Rogers GC, Buster DW, Sharp DJ. Three microtubule severing enzymes contribute to the "Pacman- flux" machinery that moves chromosomes. *J Cell Biol* 2007;**177**:231–242.

Zhang L, Hou X, Ma R, Moley K, Schedl T, Wang Q. Sirt2 functions in spindle organization and chromosome alignment in mouse oocyte meiosis. *FASEB J* [Internet] 2014;**28**:1435–1445.

Zhang Y, Kwon S, Yamaguchi T, Cubizolles F, Rousseaux S, Kneissel M, Cao C, Li N, Cheng H-L, Chua K, *et al.* Mice Lacking Histone Deacetylase 6 Have Hyperacetylated Tubulin but Are Viable and Develop Normally. *Mol Cell Biol* 2008;**28**:1688–1701.

Zhou D, Choi Y-J, Kim J-H. Histone deacetylase 6 (HDAC6) is an essential factor for oocyte maturation and asymmetric division

in mice. *Sci Rep* [Internet] 2017;**7**:8131. Springer US.

Zielinska AP, Bellou E, Sharma N, Frombach AS, Seres KB, Gruhn JR, Blayney M, Eckel H, Moltrecht R, Elder K, *et al.* Meiotic Kinetochores Fragment into Multiple Lobes upon Cohesin Loss in Aging Eggs. *Curr Biol* 2019;**29**:3749-3765.e7. Cell Press.

Zilberman Y, Ballestrem C, Carramusa L, Mazitschek R, Khochbin S, Bershadsky A. Regulation of microtubule dynamics by inhibition of the tubulin deacetylase HDAC6. *J Cell Sci* 2009;**122**:3531–3541.